CHARACTERISTICS OF DISK AND HALO POPULATIONS DERIVED FROM PHOTOGRAPHIC PHOTOMETRY

Thesis by
Donna E. Weistrop

In Partial Fulfillment of the Requirements
for the Degree of
Doctor of Philosophy

California Institute of Technology
Pasadena, California

1971

(Submitted May 25, 1971)

The future is a world limited by ourselves.

Maeterlinck, Joyzelle

Acknowledgements

Thanks are due many people for the help that has been made available to me. To Dr. Sarah J. Hill of Wellesley College, who believed women should be in astronomy when others thought they belonged at home , I will always be grateful. I am deeply indebted to Dr. Maarten Schmidt, who first suggested the thesis project and provided invaluable guidance along the way. Dr. Allan Sandage, in addition to making available plates and other data, has also given his time, for discussion and adjustment of the iris photometer. A computer program, and the knowledge necessary to run it, were provided by Dr. Bruce Peterson. My thanks go to the night assistants, Gene Hancock and Henry Schaefer at Mt. Wilson, and Dennis Palm at Palomar, for putting up with me when I said maybe it would clear, and it was pouring rain at 1 A.M. Bob Vaughan, Larry Blakeé, and Maynard Clark must also be mentioned, for electronic set-ups on Mt. Wilson and "house calls" to the iris photometer at Santa Barbara Street. Thanks also go to Rudy Ribbens for looking after the mechanical aspects of the aforementioned infernal machine. I am indebted, too, to Dr. Robert Kraft, who started me off on a life of observing. The people at NASA, the Woodrow Wilson Foundation, and the guardians of the GRA's have helped by providing sustenance. I am grateful to have had the opportunity of using the facilities of the Hale Observatories at both Mt. Wilson and Palomar.

Finally, many thanks must go to Anneila Sargent, for morale-building trips to Wil Wright's before my preliminary orals, and for frequent trips to the Konditori during the last few harried months.

Abstract

The nature of faint stars at high galactic latitudes was investigated through U,B,V photometry of several thousand stars between V = 12 and 18 near the North Galactic Pole. Magnitudes were determined from iris photometer measurements of plates taken with the 48-inch Schmidt telescope. Calibration was provided by a photoelectric sequence in the field. Several models for the luminosity function and density distribution of Population II field stars were assumed. Assuming also that all stars bluer than $(B-V)_o = .5$ and fainter than V = 17 are members of Population II, an upper limit of 7×10^{-5} solar masses per pc^3 was calculated for the local Population II density, a result significantly lower than local densities computed from the number of nearby stars suspected of halo membership. Some of the discrepancy may be due to the method used.

Having estimated the contributions to the star counts due to Population II stars and disk giants and subgiants, the remaining stars were assumed to constitute a pure disk dwarf population. Density distributions for stars in successive $(B-V)_o$ intervals were calculated and combined to form a composite disk density distribution. The agreement with Oort's K giant distribution is satisfactory. There was some indication that the faintest dwarfs are concentrated in a narrow layer in the plane, but further investigation is required. Determination of the luminosity function for the reddest disk dwarfs indicated these stars are five to ten times as numerous as was previously thought, thus accounting for a significant fraction of the missing mass in the solar neighborhood. Luminosity functions extrapolated to account for all the missing mass are indicated.

Table of Contents

Chapter I

Introduction

Several early studies of stars at high galactic latitude were made, most of them concerned with determining the stellar density distribution perpendicular to the galactic plane. Using data for stars for which spectral classifications were available ($m_{pg} \leq 13$) , van Rhijn and Schwassmann (1935) were able to determine density distributions for stars of various absolute magnitudes. Becker (1940), in a similar way, determined the distribution perpendicular to the plane of A and F stars in the southern sky. Bok and MacRae (1941), employing a different method, used a previously determined luminosity function for the plane and adjusted density distributions to fit observed star counts and mean parallaxes. By using star counts without color or spectral data, they were able to extend the analysis to include data from stars as faint as photographic magnitude 18. Oort (1932), adopting yet a third approach, used known velocity and density distributions perpendicular to the plane to derive the acceleration in the z direction within 500 pc, then inverted the argument to predict the density distribution far from the plane from the extrapolated acceleration. The results were checked by comparing predicted star counts with the observations.

More recent work may be separated into two categories. Investigations of metal-deficient field stars have generally been carried out using specific types of stars; e.g., blue stars and subdwarfs (Greenstein, 1966; Sandage, 1969b; and Sandage and Luyten, 1967, 1969) and RR Lyrae stars (Plaut and Soudan, 1963), leaving the general characteristics of the metal-deficient field population relatively unknown. For the disk population, the density distribution perpendicular to the plane has recently been studied for K giants (Oort, 1960; Hill, 1960; Upgren, 1962; and Elvius, 1965) and main sequence stars of spectral types A-G (Upgren, 1962, 1963; and Elvius, 1965); but these investigations, like earlier ones employing spectral classifications, were limited to stars brighter than photographic magnitude 13. Only Fenkart (1967) has investigated the distributions for fainter stars, but his results are limited to stars with absolute magnitude $M_G = 3\text{-}8$.

Much remains to be learned from a study of color and magnitude data for faint (V fainter than 12) field stars at high galactic latitudes. If Population II and disk members can be separated, there is the possibility of determining the local Population II density. Current estimates of the local density of metal-deficient stars are very uncertain, being based mainly on the number density of a few high velocity stars thought to be subdwarfs (Oort, 1965). The disk density distribution far from the plane is

known principally from the studies of late-type giants and Fenkart's analysis of R, G, U photometry of field stars. The last determination is, of course, strongly dependent on the method used to discriminate between disk and halo population members. Finally, by measuring colors and magnitudes for all stars in a given part of the sky to faint apparent magnitudes, it is possible to determine the luminosity function of intrinsically faint stars, thus determining the importance of such stars in the plane.

An investigation was undertaken to determine the distribution with apparent magnitude and color of all stars with V magnitudes between 12 and 18. An area of the sky centered on Selected Area 57 (R.A.(1950) = $13^h\ 6\overset{m}{.}4$, Dec.(1950) = +29° 44' : $l^{II} = 65\overset{\circ}{.}5$, $b^{II} = 85\overset{\circ}{.}5$) and covering 13.5 square degrees was chosen for the study, thus enabling observations to be made for stars at the maximum height above the plane for a given apparent magnitude limit while allowing the use of previously derived results for stars in the Selected Area, if necessary. The U, B, V magnitudes and colors of 13,820 stars were measured on plates taken with the 48-inch Schmidt telescope, with calibration from a photoelectric sequence observed with the 100-inch telescope on Mount Wilson. The photographic and photoelectric photometry, and all reduction procedures, are discussed in Chapter II.

Several models of the density distribution for metal-deficient stars were used to derive the upper limit of the local Population II density. Density distributions for disk members in successive intervals of $(B-V)_o$ were calculated, and used to derive a composite density distribution for the disk population. The luminosity function for red dwarfs in the plane was calculated and found to be larger than previously thought (Chapter III).

The influence of the assumed value of the total absorption on the results is considered in Chapter IV. Comparisons between the results derived here and those of other authors are also made. The derived local density of Population II is significantly lower than previous estimates, and possible reasons for this are considered. The composite disk density distribution is found to be in satisfactory agreement with distributions derived by other authors. The consequences for the local mass density of the luminosity function derived for intrinsically faint stars are discussed. At least some of the missing mass in the plane can be accounted for by such stars. In the Appendix, the star counts as a function of apparent magnitude only are briefly considered.

Chapter II

Observations

The Photoelectric Sequence

To calibrate the photographic material, it was necessary to establish a photoelectric sequence of stars over the area of the sky to be measured on the plates. Though some photoelectric standards in SA 57 were already available, additional observations were necessary to obtain a sufficient number of stars in the desired magnitude range, to calibrate the U and r magnitudes originally included in the survey, and to ensure the presence of photoelectric standards in all parts of the field.

Thirty-eight stars with V magnitudes between 12 and 18 were observed in U, B, V and r at the Newtonian focus of the 100-inch telescope between March 1968 and May 1969. An ITT fw-130 photomultiplier tube with S-20 cathode was used with the filters indicated in Table 1 to reproduce the Sandage and Smith (1963) four color system.

Table 1

Filters for Photoelectric Observations

U	2.8 mm Corning 9863 + 5 mm liq. chamber, 40% saturated solution of $CuSO_4 \cdot 5H_2O$
B	0.7 mm Scott BG 12 + 2 mm GG 385 + 5 mm liq. chamber, 40% saturated solution of $CuSO_4 \cdot 5H_2O$
V	2.2 mm Schott GG 495 + 1.6 mm Scott BG 18
r	2.0 mm Schott RG 610 + Corning 1-60

The filter-photomultiplier combination is essentially the same as that of Sandage and Smith, with the addition of the Corning 1-60 filter used to cut off the long wavelength end of the red pass band. The photomultiplier tube was mounted in vacuum insulated cold box V-1 and cooled with dry ice to minimize the dark count. Data collection was accomplished by a pulse-counting system consisting principally of a pre-amplifier, amplifier, pulse height discriminator, and counters. The total number of pulses, integration time and identification data were recorded automatically on both punched cards and paper tape.

The coincidence correction was measured at the telescope, using a lamp and variable power supply. Counts were made through two apertures, with areas in the ratio 10 to 1. The count rates were chosen, so that, at each light level, the rate through the smaller aperture was less than that through the large aperture at the next lower light level. Due to the use of a high speed counting system, the count rates for most stars (25000 c/s or less) were below the level at which the coincidence correction is significant (1% at 80000 c/s). The correction was included in all reductions, however.

Observations of stars brighter than sixteenth magnitude were integrated for ten seconds in each band pass, first on the star, then on the sky, until the number

of pulses counted was sufficient to provide 1% accuracy in B and V and 3% in U. For fainter stars, a dual aperture chopping system was available, which automatically subtracted sky counts from star counts sixty times per second. Measurements of faint stars were made with the star in each aperture for half the integration time. The accuracy requirement was relaxed to 2% for stars of magnitude V = 17 and 4% for those of magnitude V = 18 .

The stars to be observed were selected such that 14 were located in the center of the field, and 5 to 7 were situated toward the edges of each of the four quadrants. Of the 38 program stars, 4, with a range in color of B-V = -.12 to 1.00 and apparent magnitudes between V = 12 and 13 , were selected to serve as local standards. The local standards, indicated by an asterisk in Table 5, were used to monitor extinction changes and establish the natural system to which all other observations were reduced.

Magnitudes indicated by u, b, v were computed from the observations by multiplying the logarithm of the count rate by -2.5 and adding a constant chosen so that the magnitudes are similar to those on the Johnson system. It is necessary to take into account the effect on the observations of the air mass between star and observer, which is assumed to be a function of the star's zenith distance at the time of observation. This may be most

conveniently accomplished by reducing all observations to outside the atmosphere. The relationship between v, b-v, and u-b and the total extinction, nightly variations in the pulse counting system, and the corresponding magnitudes and colors reduced to outside the atmosphere, v_o, $(b-v)_o$, $(u-b)_o$, is given by equation (1). In equation (1), X is

$$\begin{aligned} v &= v_o + \left[k'_v + k''_v \times (b-v)\right] X + Z_v \\ b-v &= (b-v)_o + \left[k'_{b-v} + k''_{b-v} \times (b-v)\right] X + Z_{b-v} \\ u-b &= (u-b)_o + \left[k'_{u-b} + k''_{u-b} \times (u-b)\right] X + Z_{u-b} \end{aligned} \qquad (1)$$

the air mass, Z takes into account nightly variations in the system, k' is the first order term for the extinction, and k" is the coefficient in the color dependent term for the extinction. The values adopted for k" (Table 2) were kindly provided by Dr. Bruce A. Peterson. The v-r

Table 2

Second Order Extinction Coefficients

k''_v	k''_{b-v}	k''_{u-b}
-.008	+.018	-.047

measurements will not be specifically included in the discussion, as problems with the photographic values (see next section) caused the r magnitudes to be omitted from the investigation at a relatively late date. In most cases,

the photoelectric reduction for v-r was parallel to that for u-b and b-v .

The natural system was established by making several observations of each of the local standards during the night of March 29, 1968. Using these data, equation (1) was solved simultaneously for the first order extinction corrections and the magnitudes and colors of the 4 local standards reduced to outside the atmosphere. The value of Z was assumed equal to zero for this night's observations.

Having established the natural system, four to seven observations of local standards were made during the course of each subsequent observing session. These were concentrated at the beginning, middle and end of the night, bracketing all observations of program stars. The observations of the local standards for each session were used to determine k' and Z by solving equation (1), using the natural system magnitudes of the local standards. Typical values of k' are shown for each observing run in Table 3.

Table 3

Typical First Order Extinction Terms

Date	k'_v	k'_{b-v}	k'_{u-b}
March 29, 1968	.380	.187	.402
May 23, 1968	.135	.067	.245
March 15, 1969	.110	.127	.325
April 12, 1969	.246	.082	.342
May 14, 1969	.115	.072	.246

Having determined k' and Z for a set of observations, the natural system colors and magnitudes of the program stars were computed using equation (1). All calculations were performed on the IBM 7094 computer at Caltech, using computing programs made available by Dr. Peterson.

To determine the transformation between the U, B, V and natural systems, four U, B, V primary and secondary standards were measured on the night of April 29, 1968 with the observing system described plus a 13% neutral density filter. The filter was necessary to prevent the bright standards from saturating the electronic data gathering equipment. To avoid systematic effects due to a slight color dependence of the filter transparency, the 4 local standards observed during the night were also measured through the neutral density filter. Solutions for the zero point offset and first order term in the extinction were made as described, including a constant to take into account the effect of the filter on the absolute number of pulses counted, thus reducing the observations of the U, B, V standards to the natural system. The natural system magnitudes together with the U, B, V magnitudes (Johnson and Morgan, 1953; and Johnson, 1954, 1955) of the standards were used to derive the transformations (equation [2])

$$\begin{aligned} V &= v-.0874\ (b-v) - .303 \\ B-V &= 1.400\ (b-v) + .492 \\ U-B &= .999\ (u-b) + .386 \end{aligned} \qquad (2)$$

between the systems. The standard magnitudes and colors are compared with those computed from the transformation equations in Table 4. As can be seen, no systematic effects are apparent.

The transformations have been used to calculate U, B, V magnitudes and colors of all the program stars (Table 5). Unless otherwise indicated, the star name given in the first column of Table 5 is on an arbitrary system used in this study. The "Mt.W." numbers are from the Mount Wilson Catalogue of Photographic Magnitudes in Selected Areas 1-139 (Seares, Kapteyn, and van Rhijn, 1930) and the "HZ" numbers refer to Humason-Zwicky objects (Humason and Zwicky, 1947). Columns two through six are self-explanatory. Columns seven through nine present the photoelectric results of other authors for the stars. The last column indicates the source of the comparison measurements. Colors and magnitudes from Stebbins, Whitford and Johnson (1950) were transformed to the B,V system to make the comparisons.

For the 7 stars for which other V magnitudes are available, there appear to be no systematic differences between these values and the V magnitudes derived here. Comparison of the B magnitudes for those same stars indicates an average difference of +.06 mag. in the sense (Weistrop - other). The other magnitudes were taken from several authors, indicating the origin of the difference probably lies in the present work. The precise cause is

Table 4

Colors and Magnitudes for Johnson Standards

Star	V_J	$(B-V)_J$	$(U-B)_J$	V_C	$(B-V)_C$	$(U-B)_C$
δ Boo B	7.84	+.59	+.01	7.82	+.58	+.06
6° 3525	7.74	-.01	-.55	7.75	.00	-.59
HD 111631	8.49	1.41	1.27	8.48	1.40	1.26
11° 2576	9.04	1.51	1.26	9.05	1.52	1.25

Table 5

Photoelectric Standards

Name	α_{1950}	δ_{1950}	V_W	$(B-V)_W$	$(U-B)_W$	V	B-V	U-B	Ref.
221	$12^h57^m.1$	31°00'	14.55	.74	.21				
328	12 58.6	28 27	14.18	.59	-.01				
220	12 59.0	30 56	14.10	.92	.70				
223	12 59.7	31 11	15.68	1.49	1.51				
330	13 0.2	28 3	16.18	1.25	1.31				
329	13 0.4	28 17	16.55	1.38	.53				
219	13 0.4	31 8	13.15	.53	-.01				
326	13 0.8	27 57	12.38	.66	.17				
22*	13 1.4	30 50	12.78	1.00	.95				
HZ 39	13 2.3	28 23	15.53	-.40	-1.10	15.40 15.44	-.24 -.32	-1.12 -1.16	1 4
325*	13 3.1	28 31	12.94	.44	-.14				
110	13 5.1	29 11	17.05	.59	.07				
16	13 5.1	30 2	12.63	1.08	1.12				
Mt.W. 11	13 5.6	29 36	12.93	.58	-.02	12.93	.53		3
117	13 6.0	29 16	17.75	1.38	.03				
15*	13 6.0	29 26	12.43	.62	.09				
Mt.W. 40	13 6.0	29 44	14.93	.55	-.21	14.91	.49	-.22	2
Mt.W. 54	13 6.2	29 35	14.02	.70	.26	14.01	.63		3
Mt.W. 63	13 6.3	29 33	15.70	1.11	1.04	15.71	.97	.74 1.15	2
Mt.W. 71	13 6.4	29 40	17.42	1.06	.07	17.52	.85		2
111	13 6.4	30 2	15.73	.76	.25				
17	13 7.3	29 20	13.32	.48	-.01				
18	13 7.7	29 40	13.60	.64	.23				
19	13 8.1	30 3	14.76	.69	.18				
113	13 8.4	29 34	15.32	.59	.23				
543	13 10.1	31 8	14.58	.72	.15				
544	13 10.3	30 46	12.96	1.12	1.01				
538	13 10.6	31 20	12.48	.52	.02				
545	13 10.7	30 54	15.85	.69	.11				

Table 5, Continued

Name	α_{1950}	δ_{1950}	V_W	$(B-V)_W$	$(U-B)_W$	V	B-V	U-B	Ref.
541	$13^h11^m.4$	31° 5'	17.49	.69	-.26				
437	13 11.6	28 37	12.57	.69	.16				
432	13 11.7	28 20	13.01	.71	.29				
433	13 12.1	28 6	13.78	.61	.04				
540	13 12.6	31 8	14.04	.61	.09				
436	13 12.8	28 13	16.01	.94	.63				
435	13 13.1	28 23	16.81	.80	.09				
434	13 13.2	28 12	13.93	.55	.06				
HZ 43*	13 14.0	29 22	12.70	-.12	-1.17	12.68	-.10	-1.14	1

References

(1) Greenstein (1966)

(2) Sandage (1968)

(3) Stebbins, Whitford and Johnson (1950)

(4) Greenstein and Eggen (1965)

difficult to determine, but could be due to the small number of U, B, V standards used to calibrate the system. Only 4 of the stars have been observed by other authors in the ultraviolet. The average difference is .03 mag., in the same sense as above, most of this due to Mt.W. 40, for which the magnitude found here is .09 mag. fainter than Sandage's value for U. From stars No. 540 and No. 544, which were each observed on two different nights, the magnitudes appear to be internally consistent, with errors as small as .01 mag. for stars brighter than V = 15 .

Photographic Data

The photographic data consist of 24 plates taken with the 48-inch Schmidt telescope on Palomar Mountain during two observing runs in the spring of 1968. The plate emulsions and filters (Table 6) were selected to photographically reproduce the U, B, V, r photoelectric system. The sensitivity curves for the photoelectric and photographic systems are compared for each pass band in Figure 1. The photoelectric curves are the product of the transmission of the filters, measured in the Astroelectronics Laboratory at Caltech, the sensitivity of the photomultiplier tube from the manufacturer's response curve, and the effect of two reflections from an aluminized mirror (Allen, 1963). The photographic curves consist of the filter transmission curves (Kodak, 1968; and Jenaer Glaswerk

Figure 1

Comparison of photoelectric and photographic sensitivity curves. Solid line represents photoelectric curve. Photographic sensitivity is given by dashed line.

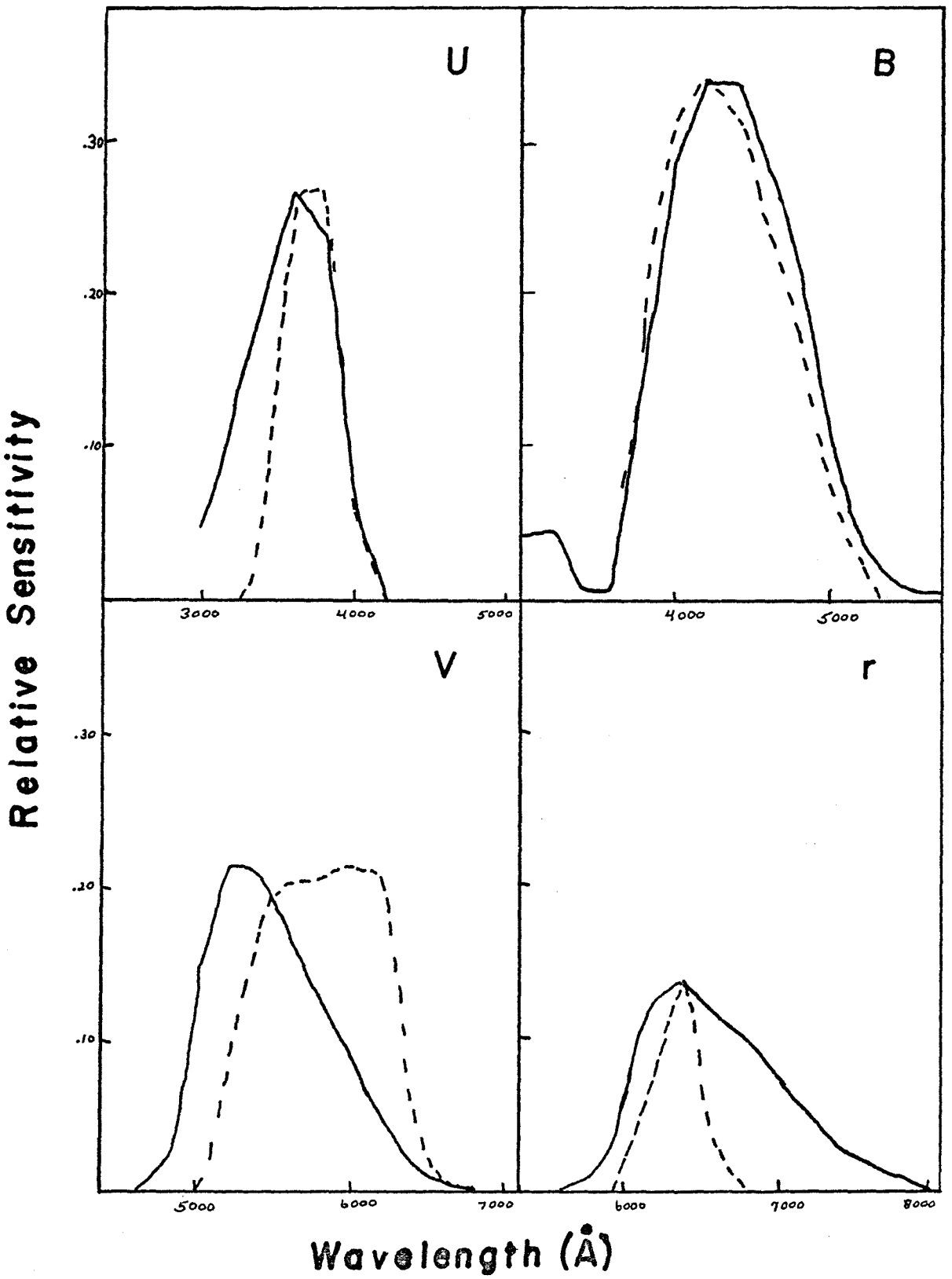
U
B
V
r
.30
.20
.10
3000
4000
5000
6000
7000
8000
Relative Sensitivity
Wavelength (Å)

Schott & Gen., 1962), emulsion sensitivity curves (Kodak, 1948), one reflection from an aluminum coated mirror, and, for U and B, the transmission of the corrector plate of the 48-inch Schmidt telescope (Minkowski and Abell, 1963).

Table 6

Plate-Filter Combinations

Magnitude	Plate + Filter	Exposure
U	103a-O + Schott UG 1	40 minutes
B	103a-O + Schott GG 13	12 minutes
V	103a-D + Wratten 12	12-15 minutes
r	103a-E + RG 1	40-50 minutes

The vertical scale is completely arbitrary. The photographic curves were normalized so that the peak sensitivity is the same as that of the corresponding photoelectric curve. Figure 1 indicates that the photographic reproduction of the B magnitudes is quite satisfactory, the U photographic magnitude does not reach as far into the ultraviolet as the photoelectric values do, the photographic V pass band is shifted to the red of that for the photoelectric magnitudes, and finally, the red photographic magnitude occupies only the blue part of the wavelength band spanned by the photoelectric value. Though some of the differences between the photographic and photoelectric sensitivity are calibrated out, it seems probable that the trouble which

arose for the V-r colors, insensitivity to changes of color as defined by B-V , was due to the fact that the photographic r corresponds to a part of the spectrum almost entirely within the pass band of photographic V. The difficulty with the V-r colors caused them to be entirely discarded, and they will therefore not be discussed in the following sections.

A total of 24 ten-inch plates, 6 each for U, B, V and r, were taken, with exposure times (Table 6) calculated to reach the limiting magnitude in each case. For four of the plates, two each in U and B, measurements of the photoelectric standards indicated the presence of unusually large errors. These plates were eliminated from the study.

Photographic Photometry

All photographic photometry was done with the Sartorius iris photometer of the Hale Observatories. The photometer is equipped with a card punching facility, so that the results of a measuring session can be reduced quickly by computer. In addition to the star name and iris reading, x and y co-ordinates, plate name and date are also punched on the cards. At the beginning and end of each four to six hour session, measurements were made of the photoelectric standards located at the plate center and in the quadrant to be measured, including six stars

near the plate center for which magnitudes and colors were supplied by Dr. Sandage. To determine the amount and direction of any systematic drift in the photometer or electronics, two standard stars, one bright, the other faint, were measured every hour. Because the plates were measured over a period of a year and a half, during which several changes in the electronic equipment were made, it was not possible to reduce all measurements on a plate to a standard system. The results of each measuring session were therefore reduced independently.

All data were reduced on the IBM 360/75 computer at Caltech, using reduction programs written specifically for the purpose. Separate determinations of the system drift during a measuring session were made for the bright and faint drift calibrators. In each case, the change in iris reading was assumed to be a quadratic function of time. Because approximately the same amount of time was required to measure each star, numbers from 1 to n were assigned the n stars measured in each session; and a star's number was assumed to be the "time" at which it was measured. The constants in the drift equation were calculated by fitting least squares solutions to the measurements of the drift calibrators. For a typical measuring session, the drift rate was 1 iris unit per hour, corresponding to approximately .02 magnitude per hour. Corrections from

the bright or faint drift equations, as appropriate, were applied to all measurements of standard and program stars.

For each measuring session, a least squares solution for the magnitude as a function of iris reading, plate distance and color, where necessary, was derived (equation [3]). In equation (3), m is

$$m = aI^2 + bI + fD + gC + h \qquad (3)$$

the magnitude to be determined, I is the iris reading, D the distance from the plate center in millimeters, C the color term, and a, b, f, g and h are constants to be determined. Since the distance of a star from the plate center is independent of the magnitude measuring apparatus, its coefficient, f, was determined from all the plate material. All the photoelectric standards on each plate in each magnitude were measured in one session and used to determine a least squares solution for equation (3) . For each magnitude the coefficients of D derived from all the plates were averaged to determine the value finally adopted, +.00095 mag./mm for U , +.00045 mag./mm for B , and -.00099 mag./mm for V . For stars anywhere on the plate, the absolute value of the distance term is less than .12 mag. in U and V and less than .06 mag. in B .

The constants a , b , g and h were determined from a least squares solution calculated for each measuring

session. For B and V, g was found to be zero within the errors (Figures 2a-b), and was therefore set equal to zero in the final solutions. In the determination of U , C in equation (3) is U-B . The values for B were taken from the photographic photometry of the B plate. The relation between the residuals for U and U-B , shown in Figure 2c, indicates that the color dependence has been adequately taken into account. The calibration equations and dependence of the magnitudes on the iris values alone are shown in Figures 3a-c for typical measuring sessions.

Results

All star-like objects brighter than V = 19 and within an eight-inch square centered on SA 57 , a total of 13,820 stars over an area of 13.5 square degrees, were measured on one plate in each color. These stars will be referred to as the "program stars" in the following discussion. From this material, all stars within 5.11 square degrees of the plate center with B-V greater than .30 and less than .90 and V brighter than 17.50 were selected and measured on the remaining plates. All objects with U-B less than -.5 and B-V less than .8 , indicating possible white dwarfs, QSO's or other objects of interest, were also measured on all remaining plates. The objects measured on all plates will be referred to as the "extended program". Of the 1450 stars originally

Figure 2

Residuals as a function of color for (a) V, (b) B, and (c) U.

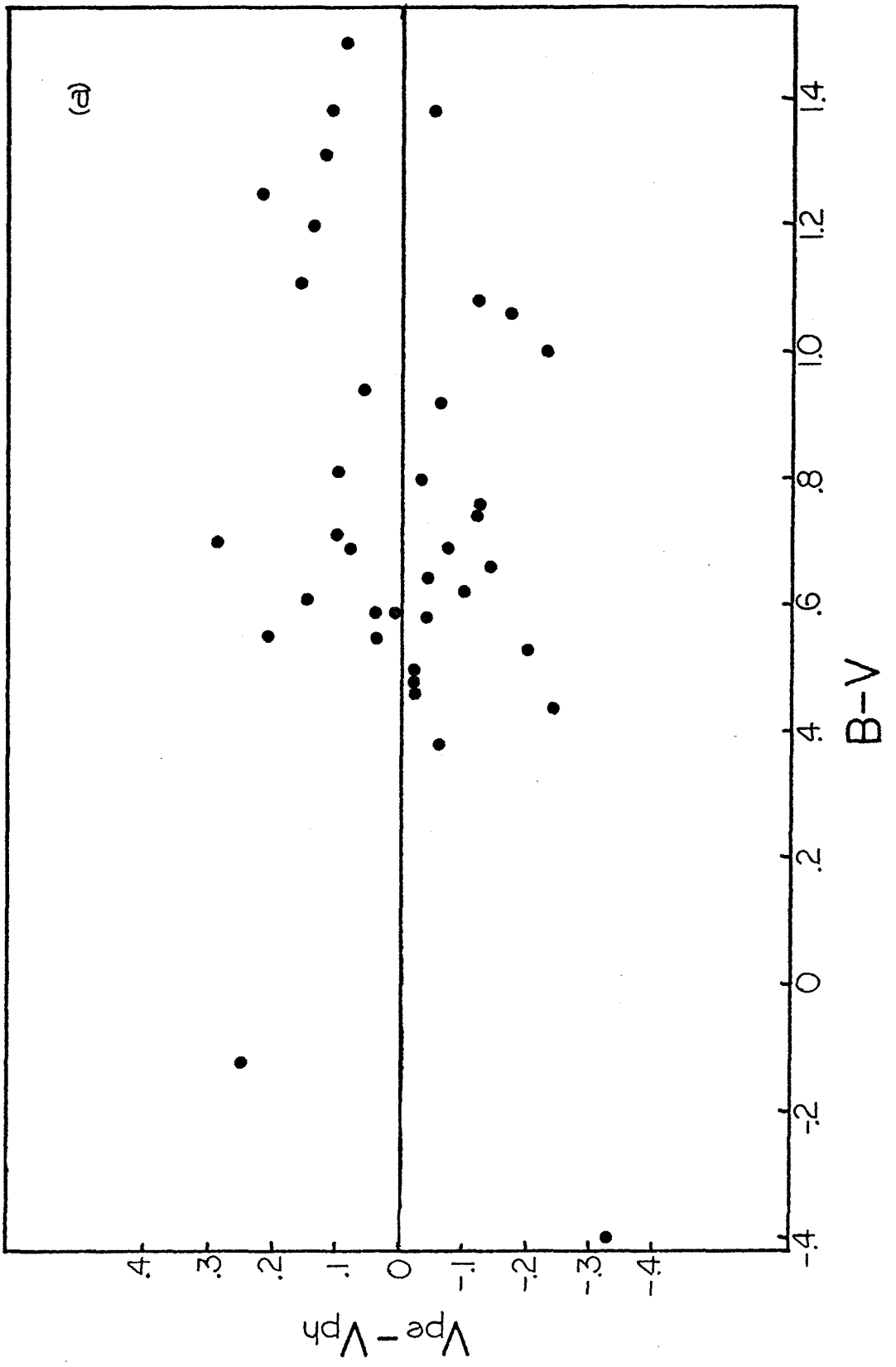
(a)
$V_{pe} - V_{ph}$
B-V
4
3
2
1
0
-1
-2
-3
-4
-4
-2
0
.2
.4
.6
.8
1.0
1.2
1.4

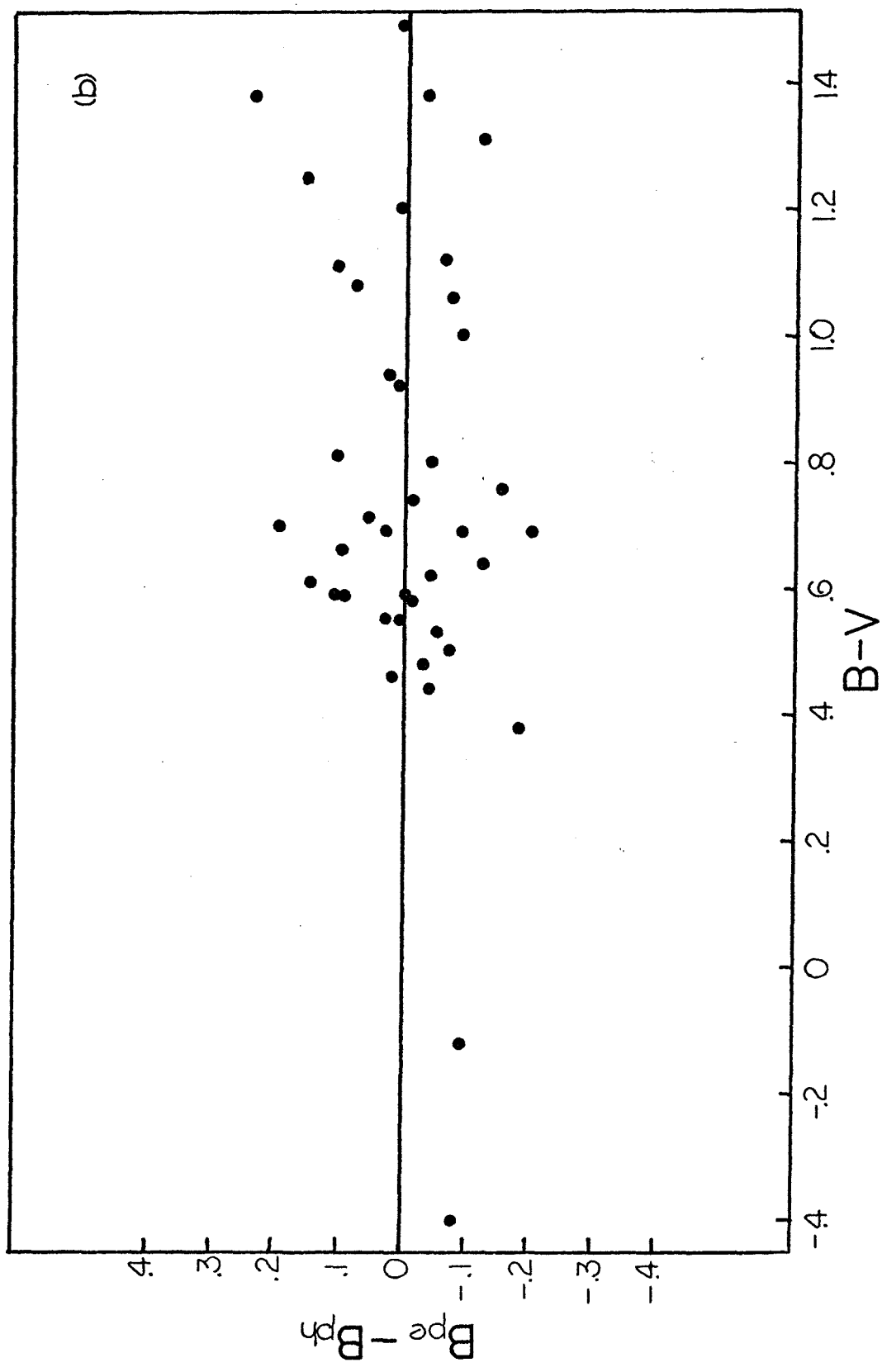
(b)
B-V
$B_{pe} - B_{ph}$
-.4
-.2
0
.2
.4
.6
.8
1.0
1.2
1.4
.4
.3
.2
.1
0
-.1
-.2
-.3
-.4

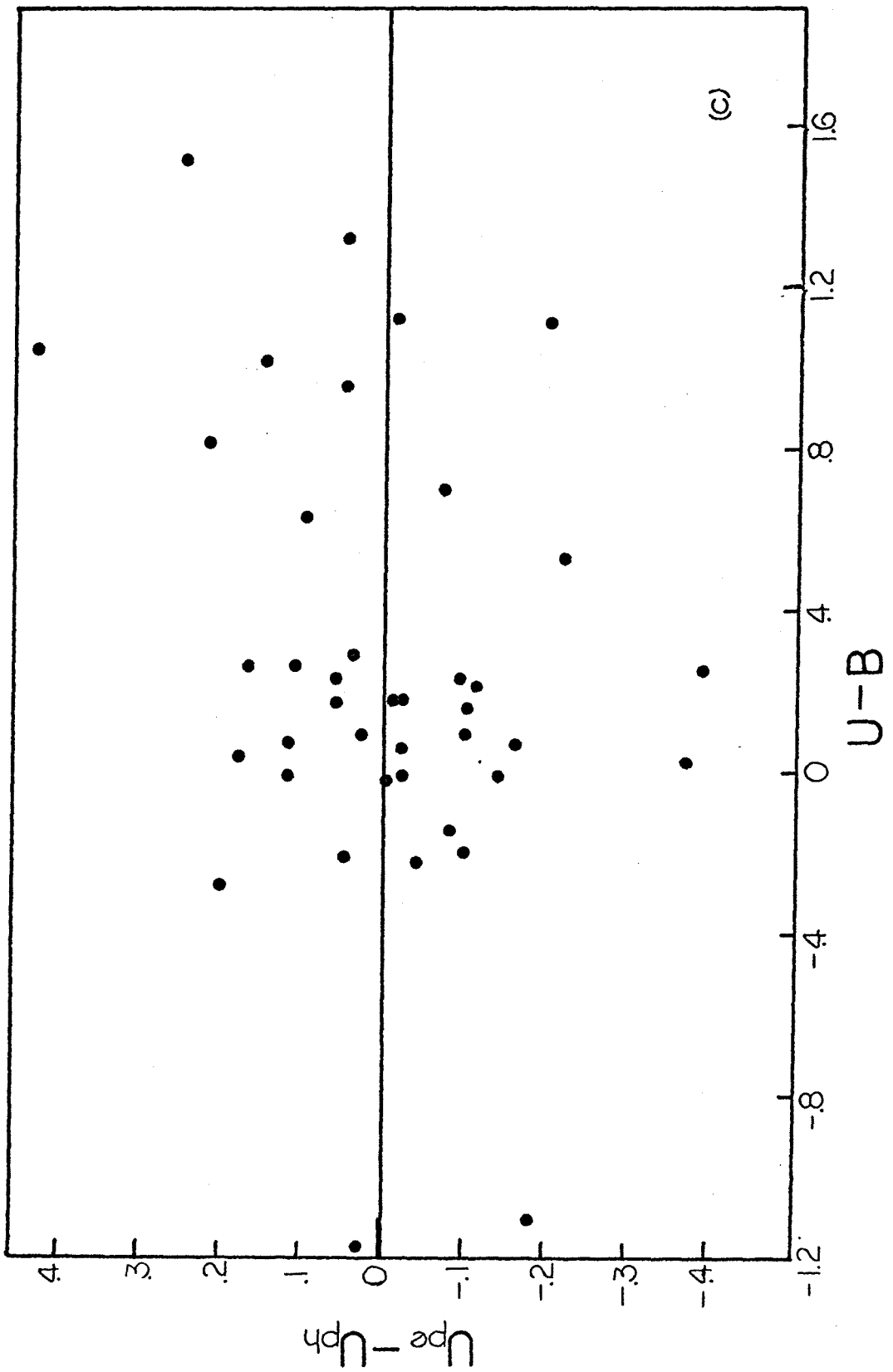
(c)
$U_{pe} - U_{ph}$
U-B
4.
3.
2.
1.
0
-1.
-2.
-3.
-4.
1.6
1.2
.8
.4
0
-.4
-.8
-1.2

Figure 3

Magnitude-iris relations for typical iris photometer measuring sessions. The date of measurement and calibration equation is given for each curve. The dashed lines indicate the changes in the adopted curves necessary to account for the shift in B-V discussed in Chapter III.

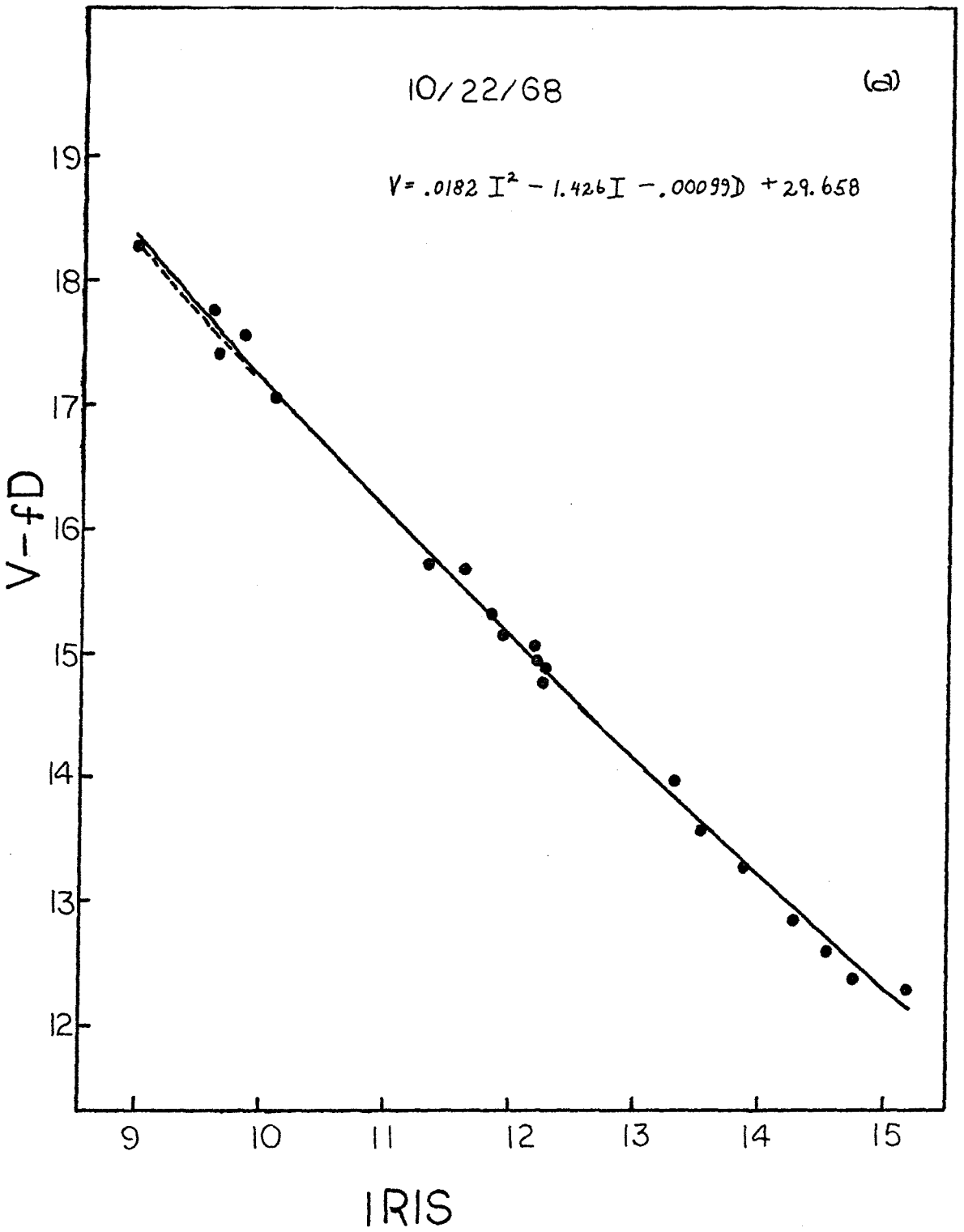
10/22/68
(a)
V = .0182 I² − 1.426 I − .0009 D + 29.658
V−fD
19
18
17
16
15
14
13
12
9
10
11
12
13
14
15
IRIS

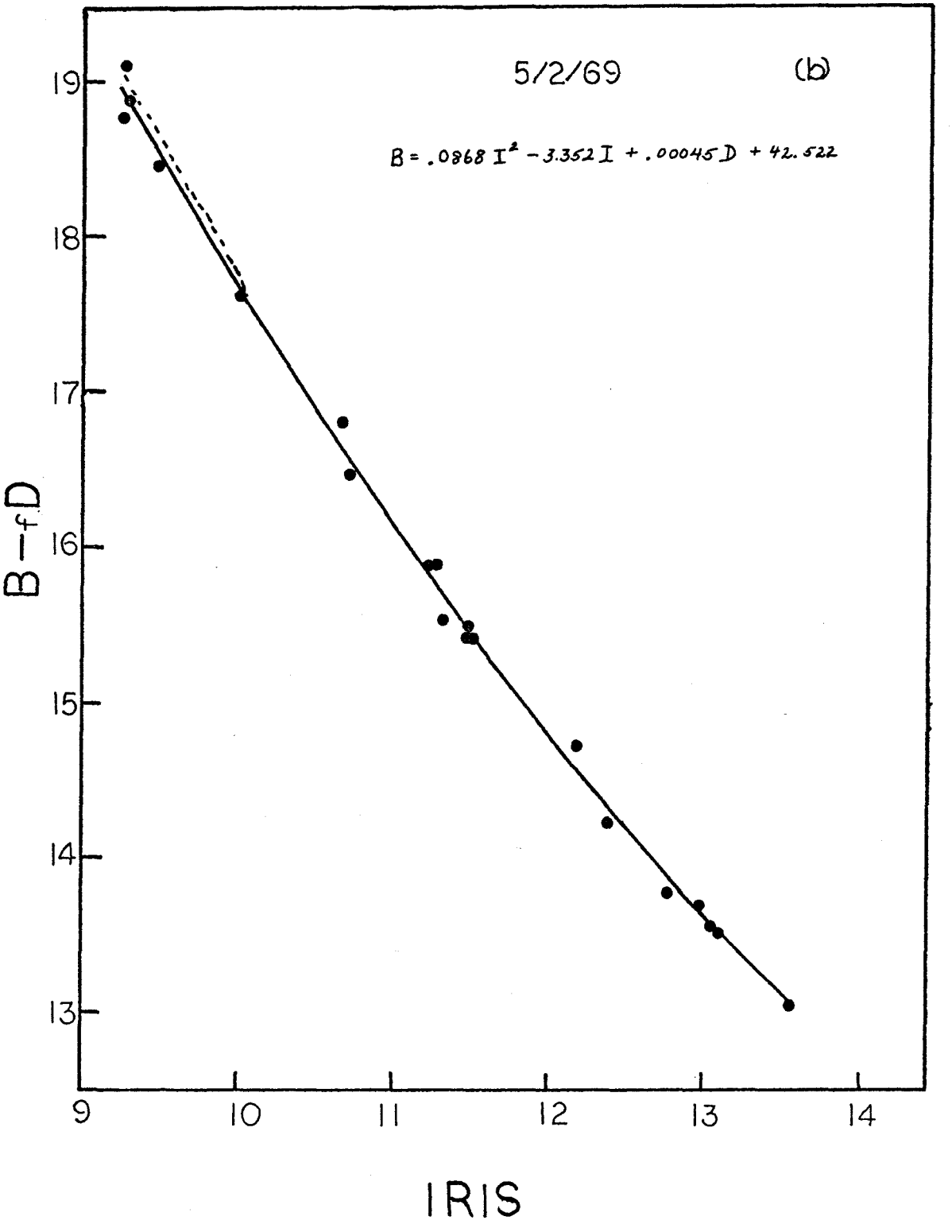
5/2/69
(b)
B = .0868 I² − 3.352 I + .00045 D + 42.522
B − f D
19
18
17
16
15
14
13
9
10
11
12
13
14
IRIS

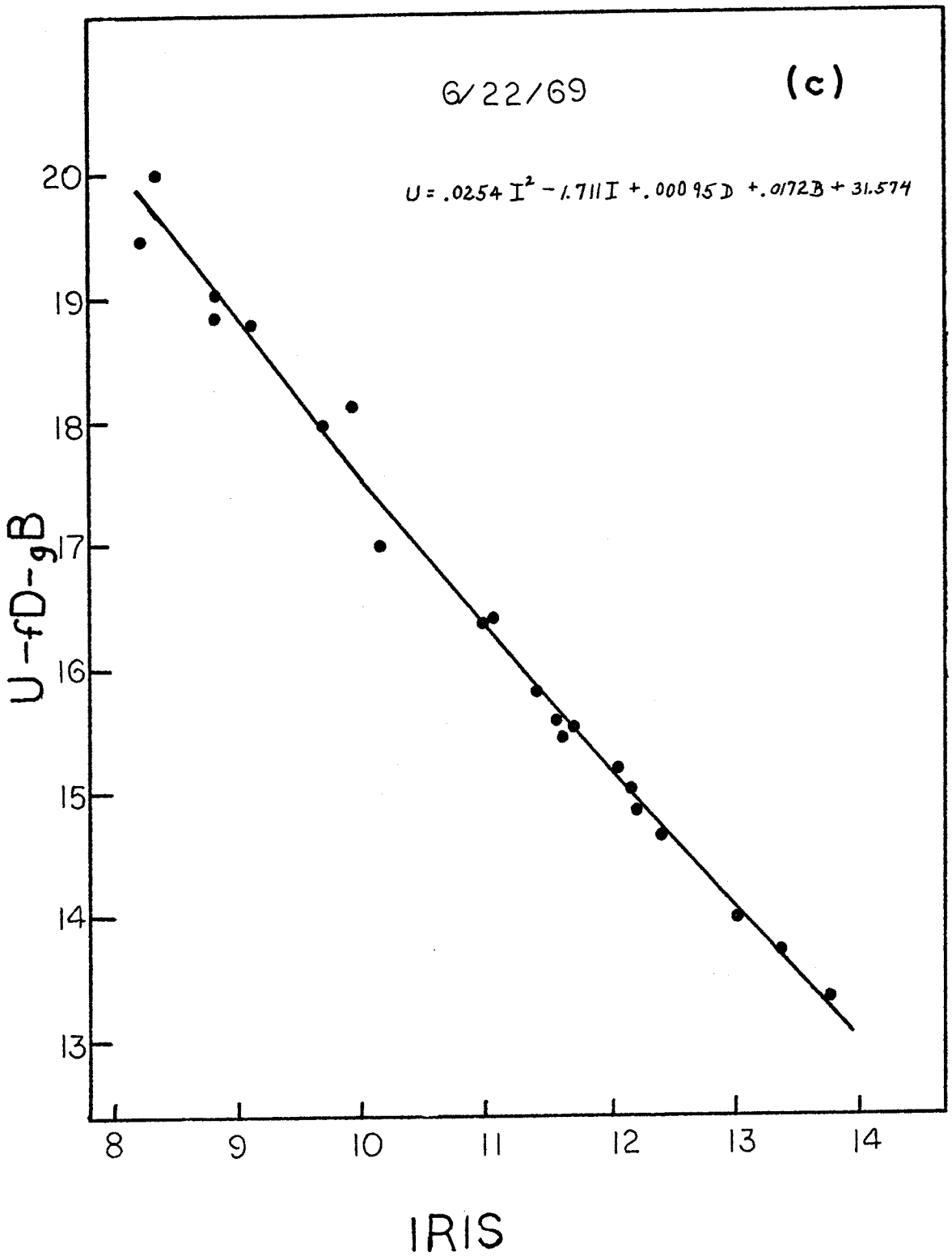
6/22/69
(c)
U = .0254 I² − 1.711 I + .00095 D + .0172 B + 31.574
20
19
18
17
16
15
14
13
U − fD − gB
8
9
10
11
12
13
14
IRIS

so designated, 50 with blended images were eliminated, as the accuracy of the magnitudes would not have been improved by further measurement. All blends, about 400 stars, were measured and included in the analyses based on the data for the program stars, however.

Magnitudes of the program stars were calculated from the iris values, color terms and plate distances, using the calibration equations derived from the standards. The magnitudes of the stars in the extended program were derived independently for each plate and then averaged. The average B magnitudes were used for the color term for U for these stars.

The internal errors, which indicate the internal consistency of the photographic photometry, have been calculated for magnitudes determined from single or multiple measurements, using the data from stars in the extended program (Table 7). The errors are about the same in each color for magnitudes determined from approximately the same number of plates (one or four to six). The external errors, which include the internal errors of the photographic photometry plus errors arising from the calibration of the photographic data with the photoelectric standards, were calculated from the root mean square deviation between photoelectrically and photographically determined magnitudes (Table 7). The single plate values were computed using measurements of the standards from

Table 7

Errors

V	No.Plates	B	No.Plates	U	No.Plates	B-V	No.Plates
				Internal			
.10	1	.11	1	.10	1		
.04	6	.06	4	.05	4		
				External			
.12	1	.10	1	.15	1		
.09	6	.08	4	.16	4		
				Adopted			
.09	6	.08	4	.16	4	.15	1

plates on which the program stars were measured. The errors for a magnitude measured on several plates were computed from the average of the magnitudes of the standards measured on each plate. The external errors determined from several plates do not show the improvement over the single plate errors exhibited by the internal errors, suggesting the presence of systematic errors in the calibration. Examination of the deviations of the photoelectric magnitudes from the calibration curves for several measuring sessions reveals several stars for which the sign and approximate size of the deviations are repeated from session to session. For example, for three typical measuring sessions, the deviations from the calibration curve for the V magnitude of star No. 111 are -.10, -.12 and -.15 mag. Thus, systematic errors appear to be present; in addition to which, the errors are larger than was predicted on the basis of the integration times for the photoelectric observations. The external errors for the U magnitudes are worse than those for B and V whether derived from one or several plates, probably reflecting both the difficulty of obtaining good U photoelectric magnitudes for faint stars, and the difference between the photoelectric and photographic sensitivity curves for U (Figure 1).

Attempts to correct for the effect of errors on

the data were made throughout the data analysis. For these calculations, the errors adopted include the external errors for U , B and V previously discussed and, for B-V , the square root of the sum of the squares of the single plate external errors for B and V , truncated to .15 mag. (Table 7, last section).

Chapter III

Data Analysis

Introduction

Ideally, we would like to derive from the data the density distribution and local density of the Population II stars, as well as the density distribution and luminosity function for the disk population. As will be discussed in the section concerned with Results for U-B and B-V Colors, the Population II density distribution can be derived using the ultraviolet excess as a population discriminant. It will be shown that such an approach is influenced considerably by the presence of errors, and the results are probably no better than density gradients derived from observations of globular clusters, subdwarfs, and other Population II objects (Oort, 1965).

The attempt to derive the Population II density distribution was therefore abandoned, and another approach adopted to calculate the upper limit to the local Population II density. The method, described more completely in the section Maximum Local Population II Density, consists of assuming all observed stars with B-V colors bluer than .5 and V between magnitude 17 and 18 are members of Population II. Assumptions concerning the density distribution and luminosity function for Population II, as well as consideration of the effect of errors on color distributions lead to predictions of the number of Population II stars as

a function of color and apparent magnitude. The distribution is scaled to fit the observed number of blue stars between V = 17 and 18, thus determining the maximum local Population II density.

The number of stars assigned to Population II as a function of apparent magnitude and color is subtracted from the observed star counts, and all remaining stars are assumed to be members of the disk population. An attempt has been made to correct the disk population star counts for the effect of errors in B-V, which distort the observed color distributions (see Correction for Errors in $(B-V)_o$). Estimates of the number of disk members which may be expected to be giants or subgiants have been made, and the numbers subtracted from the disk star counts, leaving what is assumed to be a pure dwarf disk population (see Giants and Subgiants). Dwarf density distributions have been derived as a function of color (see Dwarf Density Distributions) and the results combined to determine a general disk density distribution (Composite Density Distribution). Some evidence is presented indicating the density distribution near the plane for the faintest stars is steeper than was previously thought. New results concerning the disk luminosity function for intrinsically faint stars have also been derived (see Luminosity Functions).

The Equation of Stellar Statistics

Much of the analysis consists of determining density distributions or predicting star counts, both of which may be considered in terms of the equation of stellar statistics (equation [4]). In equation (4),

$$A(m) = \omega \int_0^{\infty} D(z,M)\ z^2\ dz \qquad (4)$$

$$A(m) = \omega \sum_{i=1}^{n} D(z,M_i)\ z^2\ dz \qquad (5)$$

$A(m)$ is the number of stars between apparent magnitudes $m-1/2$ and $m+1/2$, ω is the area of the sky over which the stars were counted (4.11×10^{-3} steradian for this investigation), $D(z,M)$ is the number of stars per cubic parsec with absolute magnitude M at height z above the plane, and z^2dz is the volume element. In this study, $A(m)$ has been observed. Values for the absolute magnitude, M , as a function of color and luminosity class have been adopted from the literature (see following sections). The distance from the galactic plane, z , is determined by $M = m + 5 - 5\log z - a(z)$, where $a(z)$ is the absorption. The dependence of the absorption on distance from the galactic plane, as well as the total amount of absorption present, have also been taken from the literature (see Maximum Local Population II Density). For purposes of computation, the right side of equation (4) will be approximated by a finite series (equation [5]).

Results for U-B and B-V Colors

An attempt was made to determine the density distribution and local density of Population II using the U-B and B-V colors of stars on the extended program. Because the errors in U, B and V are not negligible and the effect on the location of a star in the two-color diagram is complicated, models were constructed and convolved with an error function and the results compared with the observations. Such an approach is better defined than trying to assess the influence of the errors on colors of individual stars.

To construct the models, the Population II luminosity function and color-magnitude relation were assumed to be the same as those for either M 3 or M 92. The reasons for assuming the cluster characteristics to be representative of Population II will be discussed in the next section. The variable parameters in the models are the local Population II density and the Population II density distribution. Four density distributions were considered, based on the assumptions that the density of Population II in the plane varies as R^{-n}, where $n = 3$ or $n = 4$, and that Population II stars are distributed in ellipsoids of constant density with axial ratios 1:1 or 1:2. These assumptions are discussed further in the next section.

Assuming in addition a value for the local Population II density, the number of Population II stars as a function of apparent magnitude and color was predicted, using equation (5) . The predicted Population II distributions were subtracted from the observed distributions of the program stars, which had first been corrected for the effect of the errors in B-V (see Correction for Errors in $(B-V)_o$). All remaining stars were assumed to be members of the disk population.

For each model, 6 two-color diagrams were constructed, 5 for stars with V between 12 and 17 , for intervals of one magnitude, and a sixth for stars with V = 17 to 17.5 . All stars with B-V between .30 and .90 were located in the diagrams. The disk population members were assumed to be located along the Hyades two-color relation. The two-color relation of the appropriate cluster was adopted for Population II.

The effect of the errors on the colors was taken into account in the following way. The error functions in U, B and V were represented by Gaussian functions with sigma equal to the adopted errors listed in the last part of Table 7. The effect of the errors on a given number of stars with errorless magnitudes located at a point in the two-color diagram is to spread the stars along a line of zero slope (error in V) , along a line of infinite slope

(error in U) , and along a line of slope +1 (error in B) . The resulting distribution was calculated exactly from the assumed error functions, and convolved with each of the two-color diagrams constructed for the models.

To compare the model two-color distributions with those derived from stars measured on several plates, the average U-B colors for all stars within certain areas of the two-color diagram were calculated. The areas were those two defined by the blanketing lines which intersect the Hyades two-color relation at B-V = .50, .65 and .80 (Wildey, Burbidge, Sandage and Burbidge, 1962). It was possible to vary either the assumed local Population II density or the density distribution to improve the fit of the model to the observations.

Some of the results of these calculations are shown in Table 8, which presents the average U-B colors for the observations and several models, as a function of V and the area of the two-color diagram over which the stars were averaged. The models are relatively insensitive to the density distribution assumed. For both the M 3 and M 92 models for constant local density, the average U-B for stars brighter than V = 16 hardly changes as the density distribution is changed from that with the steepest (n=4 , 1:2) to that with the gentlest (n=3 , 1:1) slope. The burden of distinguishing between various density distributions falls entirely on the last two

Table 8

Comparison of Average U-B for Models and Observations

$(B-V)_{HY}$	V	12.5	13.5	14.5	15.5	16.5	17.25
				Observed Data			
.50-.65		.19	.17	.12	.08	.03	.01
.65-.80		.20	.14	.08	.09	.02	-.04
		Model M 3, n=4 , 1:2 Local Den. = $2.3 \times 10^{-5}(\eta/L)_{M3}$					
.50-.65		.14	.09	.10	.09	.06	.07
.65-.80		.12	.07	.10	.08	.05	.06
		Model M 3, n= 3, 1:1 Local Den. = $2.3 \times 10^{-5}(\eta/L)_{M3}$					
.50-.65		.14	.09	.10	.08	.04	.04
.65-.80		.12	.07	.10	.08	.03	.02
		Model M 3, n=4 , 1:2 Local Den. = $8.3 \times 10^{-5}(\eta/L)_{M3}$					
.50-.65		.13	.08	.09	.07	.03	.02
.65-.80		.12	.07	.09	.06	.01	.00
		Model M 92, n=4 , 1:2 Local Den. = $4.3 \times 10^{-5}(\eta/L)_{M92}$					
.50-.65		.14	.08	.10	.09	.05	.04
.65-.80		.12	.07	.09	.08	.04	.03
		Model M 92, n=3 , 1:1 Local Den. = $4.3 \times 10^{-5}(\eta/L)_{M92}$					
.50-.65		.13	.08	.08	.07	.02	.00
.65-.80		.12	.06	.08	.06	.00	-.03

magnitude intervals. For M 92 , the match of the average U-B colors for these intervals is not bad for the n=3 , 1:1 case, but the deviation from the observations of the average colors computed for brighter stars are so large as to inspire little confidence in such a model. In fact, for all models, the average U-B calculated for the stars with V less than 15 does not at all adequately represent the observed results, and cannot be made to do so. With such an indication of the errors in the method, the attempt to derive the Population II density distribution using U-B colors was abandoned, and the method described in the next section adopted to determine the maximum local Population II density.

Maximum Local Population II Density

To determine the upper limit to the local density of Population II stars, it is assumed that there are no members of the disk population as far as 5 kpc from the plane of the galaxy. This assumption is supported by the work of Eggen, Lynden-Bell and Sandage (1962) which indicates that all stars with velocities perpendicular to the plane large enough to attain distances of 5 kpc or more from the plane have ultraviolet excesses greater than .2 . Eggen's results for stars with (B-V) between .4 and .8 mag. (1965) indicate that only stars with ultraviolet excesses greater than .15 mag. are present at

distances beyond 1 kpc from the galactic plane. To the extent that the assumption is erroneous, the density of Population II will be overestimated.

As discussed in the preceding section, the density distribution for Population II cannot be reliably derived from the available data. The approach adopted here will be to calculate the maximum local Population II density for several assumed density distributions. The consequences of the various distributions will be considered, and some very tentative conclusions will be drawn concerning which distribution seems most likely (Dwarf Density Distributions). Following Oort (1965), the density in the plane is assumed to vary as R^{-n}, where R is the distance from the galactic center. From the Population II objects presented in Oort's table, a value of n=3 or n=4 seems most likely to represent the density distribution of these objects. It is further assumed that the Population II stars are distributed in ellipsoids of constant density, with axial ratios 1:1 or 1:2 . Thus, four possible density distributions will be considered, n=3, 1:1 ; n=3, 1:2 ; n=4, 1:1 ; n=4, 1:2 .

A reasonable representation of the Population II luminosity function must also be found. The globular clusters are the only available source for such data. Luminosity functions for M 3 (Sandage, 1957a) and M 92 (Hartwick, 1970) have been determined. All

computations were made using the luminosity functions of both clusters (giving eight different models in all), as M 92 is representative of an extremely metal-poor population, while M 3 is only moderately metal-poor (Arp, 1965; Morgan, 1959; and Sandage, 1970).

For both clusters, distance moduli, color excesses, and color magnitude relations were adopted from Sandage (1970). I am grateful to Dr. Sandage for making these data available prior to publication. Using the color-magnitude relation for each cluster, the observed luminosity functions were converted to number of stars as a function of $(B-V)_o$ with separate sequences for giants, subgiants and dwarfs, and normalized to 1.00 at the main sequence turn-off point. (Throughout, $(B-V)_o$ will be used to indicate reddening-free colors, while B-V will indicate colors to which no reddening correction has been applied.) Neither observed luminosity function extends far beyond $(B-V)_o = .70$ for stars on the main sequence, due to the faintness of the stars and the distance of the clusters. The relative luminosity functions derived were extended using the van Rhijn luminosity function (1936) and assuming a shape for the main sequence in the color-magnitude diagram similar to the one found for disk stars (see Dwarf Density Distributions). The precise nature of these assumptions is unimportant, as the number of stars

predicted using them is small. The relative stellar densities as a function of color adopted for M 3 and M 92 are shown in Table 9.

It is difficult to decide which are the best values for reddening and absorption at the North Galactic Pole. While the results of reddening studies indicate color excesses less than .05 mag. in B-V (Philip, 1968; Crawford and Barnes, 1969; Sandage, 1969a; Slettebak, Wright and Graham, 1968; Peterson, 1970; McClure and Crawford, 1971; and others), the results of galaxy counts indicate total absorption of the order $A_B = .5$ mag. towards the North Galactic Pole (Shane and Wirtanen, 1967). These values cannot be reconciled with the generally accepted value of $A/E = 3$. For this investigation we have adopted the following values for the color excesses from Sturch (1966): $E(U-B) = .02$ and $E(B-V) = .03$. These values are also consistent with Peterson's results. Though small compared to the observational errors in the study, these corrections have been taken into account in all analyses, as the effect is systematic.

The total absorption may range from .09 mag. to .47 mag. in V, the former corresponding to a normal value of A/E and the currently accepted values of the color excess, the latter, the observed value from galaxy counts combined with the color excess. For this

Table 9

Relative Luminosity Functions for M 3 and M 92

M 92

$(B-V)_o$	M_V	Rel.No.	$(B-V)_o$	M_V	Rel.No.
	Giants and Subgiants				
1.375	-2.71	.001	.725	6.43	3.081
1.225	-2.36	.002	.775	6.68	2.916
1.175	-2.18	.001	.825	6.96	2.582
1.125	-2.03	.001	.875	7.08	2.149
1.075	-1.83	.002	.925	7.27	3.071
1.025	-1.63	.005	.975	7.52	3.377
.975	-1.43	.002	1.025	7.74	2.920
.925	-1.23	.002	1.075	7.90	2.880
.875	-1.08	.005	1.125	8.10	5.180
.825	-.73	.004	1.175	8.50	12.73
.775	-.60	.010	1.225	9.29	22.16
.725	-.13	.036	1.275	10.12	27.48
.675	.54	.068	1.325	10.94	31.39
.625	1.87	.158	1.375	11.59	29.05
.575	2.87	.202	1.425	12.14	26.89
.525	3.12	.131		Horizontal Branch	
.475	3.31	.118	.625	-.30	.008
.425	3.51	.175	.575	-.13	.008
.375	3.69	.335	.525	.00	.005
	Dwarfs		.475	.17	.004
.375	4.01	1.000	.175	.47	.006
.425	4.45	1.617	.125	.57	.009
.475	4.89	1.643	.075	.67	.014
.525	5.27	1.740	.025	.80	.019
.575	5.59	1.819	-.025	.98	.014
.625	5.87	2.139			
.675	6.15	2.490			

Table 9, Continued

M 3

$(B-V)_o$	M_V	Rel.No.
Giants and Supergiants		
1.475	-2.07	.0003
1.425	-1.97	.0005
1.375	-1.86	.001
1.325	-1.74	.001
1.275	-1.61	.002
1.225	-1.48	.002
1.175	-1.35	.002
1.125	-1.22	.003
1.075	-1.06	.004
1.025	-.87	.005
.975	-.68	.008
.925	-.38	.015
.875	.08	.027
.825	.67	.049
.775	1.42	.086
.725	2.34	.158
.675	3.17	.191
.625	3.38	.094
.575	3.54	.085
.525	3.67	.100
.475	3.81	.097
.425	3.92	.514
Dwarfs		
.425	4.75	1.000
.475	5.17	.791
.525	5.53	.756
.575	5.82	.641
.625	6.07	.626
.675	6.30	.542
.725	6.41	.420
.775	6.60	.429
.825	6.70	.437
.875	6.90	.751
.925	7.10	.464
.975	7.33	.775
1.025	7.55	.702
1.075	7.76	.702
1.125	8.00	1.124
1.175	8.30	2.421
1.225	9.15	4.998
1.275	10.00	5.711
1.325	10.73	6.442
1.375	11.40	7.492
1.425	12.00	6.762
Horizontal Branch		
.475	.75	.011
.425	.79	.005
.175	.80	.008
.125	.85	.016
.075	.91	.019
.025	1.04	.005
-.025	1.22	.001

study, a value of $A_V = .10$ mag. has been adopted. It has been assumed that the distribution of the absorbing material is similar to the distribution of the gas in z (Schmidt, 1957) with a half density height of 100 pc. The extent to which the results depend on the assumed value of A_V will be discussed in Chapter IV. The possibility of variable absorption across the field has been considered in the Appendix.

Given the relative stellar densities per unit volume and relative density distribution, the assumption that no disk stars exist beyond 5 kpc defines the local Population II density. For each Population II model, $A(V, (B-V)_o)$, the number of stars between apparent magnitude V-1/2 and V+1/2 and with color in a .05 mag. interval centered at $(B-V)_o$, was computed for a unit local Population II density using equation (5). $A(17.5, (B-V)_o)$ was then convolved with a Gaussian error function with $\sigma = .15$ mag. in order to simulate the effect of errors in B-V. The predicted Population II distribution was compared with the observed $(B-V)_o$ distribution of stars at magnitude V = 17-18. The assumed value for the local Population II density was adjusted so that all stars with $(B-V)_o$ less than .5 and apparent magnitude between 17 and 18 could be assigned to Population II. In order to avoid the presence of a

clump of stars bluer than $(B-V)_o = .35$ in the remaining disk distribution, it was necessary to shift the observed $(B-V)_o$ distributions. The alternative to this procedure would be to admit the existence of members of the disk population with colors bluer than $(B-V)_o = .35$ at very large distances from the plane, or the existence of some other group of objects to account for the blue stars. The surface densities of other such candidates are all too small. The predicted number of QSO's over the entire area surveyed, down to V=18 , is ten (Sandage and Luyten, 1969). Sandage and Luyten (1967) predict a surface density of one white dwarf per square degree, 13 for the total area surveyed here, down to $B \cong 18$. Using the densities of white dwarfs derived by Eggen (1968b) approximately two white dwarfs with $(B-V)_o$ between .00 and .4 mag. are expected between V = 17 and 18 . The maximum predicted number of QSO's and white dwarfs would have to be increased by at least a factor of five to account for the number of stars bluer than $(B-V)_o = .35$ which are not assigned to Population II. The dashed lines in Figures 3a-b show the changes that would have to be made in the calibration curves (solid lines) to account for the shifts postulated ($\Delta(B-V)_o = .15$ mag. to the red for M 3 and .10 mag. to the red for M 92). Considering the scatter of the points defining the calibration curves, these

changes do not seem unreasonable.

Once the local Population II density required to account for all stars with V between 17 and 18 mag. and bluer than $(B-V)_o = .5$ has been determined, the total Population II counts as a function of apparent magnitude and $(B-V)_o$ for V = 12-18 are predicted. The counts are convolved with the error function described above and subtracted from the observed counts. All remaining stars are assumed to be members of the disk population. The procedure has been followed for all eight Population II models.

Table 10 shows the observed star counts prior to the shift in $(B-V)_o$ for stars between V = 17 and 18 . Figure 4 shows a typical example of the fit made to determine the local density for one of the Population II models. The dots indicate observed star counts while the crosses are those star counts predicted for a unit local density and then shifted in the vertical direction to make the best possible fit. The arrow indicates the size and direction of the shift in $(B-V)_o$. In Table 11, the estimated Population II counts, convolved with the error function are presented for the model using the M 92 luminosity function and n=4 , 1:2 density distribution. Also shown are the stars assigned to the disk population for this model. The appearance of "negative" stars is due to the attempt to get the best fit between Population II and the observations for the blue stars, which results in small residuals of "negative"

Table 10

Star Counts

$(B-V)_o$	V	12.5	13.5	14.5	15.5	16.5	17.5
.025		0	0	0	2	9	14
.075		0	1	2	6	13	29
.125		3	0	4	6	13	34
.175		2	2	5	14	15	49
.225		5	7	7	14	26	56
.275		9	6	14	11	34	74
.325		8	10	18	18	36	79
.375		8	15	48	38	49	90
.425		15	23	48	63	68	85
.475		17	28	48	68	77	91
.525		18	40	59	76	77	87
.575		22	46	69	65	78	101
.625		22	43	41	62	90	77
.675		20	34	65	76	69	77
.725		11	31	61	62	74	77
.775		11	27	51	55	56	88
.825		19	31	45	57	53	55
.875		11	12	41	46	35	68
.925		9	15	31	41	50	67
.975		14	10	20	36	40	52
1.025		5	19	18	28	37	62
1.075		2	10	10	34	39	61
1.125		5	5	7	21	38	58
1.175		3	8	13	14	37	67
1.225		0	11	10	27	25	57
1.275		0	4	18	18	34	63
1.325		1	5	6	20	42	60
1.375		2	4	9	17	38	62
1.425		0	2	8	12	40	80

Table 10, Continued

$(B-V)_o$	V	12.5	13.5	14.5	15.5	16.5	17.5
1.475		0	2	7	25	30	54
1.525		0	4	7	6	37	54
1.575		0	5	6	14	31	54
1.625		2	2	4	18	30	48
1.675		1	0	5	9	24	31
1.725		0	1	2	17	16	29
1.775		0	0	1	11	16	28
1.825		1	0	0	10	7	21
1.875		0	0	0	1	7	20

Figure 4

Fit of predicted Population II star counts (x) to observed star counts (●). Arrow indicates magnitude and direction of shift of $(B-V)_o$ for observed counts. Predicted counts are for model M 92, n = 4, 1:2.

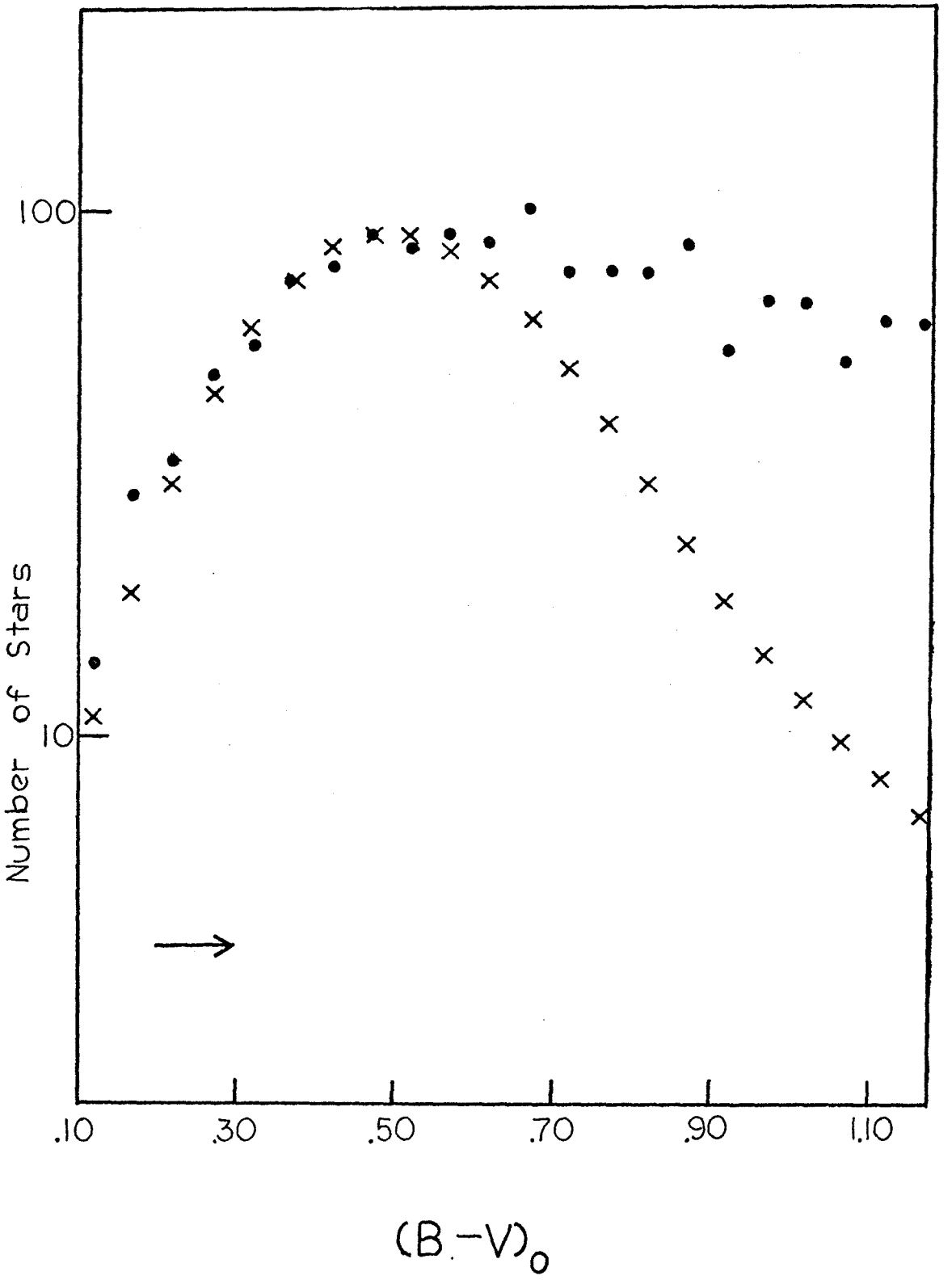
100
10
Number of Stars
.10
.30
.50
.70
.90
1.10
(B-V)o

Table 11

Estimated Population II and Disk Stars for Model M 92, n=4, 1:2

V	12.5		13.5		14.5		15.5		16.5		17.5	
$(B-V)_o$	Disk	Pop.II	Disk	Pop.II	Disk	Pop.II	Disk	Pop.II	Disk	Pop.II	Disk	Pop.II
.025								2	7	2	7	3
.075				1	1	1	4	2	9	4	15	6
.125	3		-1	1	2	2	4	2	7	6	2	12
.175	2		1	1	3	2	11	3	5	10	8	21
.225	5		6	1	5	2	9	5	10	16	1	33
.275	9		5	1	11	3	4	7	11	23	0	49
.325	8		9	1	14	4	9	9	5	31	-10	66
.375	7	1	13	2	43	5	26	12	10	39	-9	83
.425	14	1	21	2	42	6	48	15	24	44	-16	95
.475	16	1	25	3	41	7	51	17	30	47	-11	101
.525	17	1	37	3	51	8	57	19	31	46	-15	100
.575	21	1	43	3	61	8	46	19	35	43	-2	93
.625	21	1	39	4	33	8	44	18	53	37	5	82
.675	19	1	30	4	58	7	59	17	38	31	32	69
.725	10	1	28	3	55	6	48	14	50	24	21	56
.775	10	1	24	3	46	5	43	12	38	18	33	44
.825	18	1	29	2	41	4	48	9	40	13	43	34
.875	10	1	10	2	38	3	39	7	25	10	62	26

Table 11, Continued

V	12.5		13.5		14.5		15.5		16.5		17.5	
$(B-V)_o$	Disk	Pop.II	Disk	Pop.II	Disk	Pop.II	Disk	Pop.II	Disk	Pop.II	Disk	Pop.II
.925	8	1	14	1	29	2	36	5	43	7	35	20
.975	13	1	9	1	19	1	33	3	35	5	52	16
1.025	4	1	18	1	17	1	26	2	33	4	54	13
1.075	2		9	1	9	1	32	2	36	3	41	11
1.125	5		5		7		20	1	36	2	53	9
1.175	3		8		13		13	1	35	2	53	8
1.225	0		11		10		26	1	23	2	52	6
1.275	0		4		18		17	1	33	1	62	5
1.325	1		5		6		20		41	1	53	4
1.375	2		4		9		17		37	1	60	3
1.425	0		2		8		12		40		58	2
1.475	0		2		7		25		30		61	1
1.525	0		4		7		6		37		79	1
1.575	0		5		6		14		31		54	
1.625	2		2		4		18		30		54	
1.675	1				5		9		24		54	

and "positive" stars that sum to zero.

The results for the local density predicted by the eight models, in terms of the mass-luminosity ratio for the corresponding cluster, are given in Table 12. The models likely to be closest to the truth are discussed in the section on Dwarf Density Distributions.

Correction for Errors in $(B-V)_o$

The effect of the errors in $(B-V)_o$ on the disk population data must still be taken into account. The analysis for these errors is the same as that presented for observational errors in the Appendix, leading to the same series solution. Truncating the series and substituting finite differences from the data tables for the differentials of the formal solution, we obtain

$$T(x) = -e \times [O(x-a)] + (1+2e)O(x) - e \times [O(x+a)] \qquad (6)$$

where $T(x)$ is the true function, in this case the number of stars in a $(B-V)_o$ interval centered at x, $O(x)$ is the observed number of stars in the interval, a is the size of the interval, σ is the mean error in $(B-V)_o$, and $e = \sigma^2/2a^2$. For the analysis done here, $(B-V)_o$ intervals of .05 mag. were used with σ = .15 mag., giving $e = 4.5$. To eliminate spurious fluctuations, the deconvolved function was smoothed by successively averaging

Table 12

Local Population II Density

	Model		D(o) ($\mathcal{M}_\odot/pc^3$)
M 92	1:1	n=3	$3.0 \times 10^{-5} (\mathcal{M}/L)_{M92}$
		n=4	3.8×10^{-5} "
	1:2	n=3	6.8×10^{-5} "
		n=4	9.8×10^{-5} "
M 3	1:1	n=3	$3.2 \times 10^{-5} (\mathcal{M}/L)_{M3}$
		n=4	4.4×10^{-5} "
	1:2	n=3	8.0×10^{-5} "
		n=4	1.1×10^{-4} "

series of three points, i.e. $S(x) = [T(x-.05) + T(x) + T(x+.05)]/3$. The smoothed function was then reconvolved with a Gaussian function with $\sigma = .15$ and the result compared with the original function, $O(x)$. The comparisons showed no significant deviations of reconvolved $S(x)$ from $O(x)$.

The deconvolution procedure was applied to the stars determined to be members of the disk population for each of the eight Population II models considered above and a ninth model, for which the local Population II density was assumed to be zero. The colors of the stars in the ninth model were not shifted in any way. For each model the deconvolution was performed for the $(B-V)_o$ distribution of all stars between apparent magnitude 12 and 18 in intervals of one magnitude. The results of the deconvolution of the disk star counts for model M 92, n=4, 1:2 are shown in Table 13. Because of inherent uncertainties in the deconvolution, the analysis of the disk population has been performed for intervals of .10 mag. in $(B-V)_o$, as opposed to the .05 mag. intervals used in the Population II analysis. The analysis was conducted using the smoothed deconvolved functions for the six apparent magnitude intervals of each model.

Table 13

Deconvolved Disk Star Counts for Model M 92, n=4, 1:2

V	12.5	13.5	14.5	15.5	16.5	17.5
$(B-V)_o$						
.05	-1	-2	-2	-2	8	14
.15	2	-4	-2	7	14	34
.25	8	3	-1	7	3	3
.35	15	9	53	-9	2	-41
.45	29	44	101	117	64	-39
.55	50	111	115	126	76	-32
.65	47	87	111	121	102	21
.75	33	49	103	114	88	74
.85	22	34	87	84	71	106
.95	13	16	54	68	78	104
1.05	6	17	19	56	76	106
1.15	2	19	16	40	69	111
1.25	0	17	17	31	67	113
1.35	1	12	16	31	69	119
1.45	2	8	14	32	66	122
1.55	1	3	12	30	66	136
1.65	1	0	9	25	58	122

Giants

Before the dwarf density functions can be derived, some estimate of the number of giants included in the star counts must be made. Absolute magnitudes for the giants, assumed to be luminosity class III, were taken from Blaauw (1963). Since these are given as a function of spectral type, the relation between color and spectral type for giants had to be determined. This was done by plotting spectral type against B-V for all luminosity class III stars in the Catalogue of Bright Stars (Hoffleit, 1964, hereinafter referred to as BSC) for which the required data were available. The resulting relation agrees quite satisfactorily with that given by Johnson and Morgan (1953) for giants. Using these data, a graph of absolute magnitude as a function of B-V was plotted, and the magnitudes at the required colors were read from it. The finally adopted M_V-(B-V) relation for the giants is shown in Table 14. Since the giants in the BSC are all relatively nearby, the color excesses, if present, must be negligibly small. Therefore, B-V is considered equivalent to $(B-V)_o$ and is so indicated in Table 14.

The magnitudes have been derived from stars selected according to apparent magnitude. For the estimate of the number of giants, magnitudes of stars selected per unit volume of space are required. The two types of mag-

Table 14

Absolute Magnitude Calibration and
Relative Color Distribution for
Giants and Subgiants

$(B-V)_o$	M_V	Rel.No.
	Subgiants	
.55	3.00	.08
.65	3.50	.19
.75	3.50	.17
.85	3.50	.08
	Giants	
.95	.60	.26
1.05	.80	.30
1.15	.80	.23
1.25	.50	.08
1.35	.00	.04
1.45	-.20	.04
1.55	-.30	.04
1.65	-.40	.01

nitudes are related by

$$M_m = M_o - \frac{\sigma^2}{\text{Mod}} \frac{d\log A(m)}{dm} \qquad (7)$$

where M_m is the absolute magnitude for stars selected by apparent magnitude; M_o, the absolute magnitude for stars selected per unit volume; A(m), the number of stars at m; and σ, the dispersion of the absolute magnitudes around M_o (Malmquist, 1936).

A value of .60 mag. was adopted for σ, determined by fitting Gaussians to the luminosity functions of late G and early K giants as determined by Halliday (1955) and Sandage (1957b). A value of .2 was adopted for d log A(m)/dm, from the star counts of the present study.

The color distribution of the giants was determined by counting the number of luminosity class III stars in the BSC in B-V intervals of .10 mag. from B-V = .90 to 1.70. Using the absolute magnitudes adopted above, these numbers were corrected for the effect of the limiting magnitude of the BSC, which is to alter the volume surveyed for each type of star as a function of its absolute magnitude. The corrected counts were then normalized to 1.00. The adopted relative number of giants as a function of color is shown in Table 14. For the relative density distribution of the giants, an exponential

approximation to Oort's curve for K giants (1960) was adopted (Figure 5).

Using the above values and a total absorption in V of .10 mag., the number of K giants between V = 11 and 12 was estimated. From Oort and Hill (1960), the number of K giants per magnitude at V = 11.5 is approximately 25 for 13.5 square degrees. The number of K giants calculated for V = 11-12 was therefore normalized to 25 ; and, using this normalization factor, the number of giants as a function of $(B-V)_o$ and V for V = 12-18 was estimated (Table 15) . The calculated number of giants was subtracted from the star counts in the corresponding $V-(B-V)_o$ intervals.

Subgiants

Estimates of the effect of subgiants on the counts are more difficult, as much less is known about the distribution and total number of these stars. The best source of information for subgiants at the present time is the old galactic clusters. In the following calculation data from NGC 6791 (Kinman, 1965) , M 67 (Johnson and Sandage, 1955 ; and Eggen and Sandage, 1964), and NGC 188 (Sandage, 1962; and Eggen and Sandage, 1969) are used. The absolute magnitudes of the subgiants are determined by taking the mean of the absolute magnitudes for the subgiants in each cluster at the $(B-V)_o$ interval

Figure 5

Relative density distribution adopted for disk giants (solid line). Oort's curve for K giants (1960) is shown for comparison (dashed line).

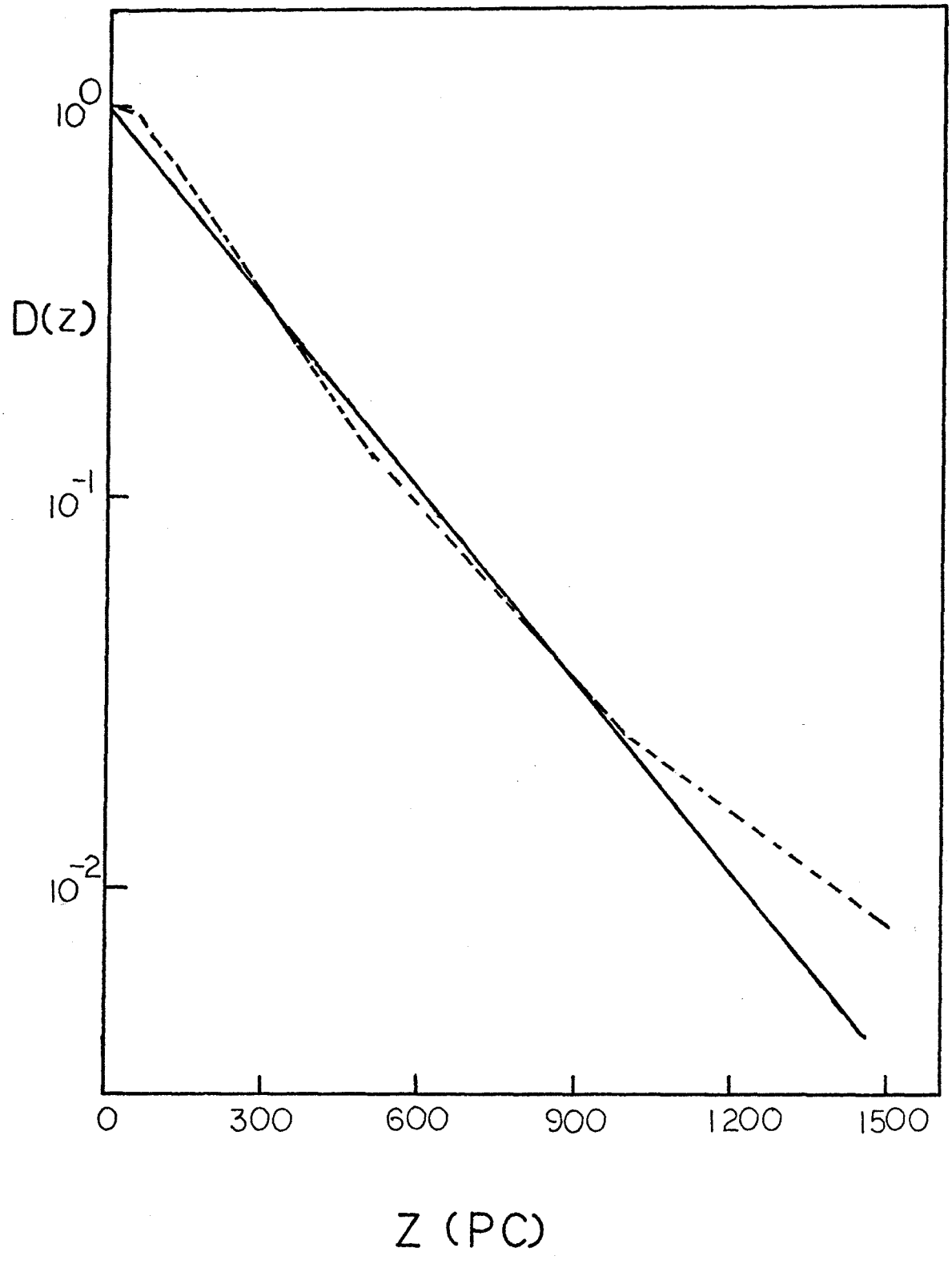
10^0
D(z)
10^{-1}
10^{-2}
0
300
600
900
1200
1500
Z (PC)

Table 15

Estimated Number of Giants and Subgiants

		Giants					
	V	12.5	13.5	14.5	15.5	16.5	17.5
$(B-V)_o$							
.95		1.8	.1	-	-	-	-
1.05		3.3	.2	-	-	-	-
1.15		2.5	.1	-	-	-	-
1.25		.5	-	-	-	-	-
1.35		-	-	-	-	-	-
1.45		-	-	-	-	-	-
1.55		-	-	-	-	-	-
1.65		-	-	-	-	-	-
		Subgiants					
.55		6.9	8.4	9.4	2.0	.1	-
.65		15.2	18.6	21.8	13.2	1.1	-
.75		13.6	16.6	19.6	11.8	1.0	-
.85		6.4	7.8	9.2	5.6	.5	-

of interest, weighted according to number. Because of the uncertainty involved, these values are then rounded to the nearest .25 mag. The magnitudes so derived correspond to magnitudes for stars selected per volume of space and therefore need not be corrected as the giant absolute magnitudes were.

Stellar evolution studies indicate that subgiants come from that part of the main sequence just above the current turn-off point. It therefore seems reasonable to relate the number of subgiants to the number of stars still on the main sequence but close to the turn-off point. The number of subgiants per $(B-V)_o$ interval relative to the number of dwarfs was determined by summing the total number of subgiants for the clusters in each interval, and dividing by the total number of dwarfs with $(B-V)_o = .6-.7$. The adopted relative number of subgiants, as well as the absolute magnitudes, are shown in Table 14. The relative density distribution of the subgiants was assumed to be similar to that for the dwarfs with $(B-V)_o = .6-.7$.

To estimate the number of subgiants an iterative technique was used. As a first approximation, all the stars between $(B-V)_o = .6$ and $.7$ assigned to the disk population were assumed to be dwarfs. The density distribution of these was then derived as described below. With the density distribution, extrapolated where necessary, and

the relative numbers of subgiants and absolute magnitudes, the number of subgiants with $(B-V)_o$ = .6-.7 was estimated using equation (5). These numbers were then subtracted from the total number of stars at the appropriate V and $(B-V)_o$ = .6-.7 and the remaining stars used to determine a new dwarf density distribution. The procedure was iterated until the newly calculated dwarf distribution was the same as the assumed one. Five iterations are generally sufficient to obtain convergence. Once the dwarf density distribution has been determined, the number of subgiants in each $(B-V)_o$ interval and at each apparent magnitude is estimated. Typical estimates of the number of subgiants calculated are shown in Table 15. The estimated number of subgiants is subtracted from the star counts in the corresponding color-magnitude interval. The remaining stars are all assumed to be dwarfs.

Dwarf Density Distributions

The absolute magnitude calibration for the dwarfs bluer than $(B-V)_o$ = 1.40 was adopted from Blaauw, using the relation between color and spectral type given by Johnson and Morgan (1953). For stars redder than $(B-V)_o$ = 1.40 , the absolute magnitudes were determined from data given by Eggen (1968a) by averaging the absolute magnitudes for all stars with $(B-V)_o$ within .10 mag. intervals. The color-magnitude diagram for Eggen's data is shown in

Figure 6, together with the adopted color-magnitude relation. The absolute magnitude calibration for all dwarfs is given in Table 16. These magnitudes, like those for the giants previously discussed, are for stars selected according to apparent magnitude.

Using the data given by Gliese (1956), an absolute magnitude dispersion of .30 mag. was adopted for all stars bluer than $(B-V)_o = 1.40$. This result is a mean of the values found by Gliese for single and double stars and for stars with various space velocities, weighted according to the number of stars in each group. An absolute magnitude dispersion of .75 mag. was assumed for stars redder than $(B-V)_o = 1.40$. The value is an estimate based on the change in absolute magnitude over an interval of .10 mag. in $(B-V)_o$ for these colors and the scatter in the color-magnitude relation for the stars used to calibrate the absolute magnitudes (Figure 6). The two effects are of approximately equal importance.

Individual density distributions were calculated using equation (5) for stars in intervals of .10 mag. in $(B-V)_o$ for $(B-V)_o = .40\text{-}1.70$. The absolute magnitude distribution was assumed to be Gaussian, centered at corrected absolute magnitude, M_o , and with dispersion .30 mag. or .75 mag., as specified above. The first approximation to the density distribution was made by assuming all

Figure 6

Absolute magnitude calibration for stars redder than $(B-V)_o = 1.40$.

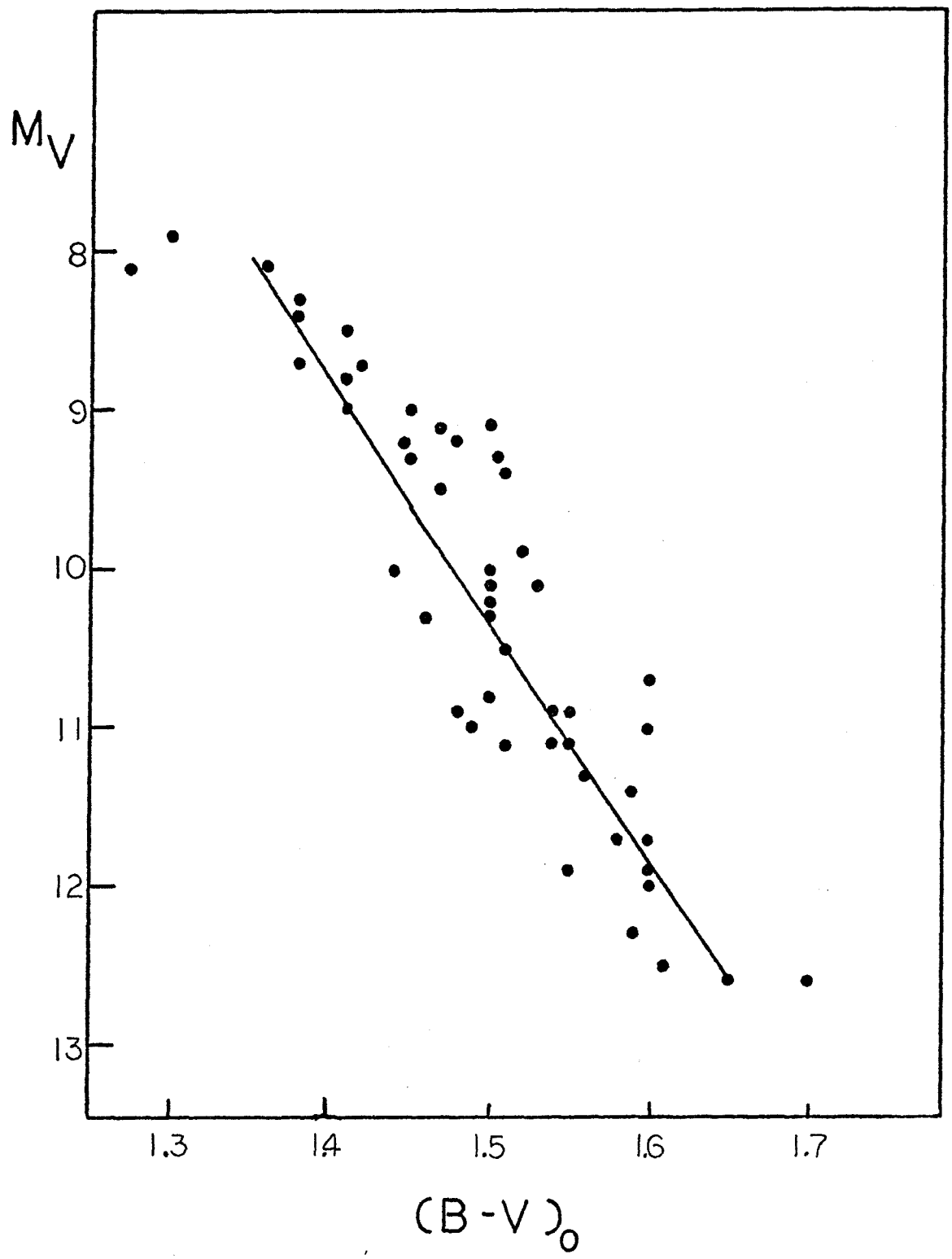
M_V
8
9
10
11
12
13
1.3
1.4
1.5
1.6
1.7
$(B-V)_0$

Table 16

Absolute Magnitude Calibration for

Disk Dwarfs

$(B-V)_o$	M_V	$(\Delta M)^{-1}$
.45	3.30	1.43
.55	4.05	1.25
.65	4.80	1.43
.75	5.60	1.67
.85	6.00	2.50
.95	6.35	2.50
1.05	6.65	3.33
1.15	7.05	2.50
1.25	7.50	2.00
1.35	8.10	.91
1.45	9.60	.56
1.55	11.10	.71
1.65	12.60	.71

dwarfs have absolute magnitude M_o , deriving the volume corresponding to the apparent magnitude, and dividing the number of dwarfs by the volume. Using this distribution, the number of stars, $A(m,(B-V)_o)$, was predicted using equation (5) and compared with the "observed" number, which has in fact been deconvolved and corrected for giants and subgiants as previously described. The density distribution was corrected by the ratio of the observed counts to the computed counts at each apparent magnitude, and the iterations continued until convergence was attained. For most intervals, the result converged within 10 iterations, though 15 were necessary for some of the redder colors. In most cases, the agreement between computed and observed counts was well within the square root of the counts, the poorer results coming for intervals containing few stars or which formally contain "negative" stars due to the subtraction of the Population II contribution.

The individual density distributions were derived for the numbers of dwarfs predicted by each of the Population II models. The results for $(B-V)_o$ intervals .45 to .85 are shown for each of the models in Figures 7a to 7i . The most striking feature of the diagrams is the difference in internal consistency between the models for M 3 and M 92 . We would expect the individual D(z) curves to behave similarly, with the exception of a possible scale

Figure 7

Density distributions for disk dwarfs calculated for various Population II models. Individual curves are shown for $(B-V)_o$ = .4-.5 (●), .5-.6 (x), .6-.7 (△), .7-.8 (□), and .8-.9 (o).

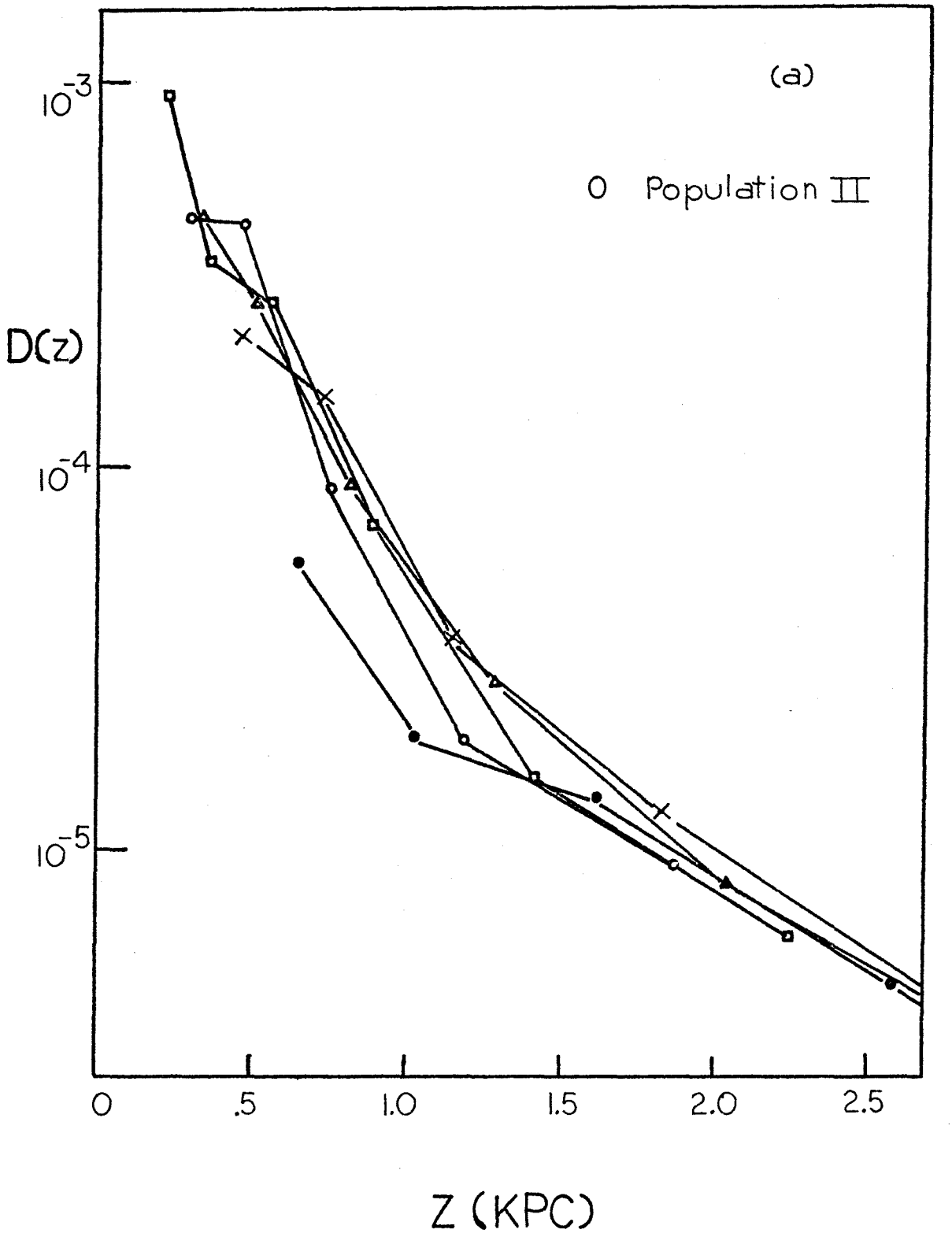
(a)
O Population II
D(z)
10^{-3}
10^{-4}
10^{-5}
0
.5
1.0
1.5
2.0
2.5
Z (KPC)

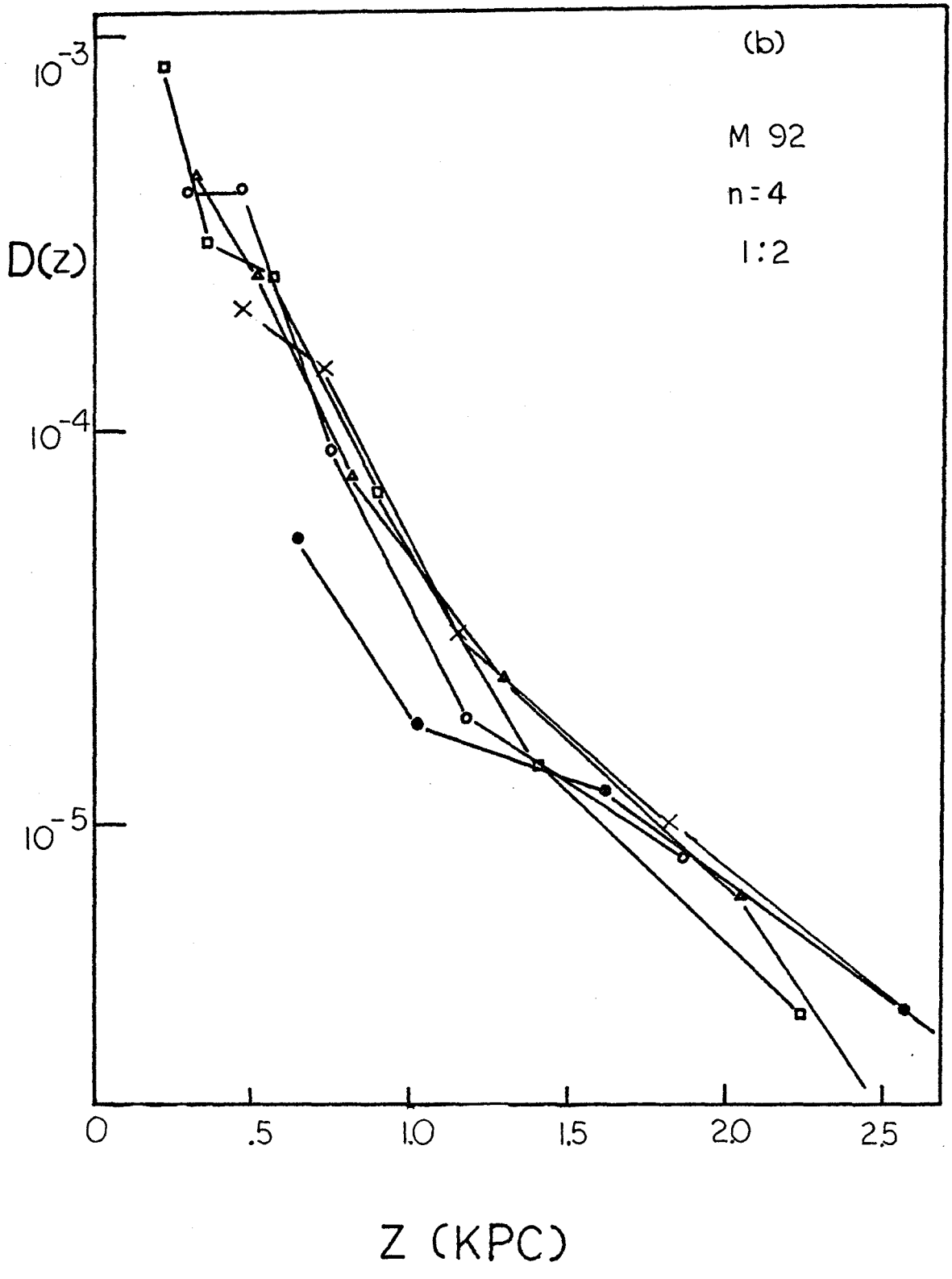
(b)
M 92
n=4
1:2
D(z)
10^{-3}
10^{-4}
10^{-5}
0
.5
1.0
1.5
2.0
2.5
Z (KPC)

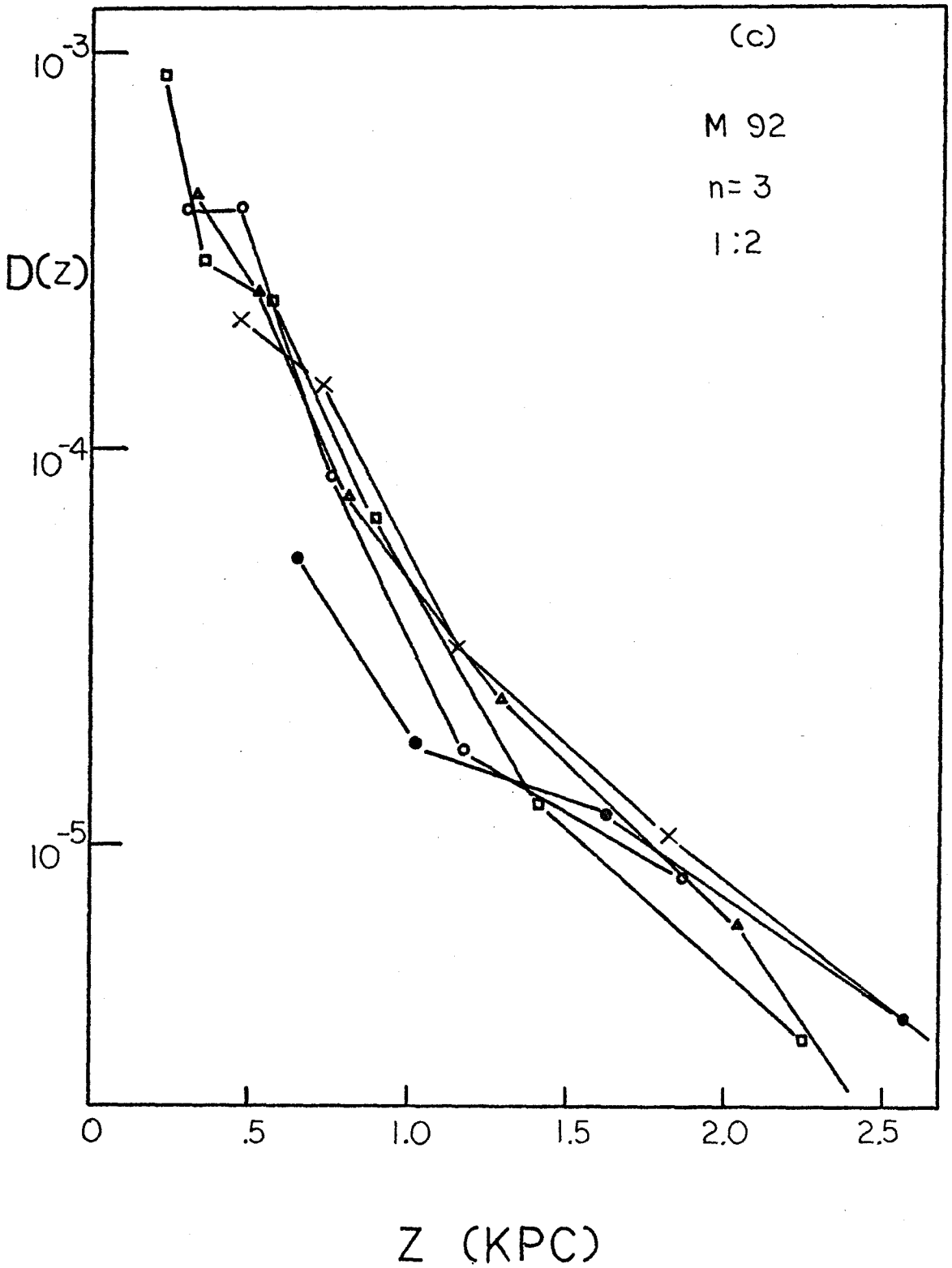
(c)
M 92
n= 3
1:2
D(z)
10^{-3}
10^{-4}
10^{-5}
0
.5
1.0
1.5
2.0
2.5
Z (KPC)

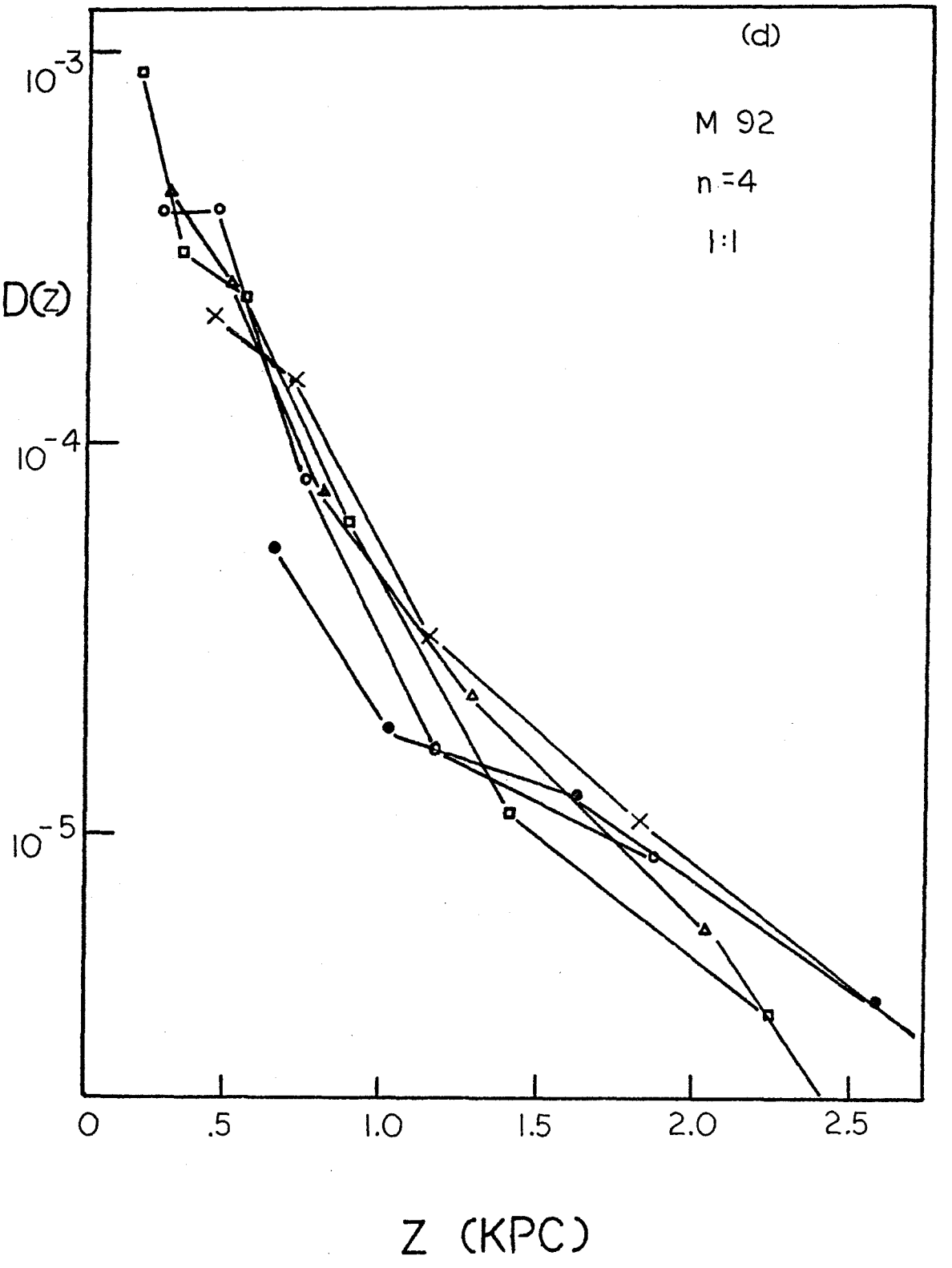
(d)
M 92
n=4
1:1
D(z)
10^{-3}
10^{-4}
10^{-5}
0
.5
1.0
1.5
2.0
2.5
Z (KPC)

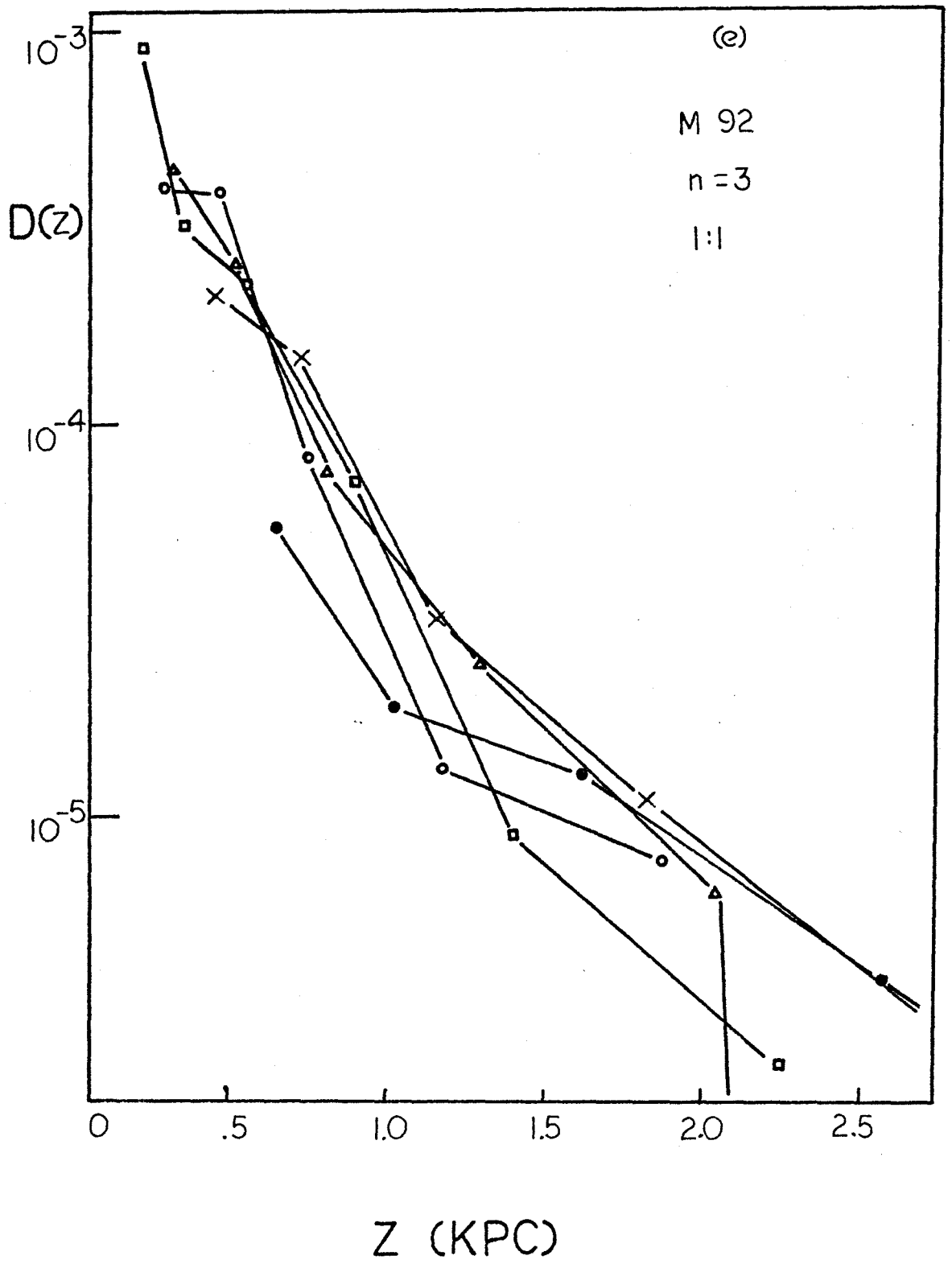
(e)
M 92
n = 3
1:1
D(z)
10^{-3}
10^{-4}
10^{-5}
0
.5
1.0
1.5
2.0
2.5
Z (KPC)

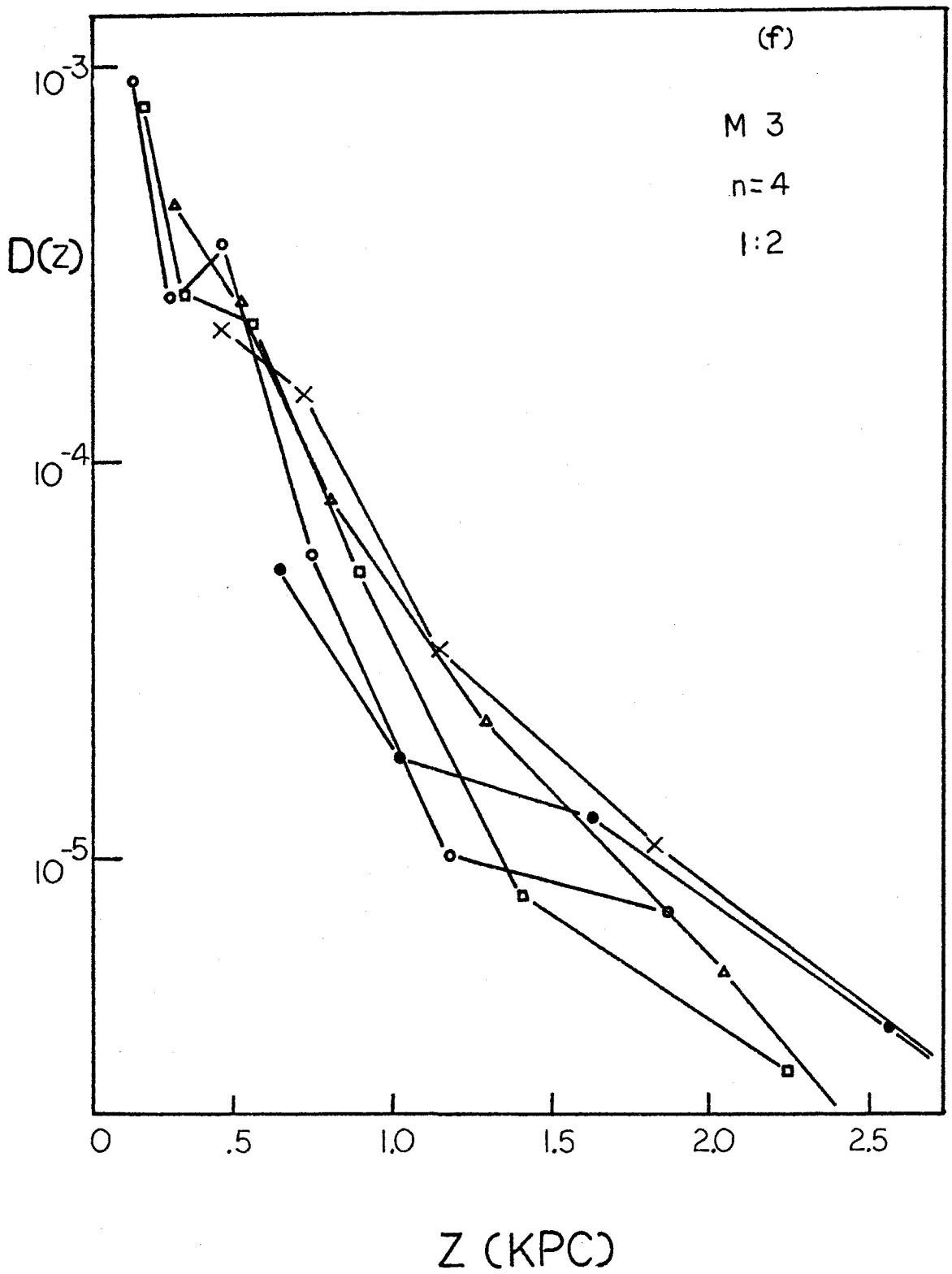
(f)
M 3
n=4
1:2
D(z)
10^{-3}
10^{-4}
10^{-5}
0
.5
1.0
1.5
2.0
2.5
Z (KPC)

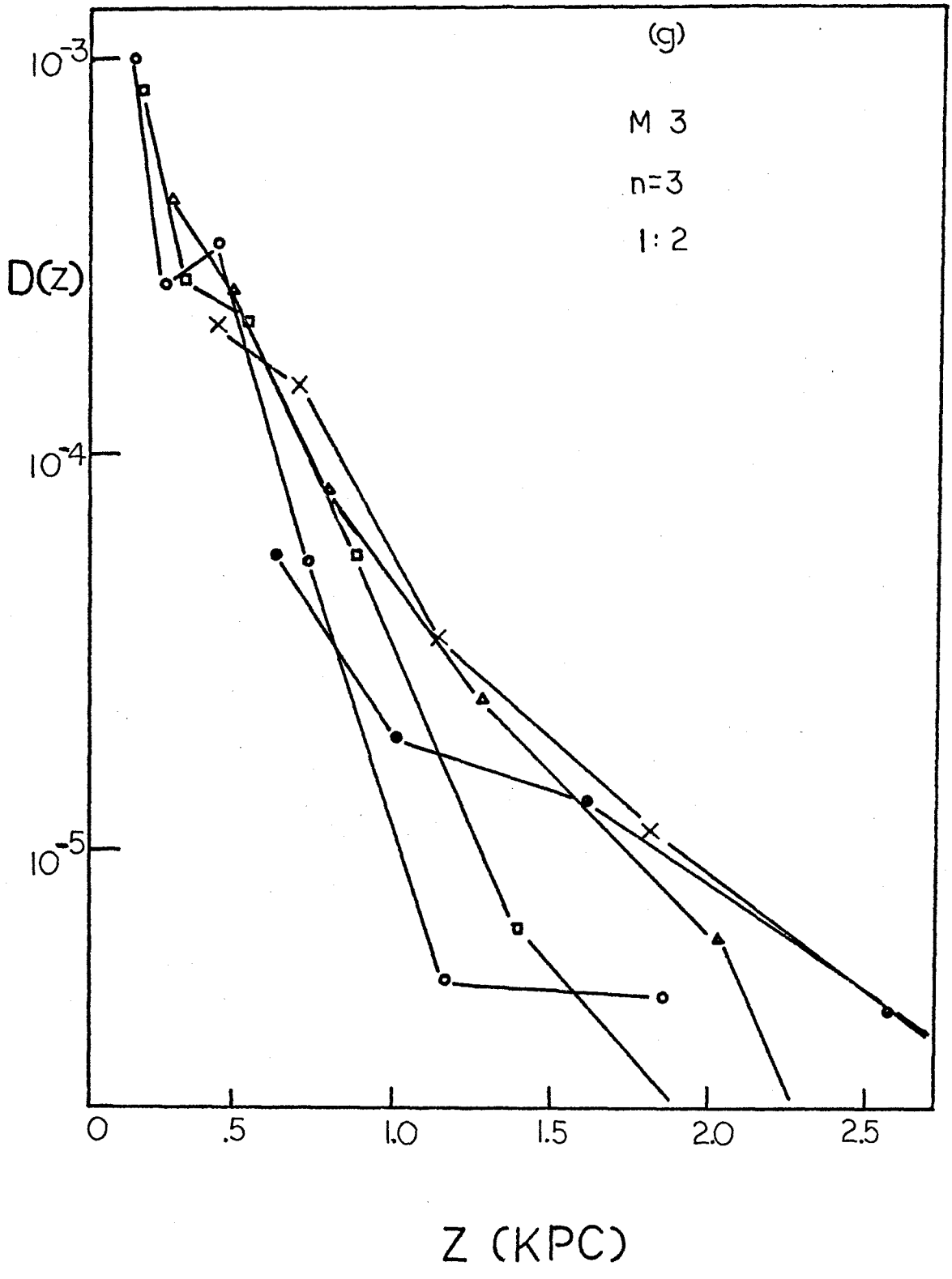
(g)
M 3
n=3
1:2
D(Z)
10^{-3}
10^{-4}
10^{-5}
0
.5
1.0
1.5
2.0
2.5
Z (KPC)

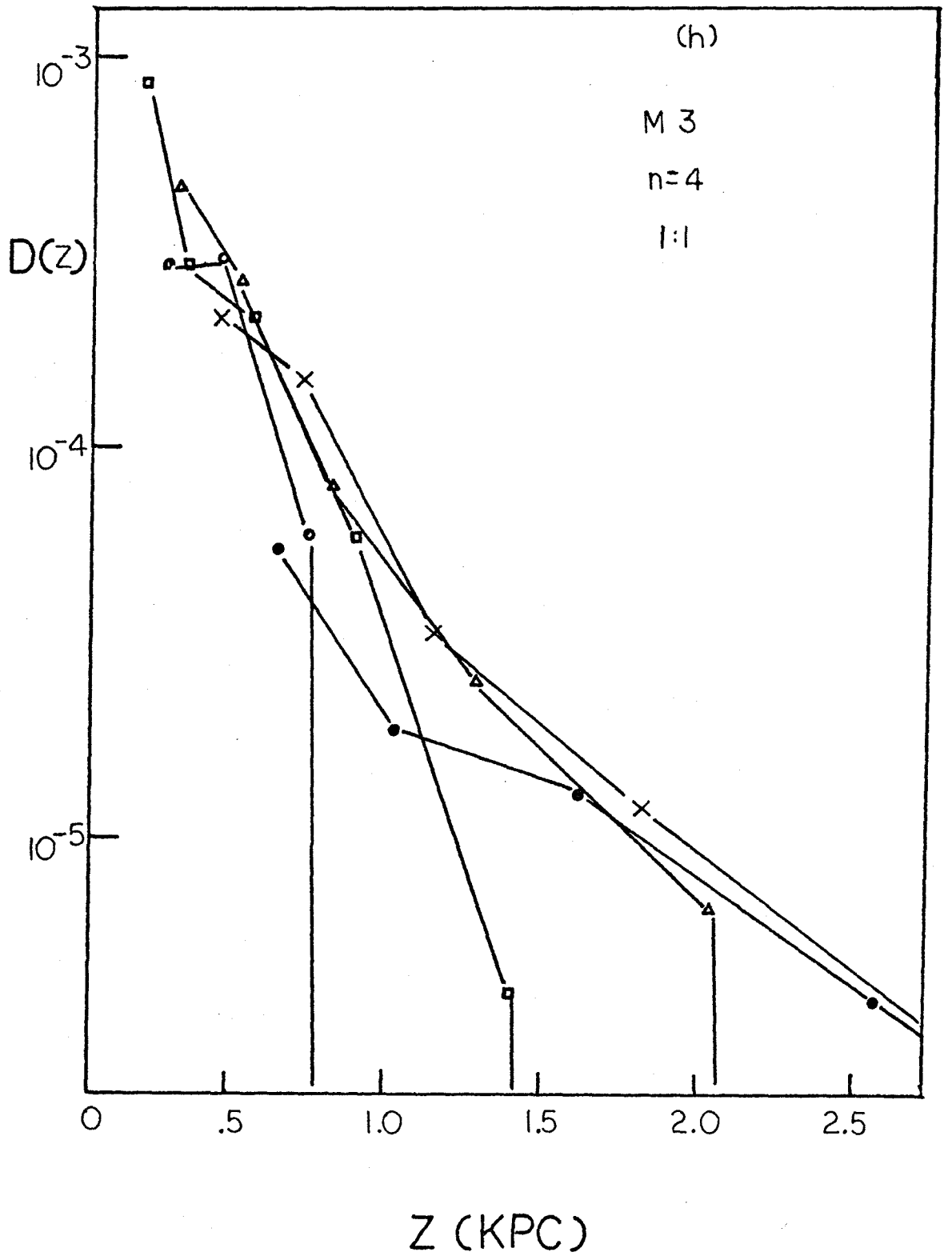
(h)
M 3
n=4
1:1
10^{-3}
10^{-4}
10^{-5}
D(z)
0
.5
1.0
1.5
2.0
2.5
Z (KPC)

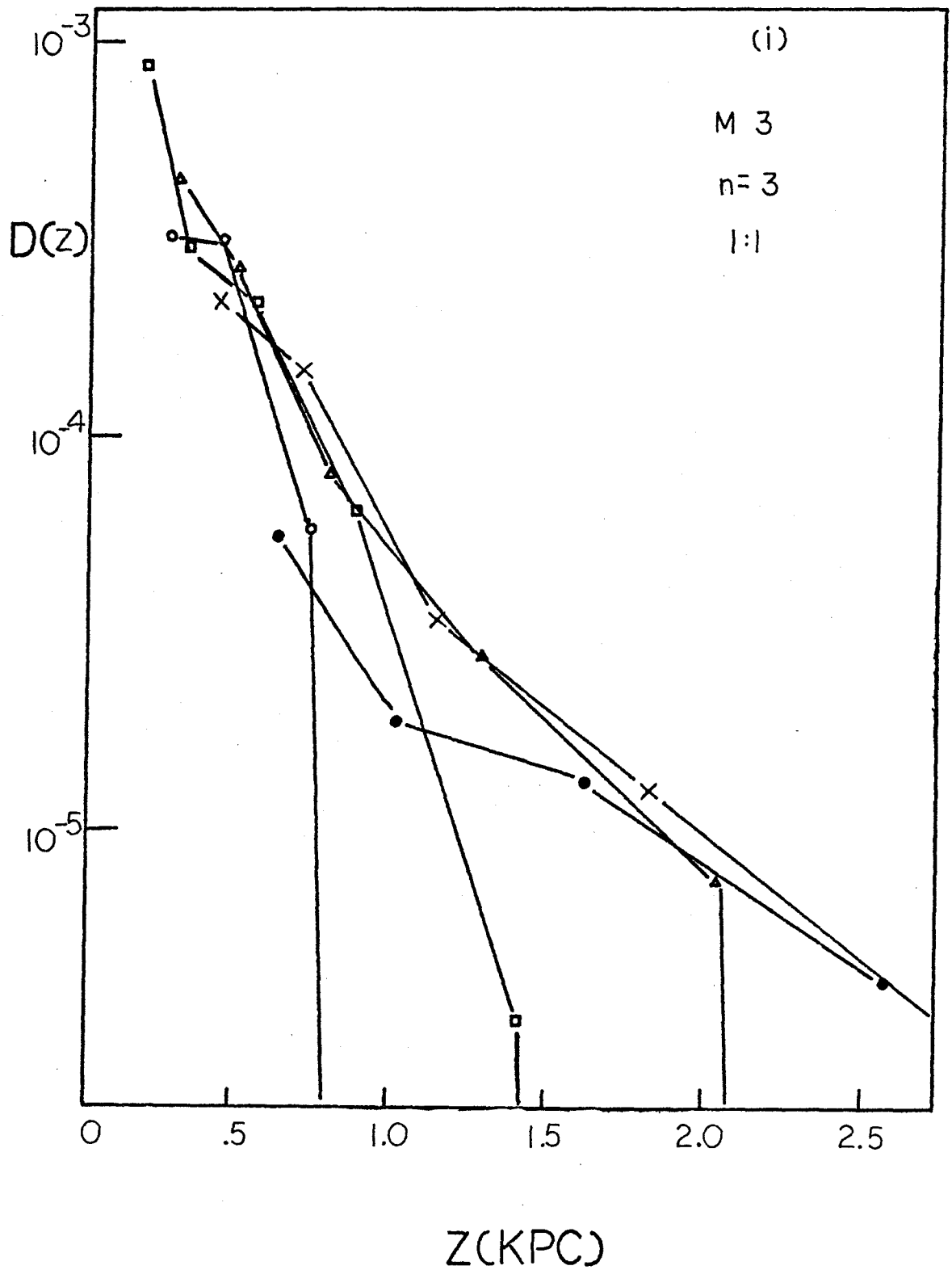
(i)
M 3
n= 3
1:1
D(z)
10^{-3}
10^{-4}
10^{-5}
0
.5
1.0
1.5
2.0
2.5
Z(KPC)

factor, but this is not the case for most of the M 3 results. Model M 3 , n=4 , 1:1 , for example, indicates an absence of stars with $(B-V)_o = .75$ beyond 1.5 kpc , yet stars of $(B-V)_o = .55$ are present to at least 3 kpc. Nothing in our present knowledge of stellar distributions would explain such a result. Inconsistencies of this sort eliminate M 3 models n=3 , 1:1 ; n=4, 1:1 ; and n=3, 1:2 from further consideration. The density models for M 92 are generally self-consistent. Only n=3, 1:1 can be definitely eliminated, based on the behavior of the density distribution for $(B-V)_o = .65$ compared to that for $(B-V)_o = .55$. None of the other models show inconsistencies significant enough to justify their elimination. Nevertheless, a definite trend is indicated, in that the n=4, 1:2 model does define a narrower D(z) curve than the data for models n=4, 1:1 and n=3, 1:2 .

The difference in the models for M 3 and M 92 originates in the differences between the luminosity functions for the two clusters. The subgiants in the clusters play a large role in determining the number of stars assigned to Population II, as can be seen in Table 17, which indicates the dwarf and nondwarf contributions to the total number of Population II stars at V = 16.5 and 17.5 for the clusters with density models n=4, 1:1 . The M 3 luminosity function contains relatively more red subgiants

Table 17

Dwarf and Nondwarf Contributions to

Population II for M 3 and M 92, n=4, 1:1

$(B-V)_o$	M 3				M 92			
	V=16.5		V=17.5		V=16.5		V=17.5	
	Dwarfs	Nondwarfs	Dwarfs	Nondwarfs	Dwarfs	Nondwarfs	Dwarfs	Nondwarfs
.375					41	18	125	54
.425	33	50	116	142	35	13	118	35
.475	14	24	50	46	26	14	90	31
.525	9	12	35	34	14	19	52	42
.575	6	13	21	36	11	37	40	89
.625	4	19	15	50	9	72	34	90
.675	2	39	9	100	5	37	20	37
.725	1	83	5	181	5	20	18	15
.775	1	66	5	100	3	5	12	2
.825	1	57	4	57	2	2	8	1
.875	2	33	4	29	2	2	6	2
.925	1	18	3	14	2	1	7	1
.975	1	8	4	6	1	1	5	1

than M 92. Consequently, for the M 3 models, more relatively red stars are assigned to Population II, leaving the observed anomalies in the disk density distributions.

Though the n=4, 1:1 and n=3, 1:2 models for M 92 cannot be definitely ruled out, the analysis in the following sections will be performed for the n=4, 1:2 density model for each cluster, which seems to be the most likely. The field Population II luminosity function is probably more similar to that for M 92 than for M 3 , but data for both clusters will be considered for comparison purposes. The zero Population II model is presented for comparison purposes only. Its similarity to the density distributions for the preferred models indicates the small degree to which the assumptions about Population II influence the overall results for the disk population.

Composite Density Distribution

The similarity in shape of the density distributions for stars of various colors for model M 92, n=4, 1:2 may be seen in Figures 7b, 8 and 9 . In general the agreement is quite good, suggesting the possibility of determining a well-defined composite disk density distribution from these individual distributions. A major difficulty arises, however, because stars of different colors (and, therefore, different absolute magnitudes) define the density distribution for different ranges of z . These

Figure 8

Density distributions of red disk dwarfs calculated for model M 92, n = 4, 1:2.

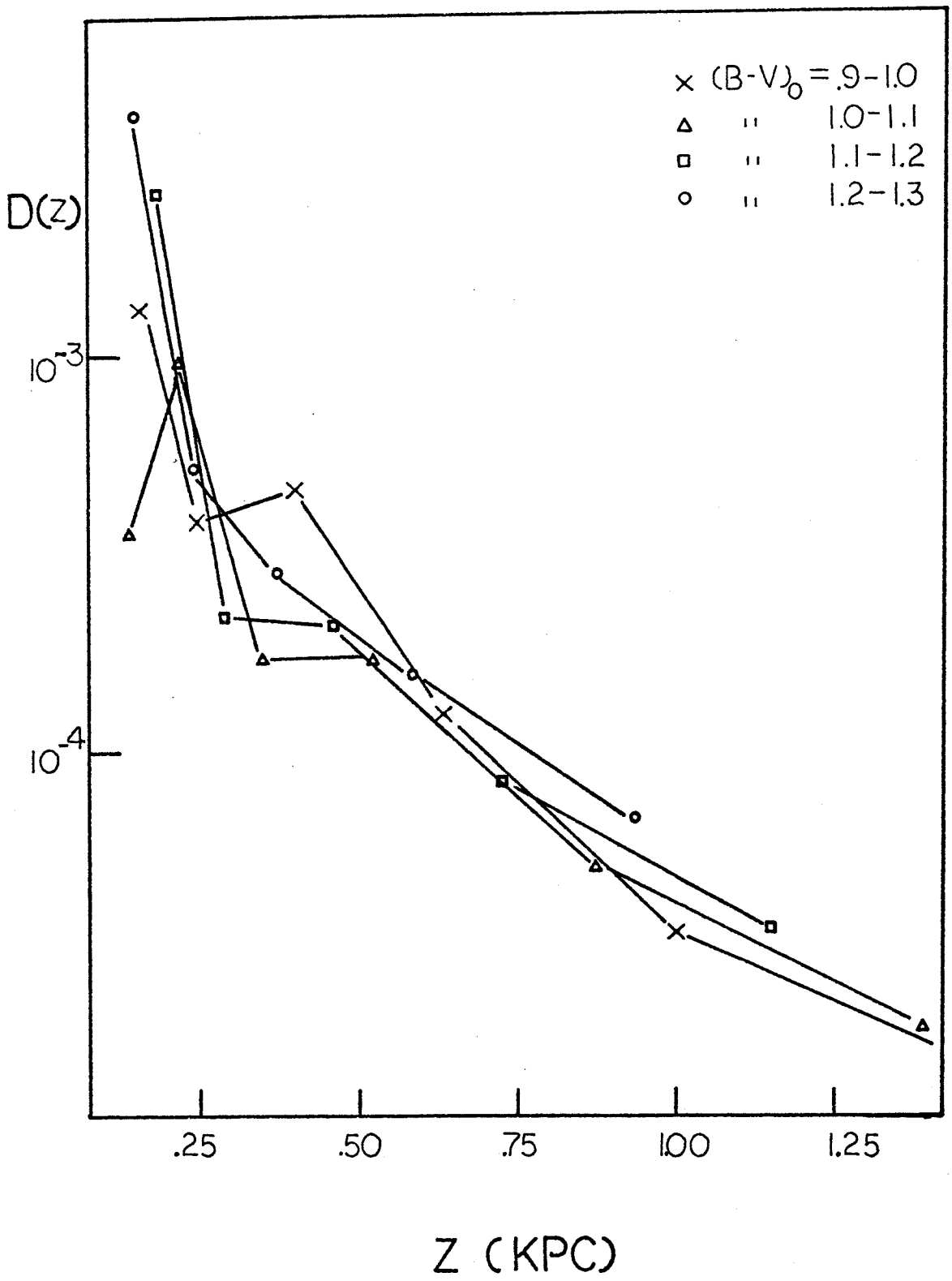
× (B-V)0 = .9-1.0
△ " 1.0-1.1
□ " 1.1-1.2
○ " 1.2-1.3
D(z)
10^-3
10^-4
.25
.50
.75
1.00
1.25
Z (KPC)

Figure 9

Density distributions of very red disk dwarfs calculated for model M 92, n = 4, 1:2.

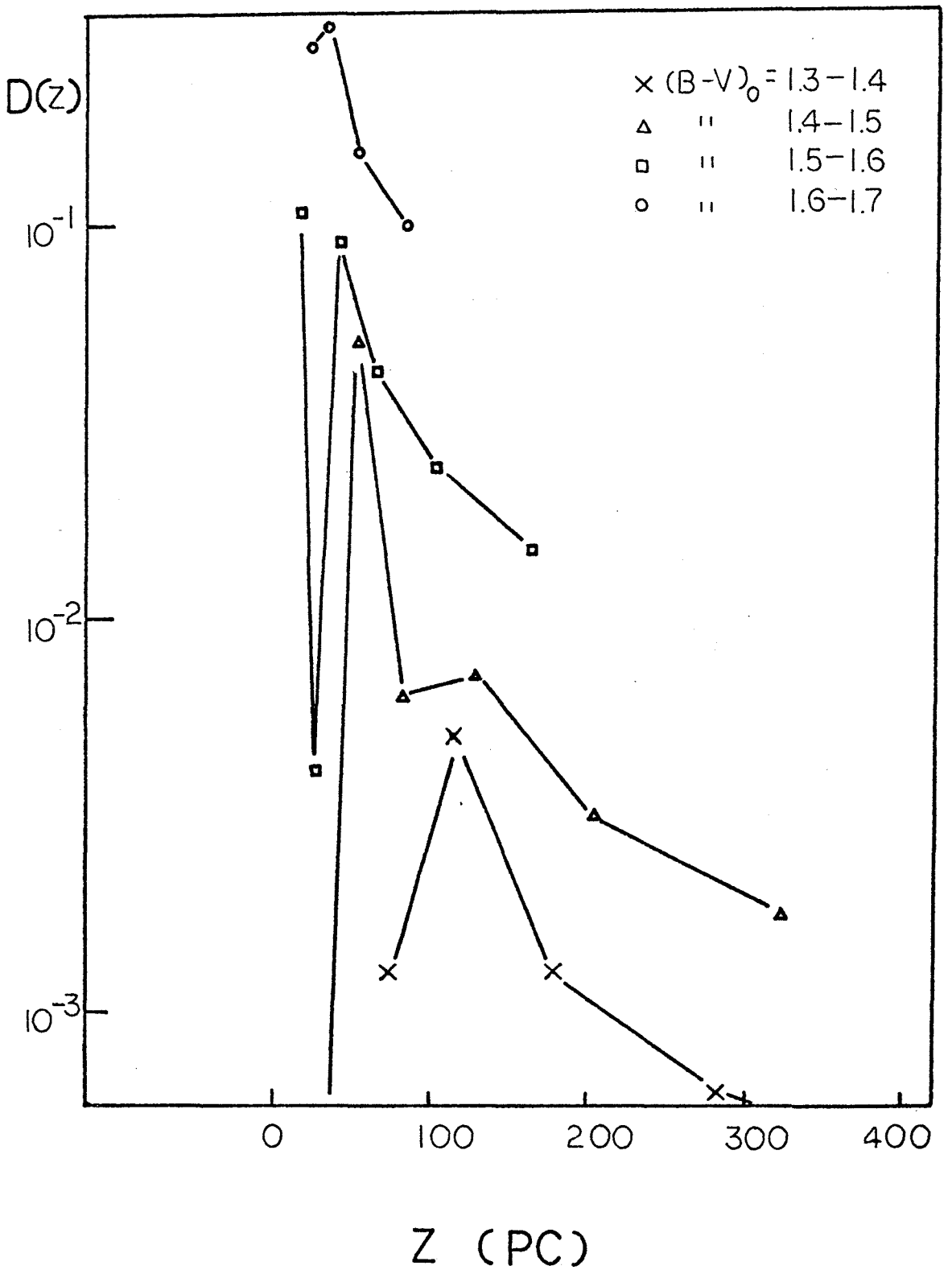
D(z)
× (B-V)0 = 1.3–1.4
△ " 1.4–1.5
□ " 1.5–1.6
○ " 1.6–1.7
10-1
10-2
10-3
0
100
200
300
400
Z (PC)

individual distributions must somehow be combined into one composite curve which encompasses the results for all z . The problem is further complicated by the effect of the estimates made for the number of giants and subgiants. Because of the uncertainties inherent in those estimates, densities strongly influenced by the predicted number of giants and subgiants were not included in the construction of the composite curve. Since such densities were always at distances closest to the plane for the particular color interval, the effect was to decrease even more the range in z for which the density distributions overlap. The method used to overcome this difficulty and derive the composite density distribution is described below. Results based on the model M3, n=4, 1:2 are also given, for comparison purposes, although the agreement among the individual density distributions calculated for this model for stars bluer than $(B-V)_o = .90$ is not as good as that for the M 92 model (Figure 7f). The density distributions for redder stars are essentially the same as those for the M 92 model.

Intervals in z were established with widths corresponding to $\Delta m = .50$ mag. The average difference in log D(z) in adjacent intervals was determined using only those individual D(z) curves defined in both intervals. Those parts of the individual D(z) curves defined by counts for which the estimated giant or subgiant contribution was one third or

more of the total number were eliminated. Densities from the individual curves were calculated by interpolating logarithmically between the points on the curve to the z at the middle of each interval. The differences in log D(z) for adjacent intervals were averaged, using the relative densities at a given z as weights. The weights were determined by fitting the individual D(z) curves to the composite D(z) from the previous iteration. For the first iteration, the values of the van Rhijn luminosity function at the appropriate M_V were used as weights. The difference between the average log density of the adjacent intervals was subtracted from the previously determined point on the composite curve to find the value of the new point. The composite distribution was normalized by setting D(z=0) = 1.00. Once a composite curve had been established, new weights for the individual D(z) curves were determined, and the process was iterated until the weights computed from the new composite curve were the same as the weights from the previously computed curve. Ten iterations were more than sufficient to obtain convergence in all cases.

The composite curves for the cluster models and the zero Population II model are shown in Figures 10a to 10c . The results have not yet been normalized to D(0) = 1.00 . The curves for the clusters are essentially the same, except for the normalization. The agreement with

Figure 10

Composite disk density distributions for three Population II models. The dashed lines indicate the exponential extrapolation to the plane discussed in the text. In (a) the $(B-V)_o$ colors of the stars determining each part of the curve are indicated. The vertical scales have not yet been normalized to D(0) = 1.00.

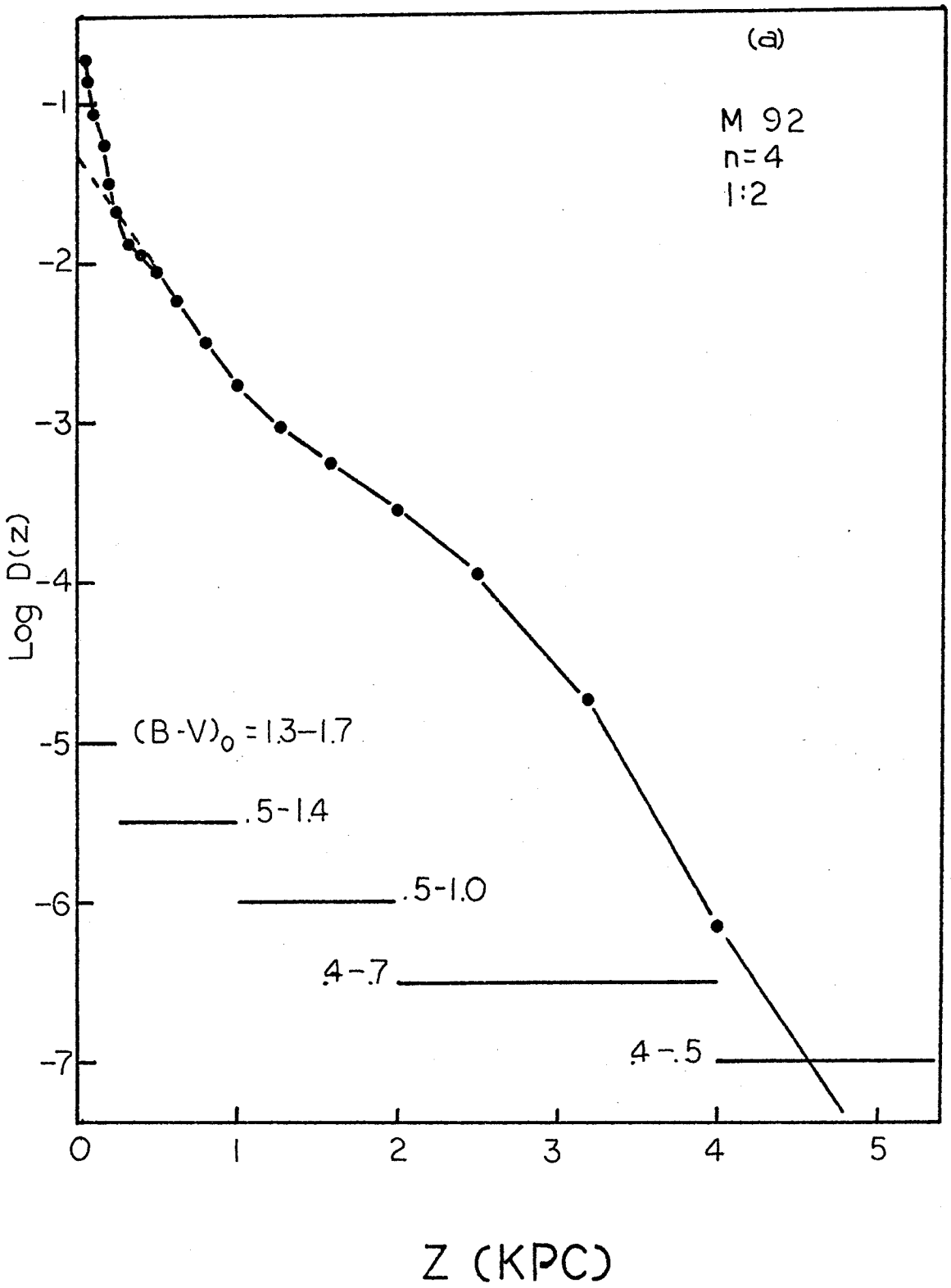
(a)
M 92
n=4
1:2
Log D(z)
-1
-2
-3
-4
-5
-6
-7
$(B-V)_0$ = 1.3–1.7
.5-1.4
.5-1.0
.4-.7
.4-.5
0
1
2
3
4
5
Z (KPC)

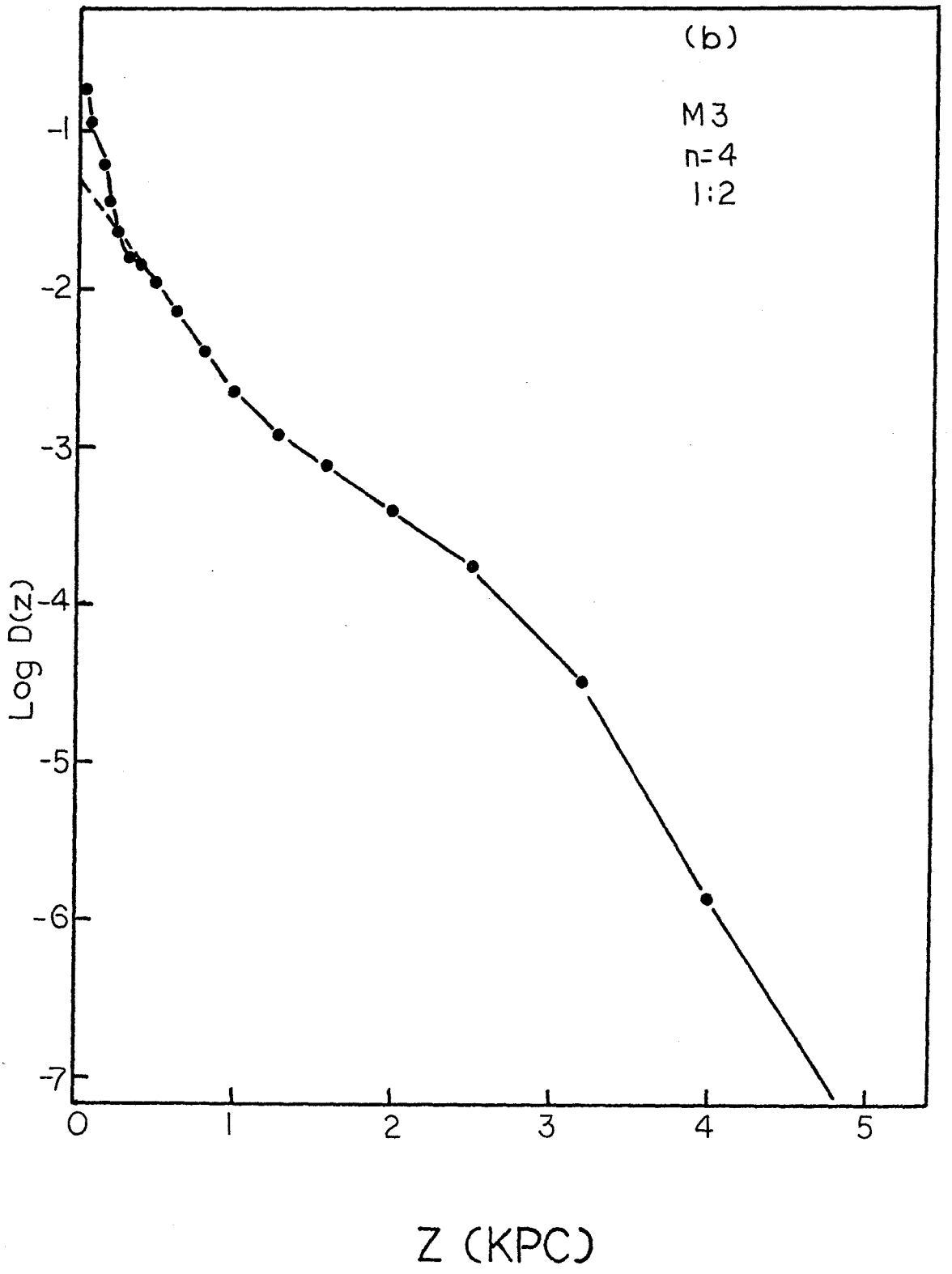
(b)
M3
n=4
1:2
-1
-2
-3
-4
-5
-6
-7
Log D(z)
0
1
2
3
4
5
Z (KPC)

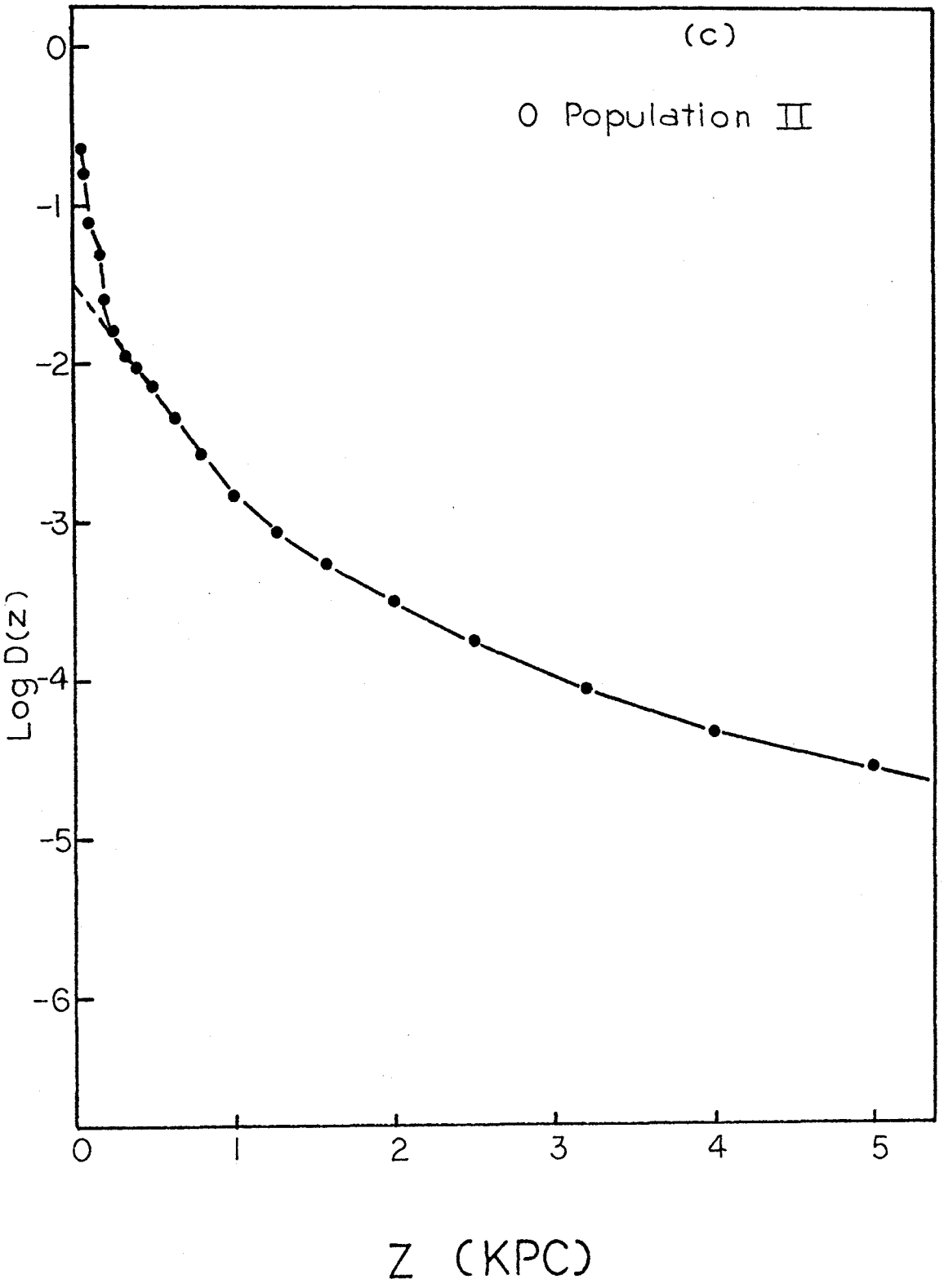
(c)
O Population II
0
-1
-2
-3
-4
-5
-6
Log D(z)
0
1
2
3
4
5
Z (KPC)

the zero Population II case is good to 2 kpc, reiterating that the results for the disk are essentially independent of the assumptions made concerning Population II. The results beyond 3 kpc are tentative, as only the bluest disk stars studied penetrate to these distances, and these are most effected by the Population II assumptions.

It will be noted that Figures 10a to 10c also indicate a very steep increase in D(z) within 200 pc of the plane. Because such a steeply increasing D(z) is in conflict with previously determined density distributions, attempts were made to check the validity of this result. The effects of the apparent magnitude limits imposed on the observed material and the densities omitted due to strong dependence on giant and subgiant estimates are such that the composite D(z) for small z reflects the individual D(z) curves for the reddest dwarfs observed. This can be seen in Figure 10a , where the colors of the stars which are the major contributors to each part of the composite curve are indicated. Attempts were made to account for the observed counts of these stars ($(B-V)_o$ greater than 1.30) without resorting to a steep D(z) . The composite D(z)'s were extrapolated to z = 0 as indicated by the dashed lines in Figures 10a to 10c . The linear extrapolation is equivalent to assuming D(z) is exponential close to the galactic plane. The extra-

polated composite D(z)'s were then used to predict the counts for the stars in question using equation (5).

The results using the absolute magnitudes, dispersion in absolute magnitude, and absorption adopted previously were unsatisfactory, except for the stars with $(B-V)_o$ = 1.30 - 1.40 . The observed counts for these stars were adequately represented by the extrapolated density distribution and other previously adopted parameters, and so no stars bluer than $(B-V)_o$ = 1.40 will be considered in the following discussion. A change in the absolute magnitude calibration would not improve the fit of the predicted counts to the observations, as that consists of a scale change only, while, as may be seen in Figure 11, it is the slope of the predicted and observed counts which do not agree. Calculations of the number of stars expected using the extrapolated D(z) and several values for the absolute magnitude dispersion were made. Typical examples of these predictions may be seen in Figure 11 along with the star counts to be fit, for stars with $(B-V)_o$ = 1.40-1.50 . Only for a dispersion of 2.00 magnitudes were the fits satisfactory, except for the stars for which $(B-V)_o$ = 1.60-1.70 , which could not be fit even with this large dispersion. Yet, an examination of Eggen's data (Figure 6) seems to preclude such a large dispersion in the absolute magnitudes. Finally, an attempt was made to

Figure 11

Predicted star counts as a function of absolute magnitude dispersion for stars with $(B-V)_o$ = 1.4-1.5.

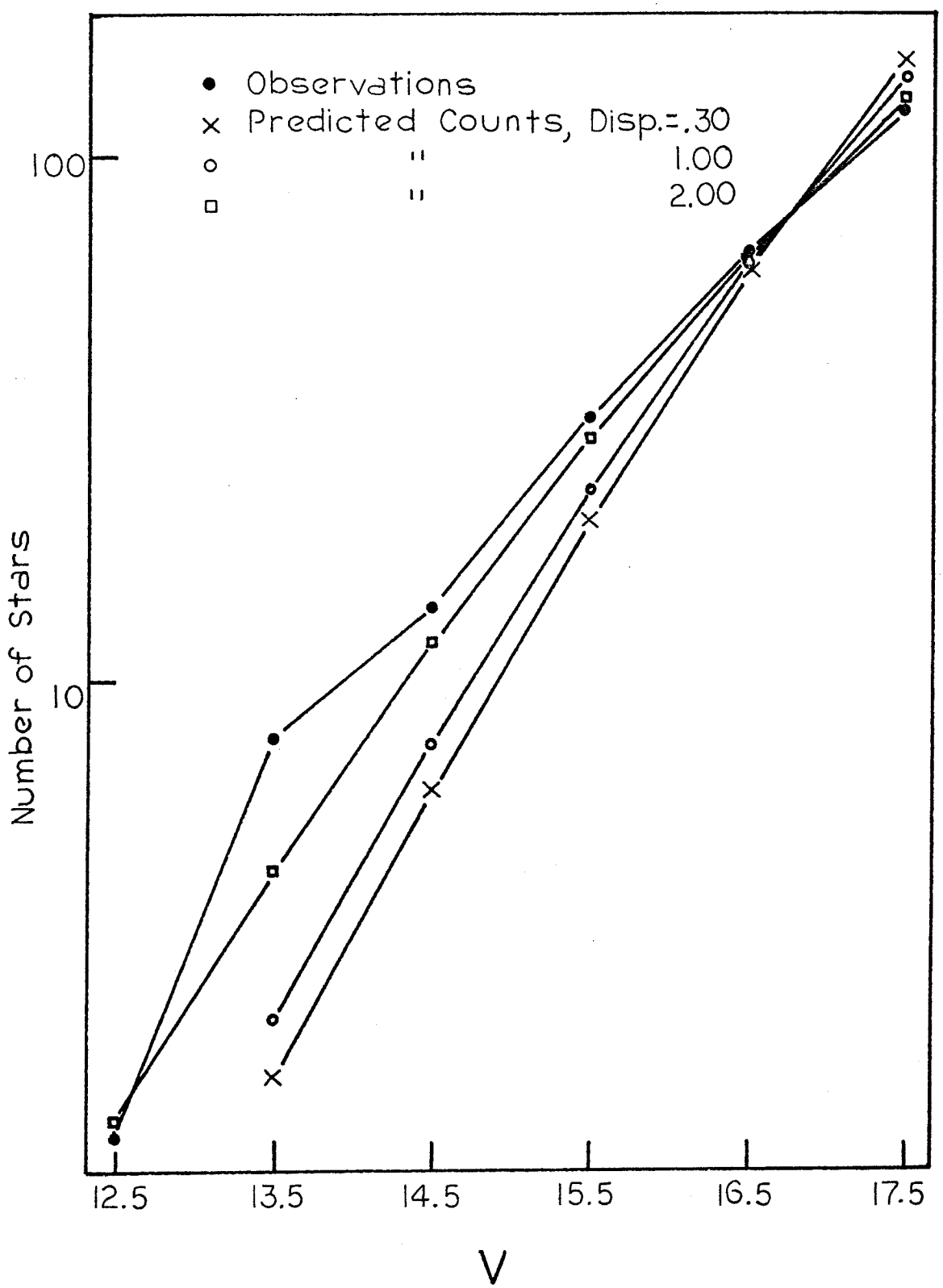
Observations
Predicted Counts, Disp.=.30
" 1.00
" 2.00
100
10
Number of Stars
12.5
13.5
14.5
15.5
16.5
17.5
V

fit the observed counts by increasing the assumed absorption to .50 mag., but the slope of the observed relation between star counts and apparent magnitude was not reproduced. The only alternative, therefore, is the acceptance of a steep D(z) as determined by the data.

Because of the controversial nature of the result just described, three possibilities will be considered in the remaining analysis. The first, referred to as Case I, will assume that the true disk density distribution is that given by the composite D(z) extrapolated with an exponential to z=0 (Figure 10, dashed line) and normalized to D(o) = 1.00 . For Case II, composite curves were derived using just the data for stars with $(B-V)_o$ greater than 1.40 . The individual points for the M 92 model are shown in Figure 12, along with the smoothed curve hand-fitted to them. The smoothed curves were fitted to the D(z) for Case I, so that for small z the curve is determined by the composite for the red stars, while for large z the shape of the curve is the same as that in Case I. Case II assumes that this is the true density distribution for all disk stars. For Case III it is assumed that stars bluer than $(B-V)_o = 1.40$ are distributed like Case I and the redder stars are distributed like Case II. Figure 13 compares the composite D(z) for Cases I and II for the M 92, n=4, 1:2 model.

Figure 12

Composite disk density distribution derived from dwarfs with $(B-V)_o$ greater than 1.4. The filled circles indicate computed points. The adopted smooth curve is given by the solid line. The Case I distribution, shifted vertically to fit the adopted curve, is indicated by the dashed line. The vertical scale has not yet been normalized to D(0) = 1.00.

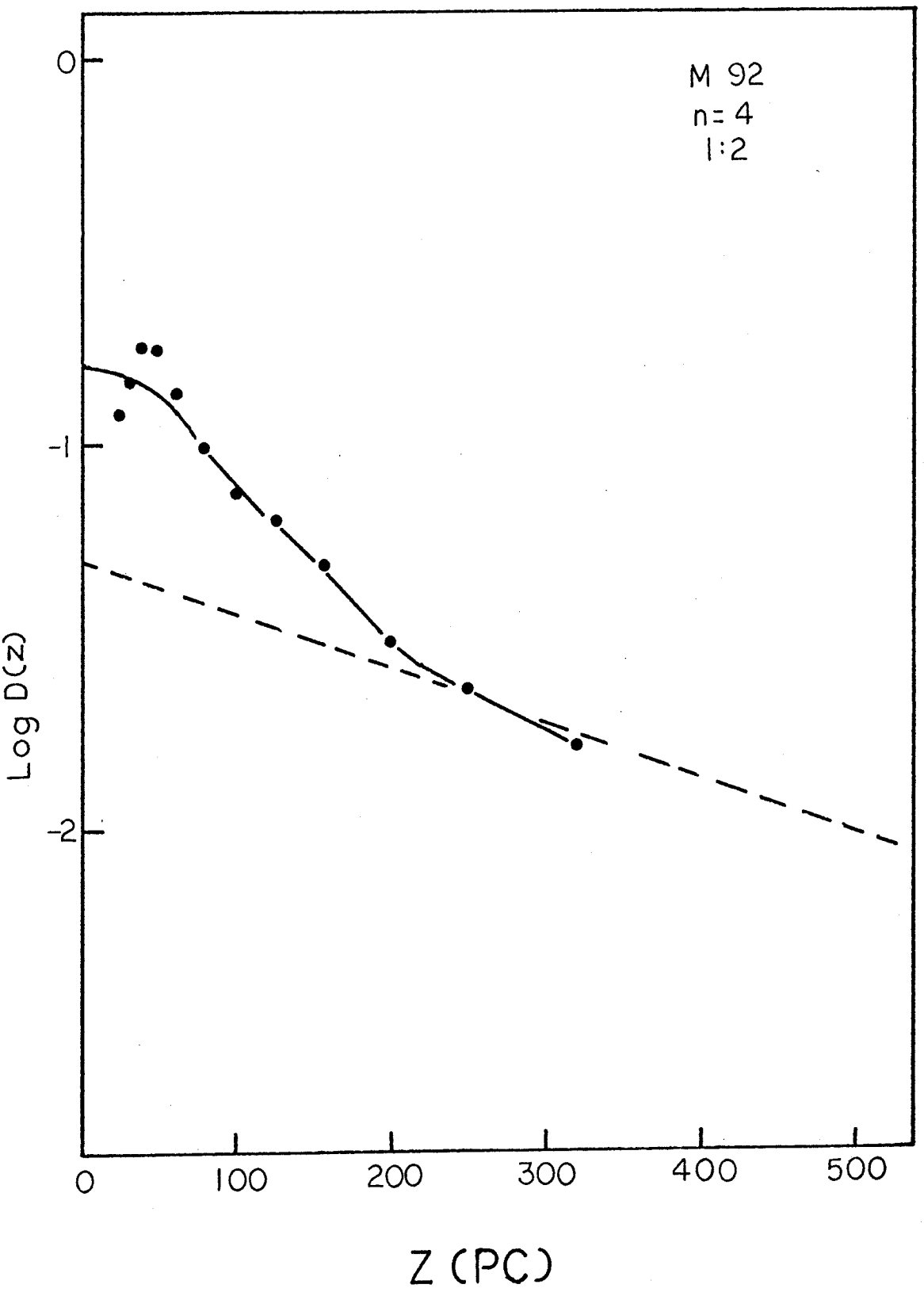
M 92
n= 4
1:2
0
-1
-2
Log D(z)
0
100
200
300
400
500
Z (PC)

Figure 13

Comparison of density distributions adopted for Cases I (●), and II (x). The dashed line indicates the extrapolation to the plane for Case I. Data are for model M 92, n = 4, 1:2.

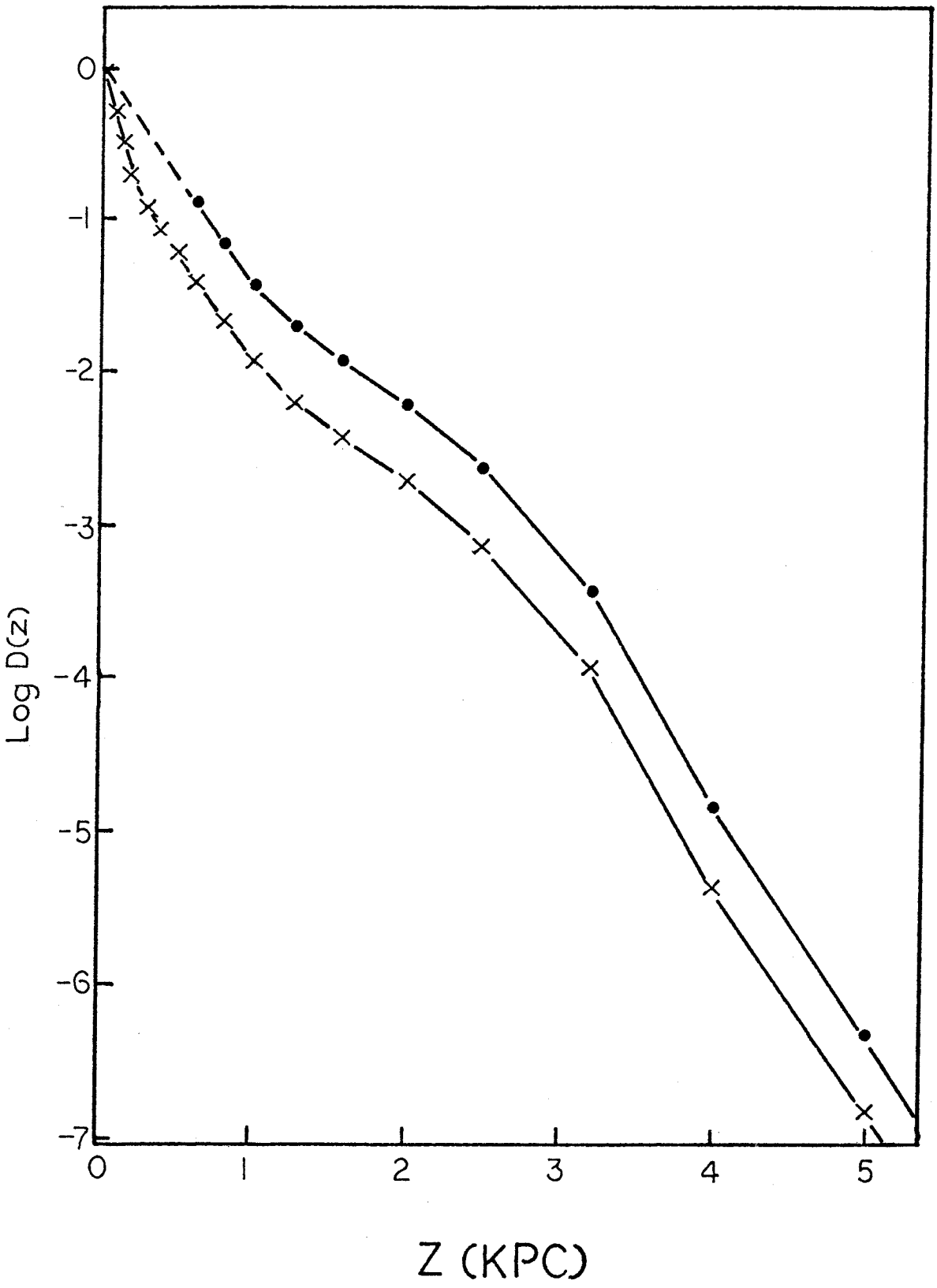
0
-1
-2
-3
-4
-5
-6
-7
Log D(z)
0
1
2
3
4
5
Z (KPC)

Luminosity Functions

If star counts for narrow intervals of color or absolute magnitude are available, the stellar density in the plane for the stars in each interval is just a scale factor that can be determined by fitting the predicted counts (equation [5]) to the observed counts. Using the parameters and composite D(z) curves derived above, the number of stars was predicted for each $(B-V)_o$ interval, assuming unit density in the plane. The density was then derived by summing the predicted counts for each interval, and scaling the total to the sum of the observed counts for the interval. To transform the present result to a luminosity function, the density of stars for each color interval must be multiplied by a factor which is just the inverse of the increment in absolute magnitude corresponding to the limits of the $(B-V)_o$ interval (Table 16). The luminosity functions derived for Cases I, II , and III are shown in Figure 14 for model M 92, n=4, 1:2 . Also shown are the McCuskey (1956) and van Rhijn luminosity functions for comparison. The Case III luminosity functions for M 3 and M 92 are compared in Figure 15. The difference between the two can be attributed to the difference in the luminosity functions of the clusters, specifically, the relatively larger number of subgiants in M 3. The two disk luminosity functions are essentially the same for

Figure 14

Luminosity functions computed for model M 92, n = 4, 1:2 (●). The van Rhijn (x) and McCuskey (o) luminosity functions are shown for comparison.

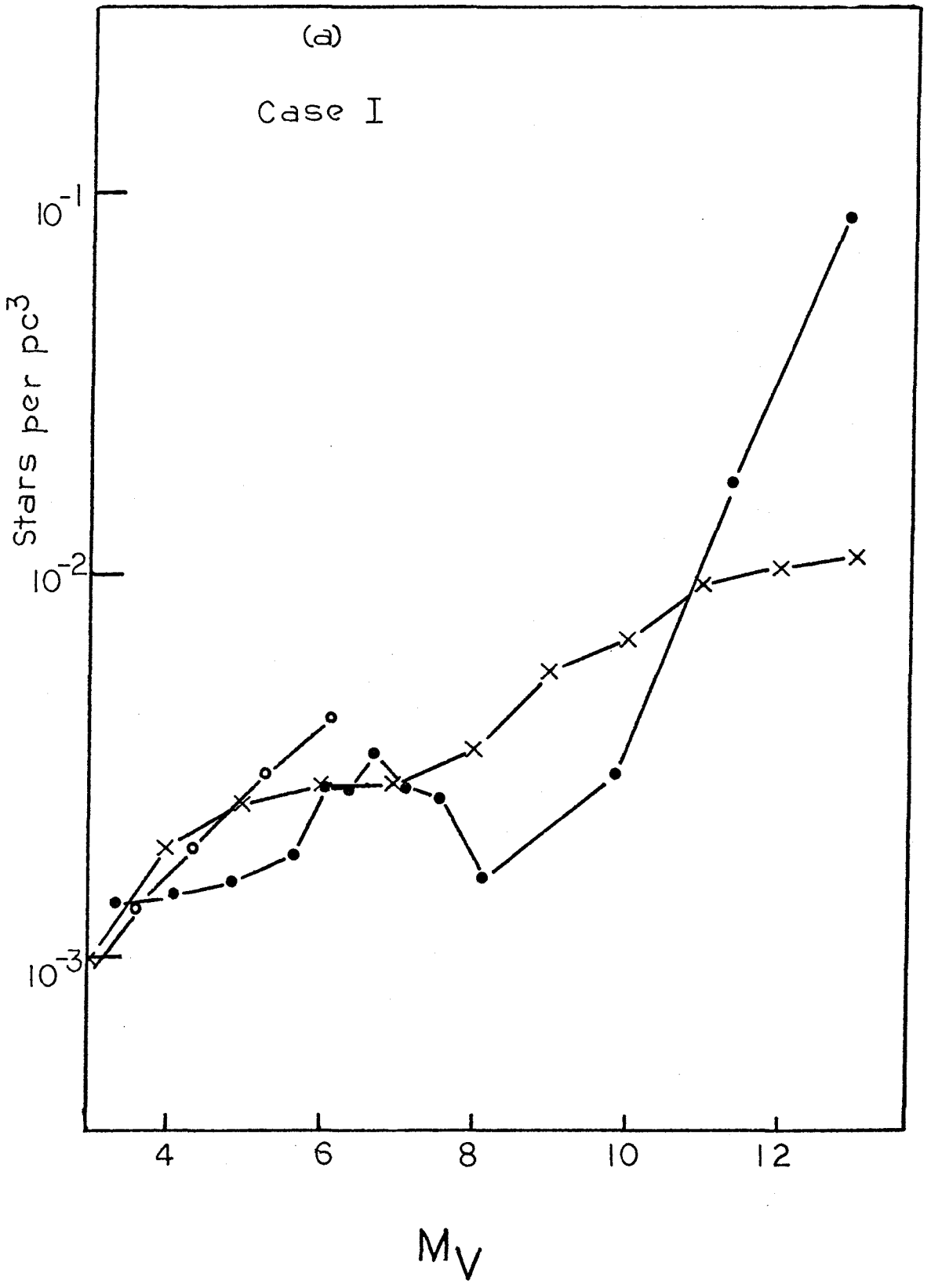
(a)
Case I
10^{-1}
10^{-2}
10^{-3}
Stars per pc^3
4
6
8
10
12
M_V

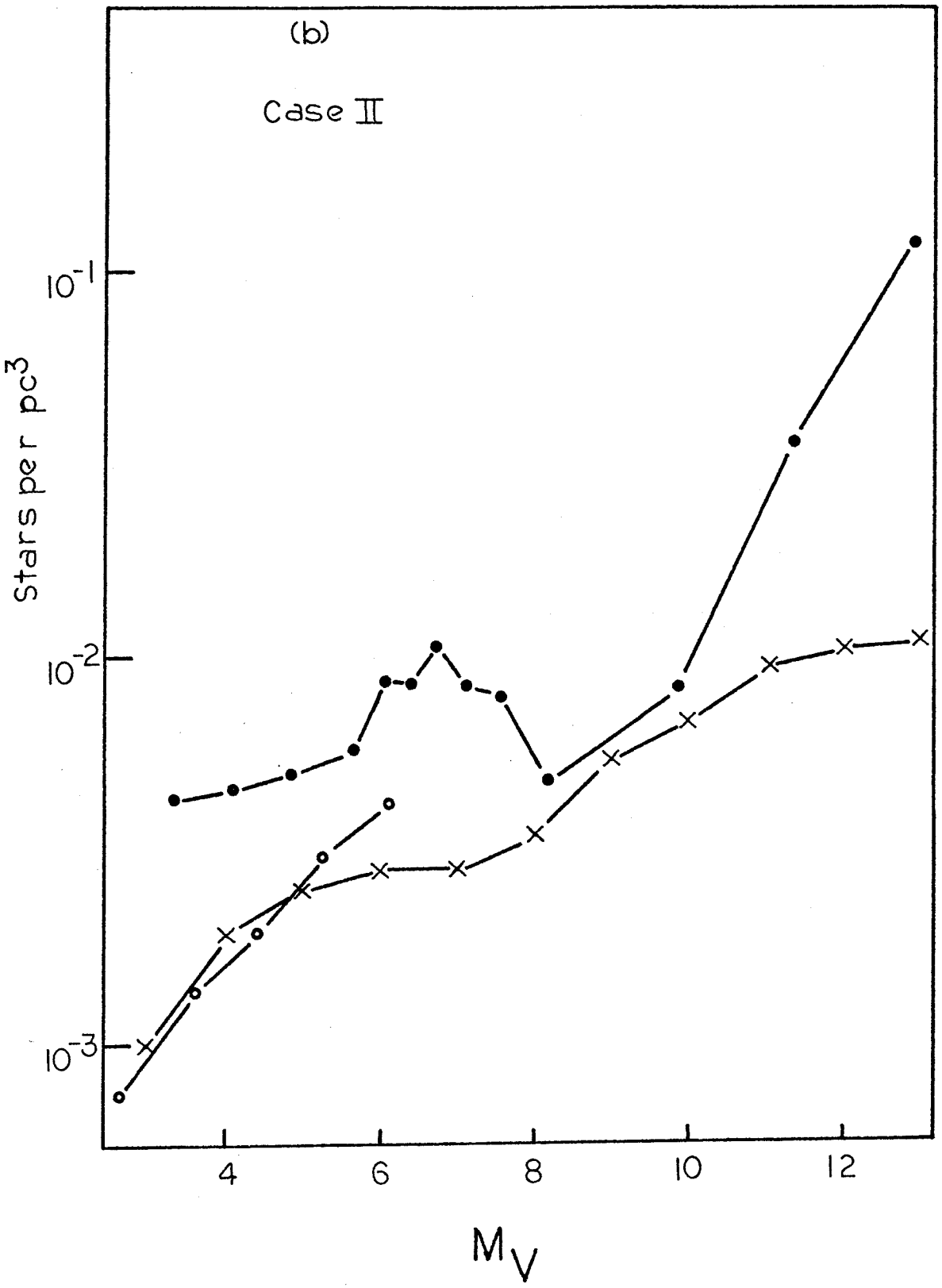
(b)
Case II
10^{-1}
10^{-2}
10^{-3}
Stars per pc^3
4
6
8
10
12
M_V

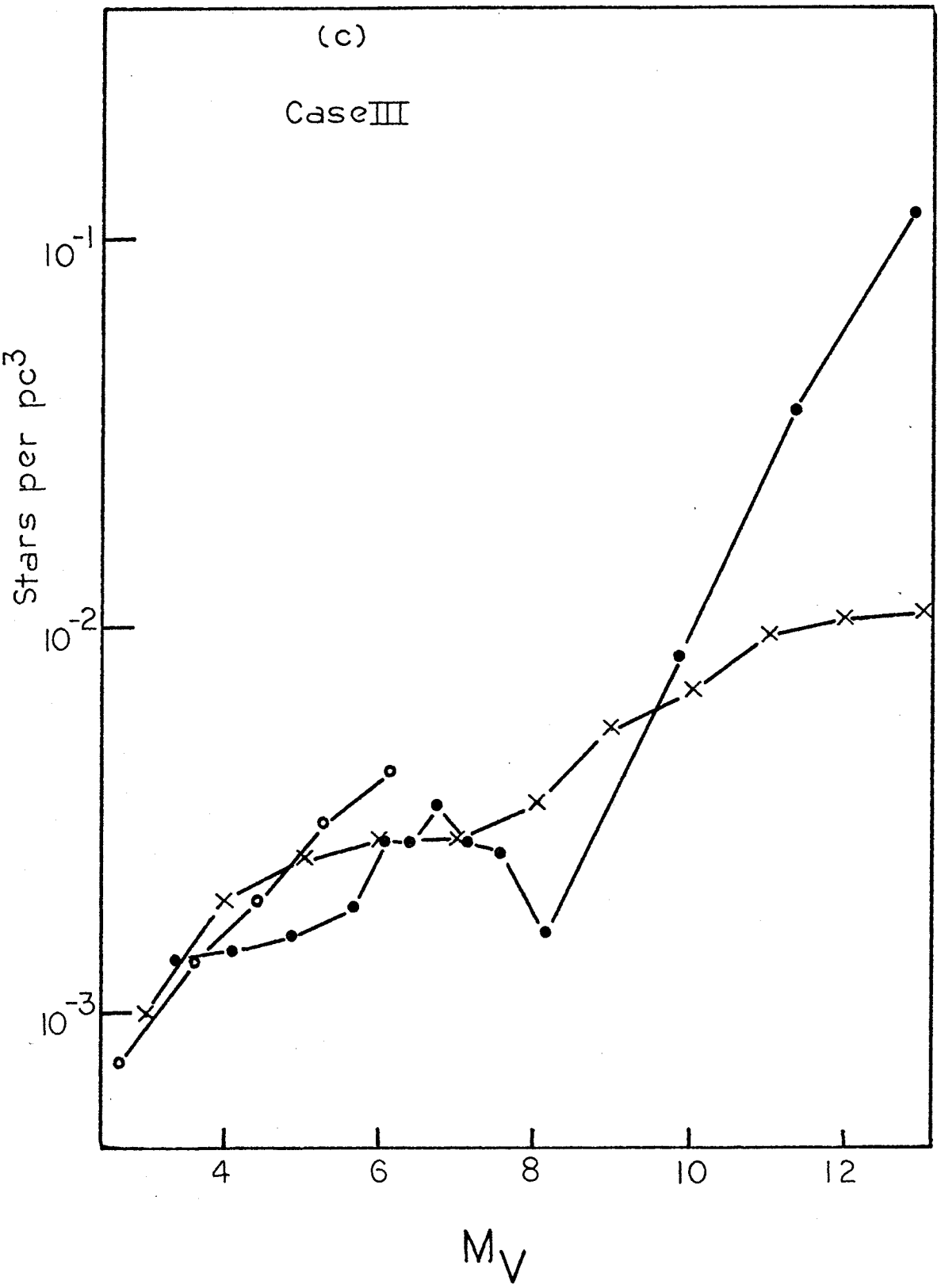
(c)
Case III
10^{-1}
10^{-2}
10^{-3}
Stars per pc^3
4
6
8
10
12
M_V

Figure 15

Comparison of luminosity functions for models M 3 and M 92, n = 4, 1:2, Case III.

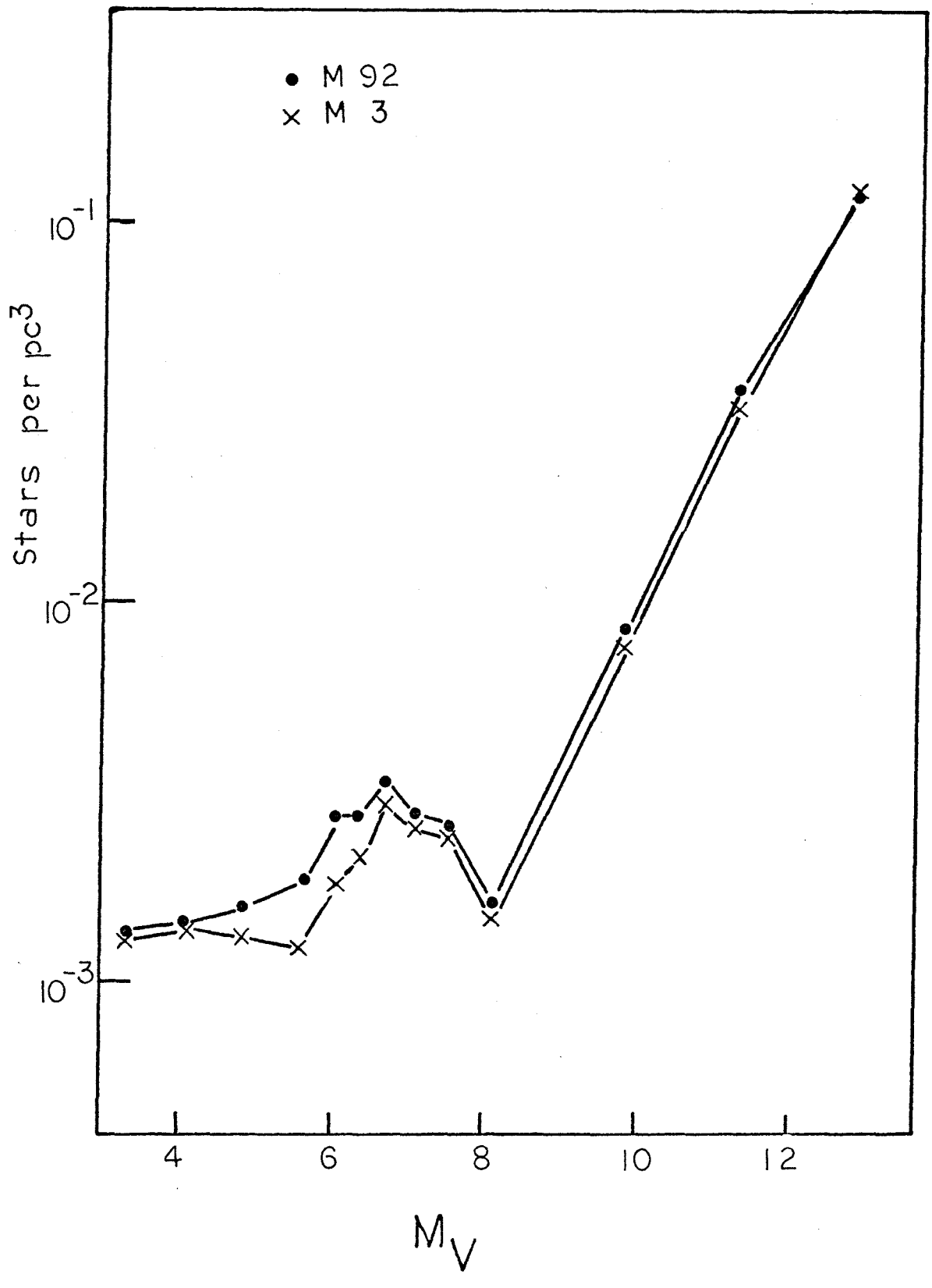
• M 92
× M 3
10^{-1}
10^{-2}
10^{-3}
Stars per pc^3
4
6
8
10
12
M_V

stars fainter than $M_V = 7$.

The bump between absolute magnitudes 6 and 8 in the luminosity functions seems well-established, as there are several points contributing to it. The existence of the decrease beyond absolute magnitude 8 is subject to doubt, however, as it is defined by one point only. It should be noted that the luminosity functions for Cases I and II just bracket the van Rhijn luminosity function for absolute magnitude brighter than 10 . This is not surprising, as the true $D(z)$ might reasonably be expected to lie somewhere between Cases I and II. The most remarkable feature of the luminosity function is the steep rise beyond absolute magnitude 9 . This result seems well established, as it is present for all three density distribution cases considered for the disk, whether the Population II model for M 3 , M 92 or zero density is assumed. As will be seen in the next chapter, it has significant consequences for the mass in the neighborhood of the sun as determined by non-dynamical means.

In view of the uncertainties involved in the $D(z)$ determination close to the plane, which in turn has a large influence on the luminosity function calculated for the stars brighter than absolute magnitude 9 , and the result that Cases I and II bracket the van Rhijn luminosity function, the best estimate for the luminosity

function from these data would seem to be the van Rhijn function for stars brighter than $M_V = 9.5$ and the Case III luminosity function as shown in Figure 14c for fainter stars.

The mass-luminosity relation adopted is that used by Schmidt (1959), which provides a good fit to the data given by Harris, Strand and Worley (1963) and Eggen (1967). The result of applying the mass-luminosity relation to the luminosity functions for Cases I, II and III are shown in Table 18. Also shown are the results for the van Rhijn luminosity function and two combined luminosity functions, consisting of van Rhijn's data for bright stars and the data derived for model M 92, n=4, 1:2, Case III for stars fainter than absolute magnitude 9.5 and, for comparison, van Rhijn's function plus the data for M 92, n=4, 1:2, Case I for stars fainter than absolute magnitude 10.5 (see Figures 14a and 14c). The masses derived using the van Rhijn luminosity function include contributions for all stars fainter than $M_V = -5.0$. The differences among the various determinations reflect the differences in the luminosity functions assumed. The dominant contribution to the total mass is made by the large number of faint stars in all cases. The results for the models considered to be most likely (Case II and van Rhijn – Case III) indicate a mass density of between .06 and .07 solar masses per pc^3 for the type of stars considered here.

Table 18

Local Mass Density of Stars

M_V	Mass Density (10^{-2} solar masses per pc^3)					
	CaseI	CaseII	CaseIII	v.Rhijn	v.Rh.-III	v.Rh-I
≤2				.27	.27	.27
3	.20	.62	.20	.14	.14	.14
4	.16	.53	.17	.23	.23	.23
5	.16	.50	.15	.24	.24	.24
6	.21	.68	.21	.23	.23	.23
7	.21	.65	.21	.20	.20	.20
8	.12	.35	.12	.22	.22	.22
9	.12	.35	.20	.31	.31*	.31
10	.17	.45	.46	.32	.46	.32*
11	.38	.86	.89	.32	.89	.38
12	.80	1.41	1.40	.24	1.40	.80
13	1.60	2.10	2.08	.18	2.08	1.60
Total	4.1	8.5	6.1	2.9	6.7	5.0

*Entries above line were computed using van Rhijn luminosity function. Others were computed using designated luminosity function from this study.

Chapter IV

Discussion

Absorption

The influence of the total absorption on the results was investigated by repeating all calculations for models M 92, n=4, 1:2 and M 3, n=4, 1:2 , assuming values for the total absorption of .00 mag. and .50 mag. The effect on the local Population II density may be seen in Table 19, where the new results are compared with those obtained using a total visual absorption of .10 mag. As might have been expected, assuming zero absorption changes the local Population II density very little. A total absorption of .50 mag. increases the density twenty to thirty percent. The magnitude of the change is not disturbing. Even if the local Population II density is thirty percent higher than has been derived, the main import of the result, that it is considerably lower than had previously been thought, is preserved.

Figures 16a-b compare the Case I disk density distributions for the three values of the absorption. As might have been expected, the curves are quite similar for small z but diverge strongly beyond 2 kpc. The curves fall off more rapidly for the case of .50 mag. absorption than for the others; since, for given apparent and absolute magnitude, the assumption of increased absorption locates

Table 19

Influence of Absorption on the Local Population II Density Derived

Absorp. Model	.00 mag.	.10 mag.	.50 mag.
M3 n=4 1:2	$1.1\times10^{-4}(\eta/L)_{M3}$	$1.1\times10^{-4}(\eta/L)_{M3}$	$1.4\times10^{-4}(\eta/L)_{M3}$
M92 n=4 1:2	$9.0\times10^{-5}(\eta/L)_{M92}$	$9.8\times10^{-5}(\eta/L)_{M92}$	$1.3\times10^{-4}(\eta/L)_{M92}$

Figure 16

Composite disk density distributions for Case I, models M 3 and M 92, n = 4, 1:2, for three values of absorption. Dashed lines indicate extrapolation to plane.

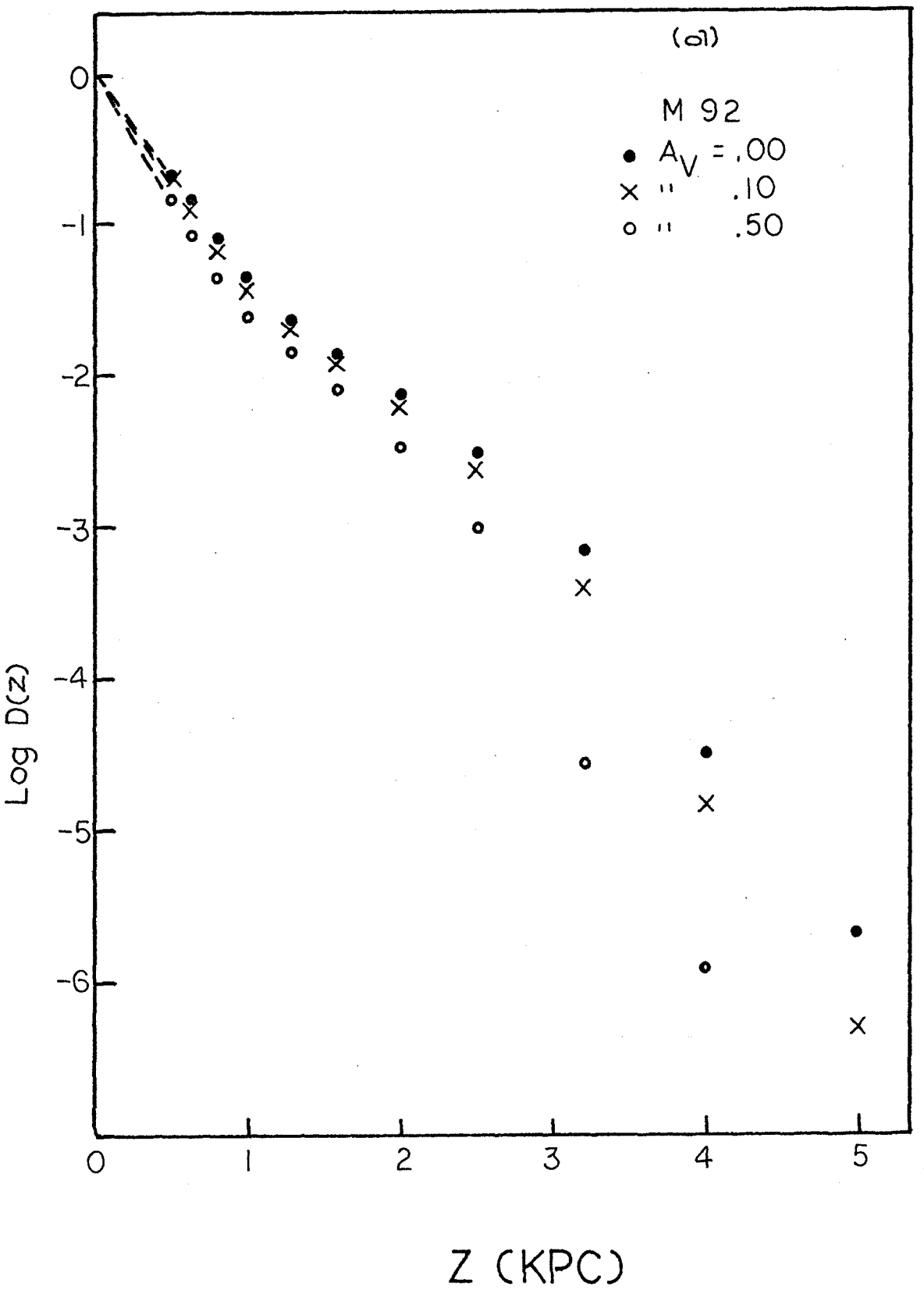
(a1)
M 92
A_V = .00
" .10
" .50
0
-1
-2
-3
-4
-5
-6
Log D(z)
0
1
2
3
4
5
Z (KPC)

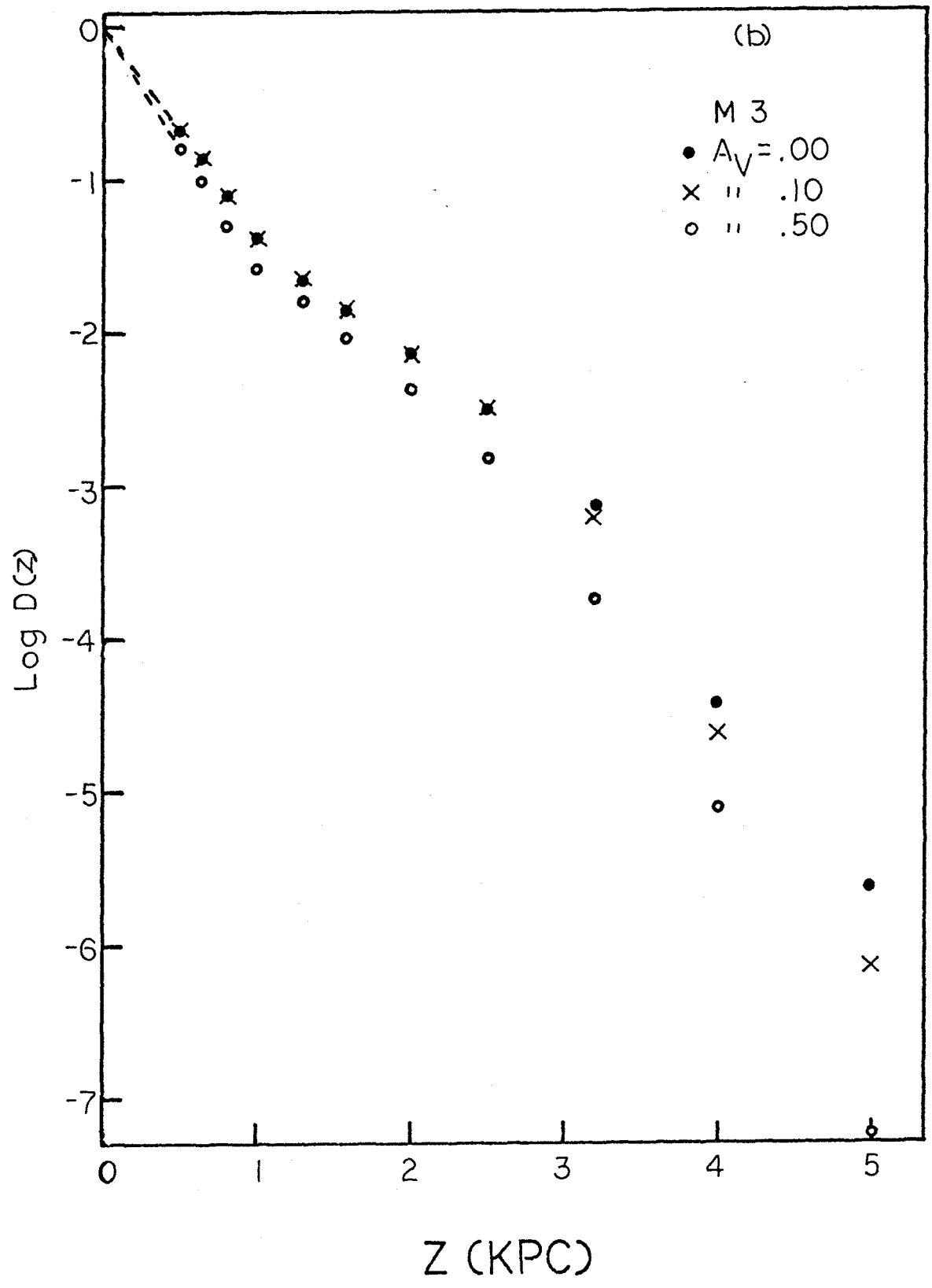
(b)
M 3
● A_V=.00
× " .10
○ " .50
0
-1
-2
-3
-4
-5
-6
-7
Log D(z)
0
1
2
3
4
5
Z (KPC)

the star closer to the observer. The slope of the curves is sufficiently steep that the corresponding density increase due to the decreased volume, a factor of approximately two, is not sufficient to overcome the consequences of the change in distance, a decrease of about 20%. The same effect causes the curve for zero absorption to be relatively flatter than the .10 mag. absorption case, though the difference is negligible for distances less than 2000 pc.

The Case II composite distributions are compared similarly in Figures 17a-b. For the M 92 model, the slope is sufficiently gentle that the effect of the increased density prevails over that of the decreased distance, so that the density distribution for the .50 mag. assumed absorption decreases more slowly than the .10 mag. case. The slope of the M 3 distribution is such that the curves for all three absorption assumptions are similar. There are, of course, additional, smaller influences on the curves, such as changes in the number of stars assigned to the disk population, for the three assumed absorptions. Such differences generally amount to five stars or less. Differential absorption effects also play a role for very nearby stars. For the first few parsecs, there is relatively little absorption, but almost the full amount influences data from stars beyond 100 pc. The unequal

Figure 17

Smoothed Case II composite disk density distributions for models M 3 and M 92, n = 4, 1:2, for three values of absorption.

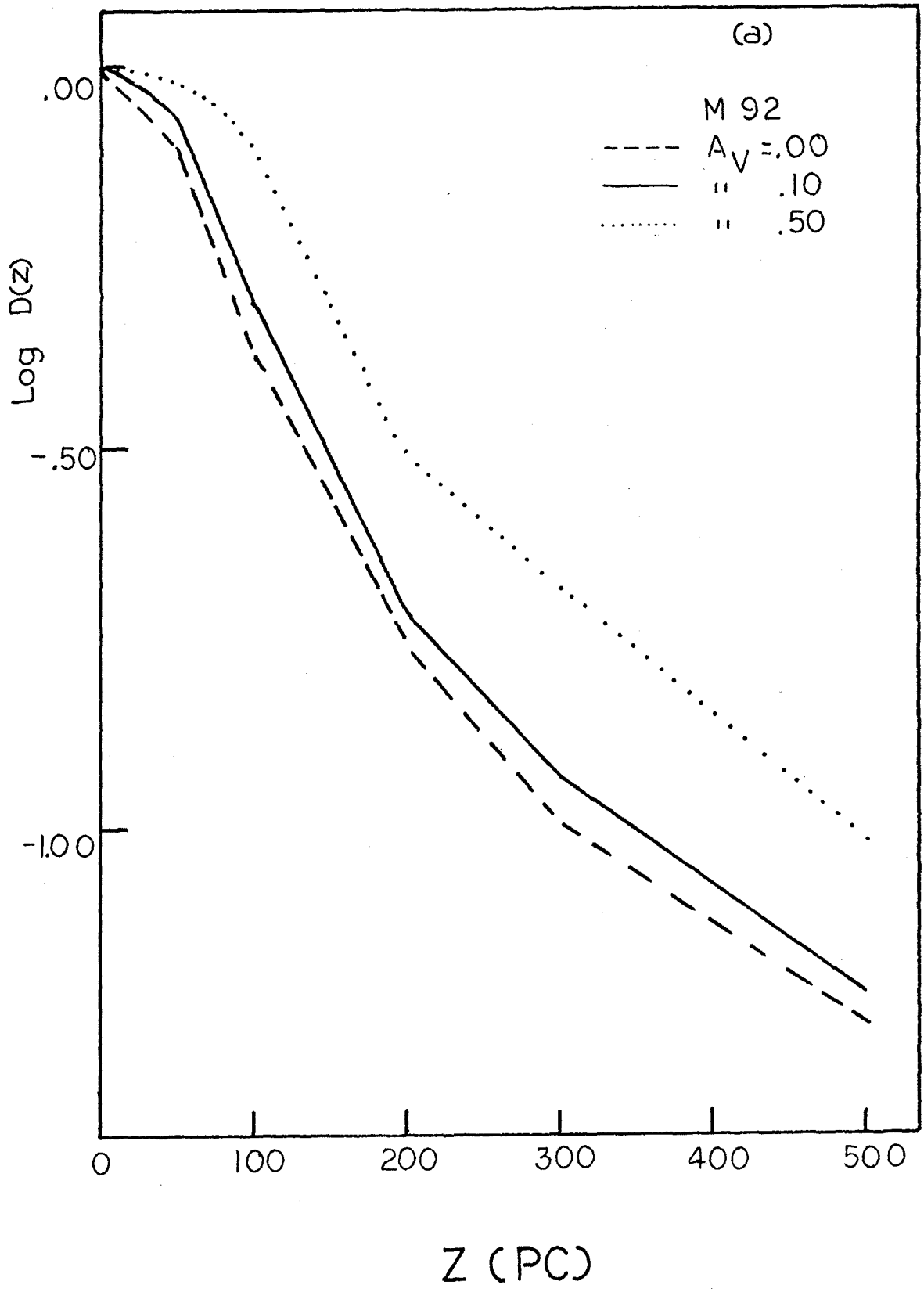
(a)
M 92
---- A_V =.00
—— " .10
..... " .50
.00
-.50
-1.00
Log D(z)
0
100
200
300
400
500
Z (PC)

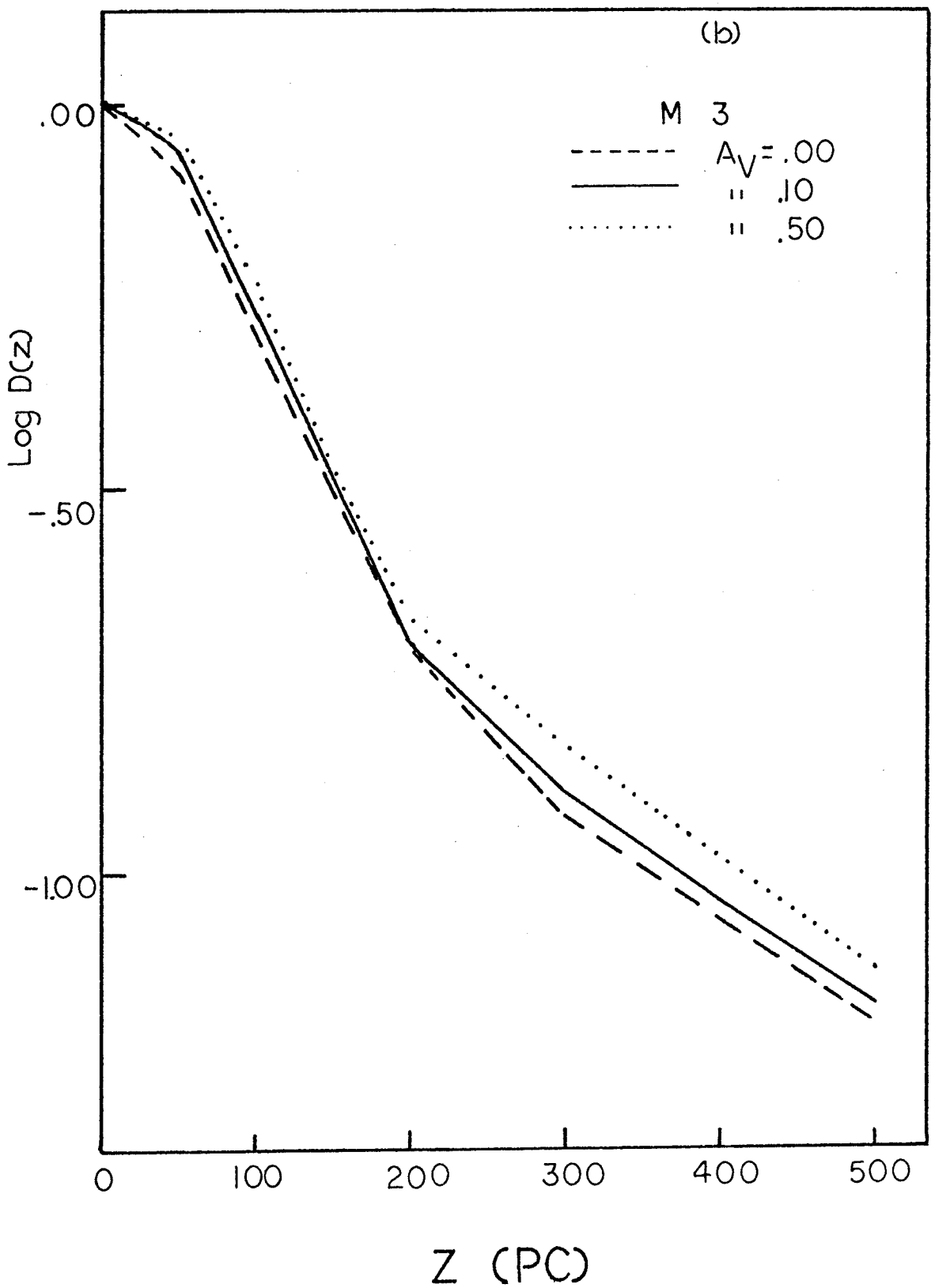
(b)
M 3
A_V = .00
" .10
" .50
.00
-.50
-1.00
Log D(z)
0
100
200
300
400
500
Z (PC)

effect of the absorption increases the size of the dip already noted for points closer than 50 pc (Figure 12), if .50 mag. of absorption is assumed, thus producing a gentler slope in the smooth curve drawn through the points.

The major change in the luminosity function due to increased total absorption is an increase in the number density of all stars, as may be seen in Figure 18, which compares the Case III luminosity functions for model M 3, n=4, 1:2 for the three values of total absorption assumed.

Table 20

Derived Mass Density (Solar Masses per pc^3)

as a Function of Absorption

Absorp.	.00	.10	.50
Model			
M 3, n=4, 1:2			
Case I	.036	.041	.063
Case II	.075	.078	.098
Case III	.054	.058	.078

The result is just as one would expect, as assuming an increased amount of absorption is equivalent to requiring the observed number of stars to occupy a decreased volume. The intrinsically faintest stars are nearest, and therefore least effected by the absorption, explaining the smaller increase in the luminosity function for faint absolute

Figure 18

Luminosity functions computed assuming model M 3, n = 4, 1:2, Case III for three values of absorption.

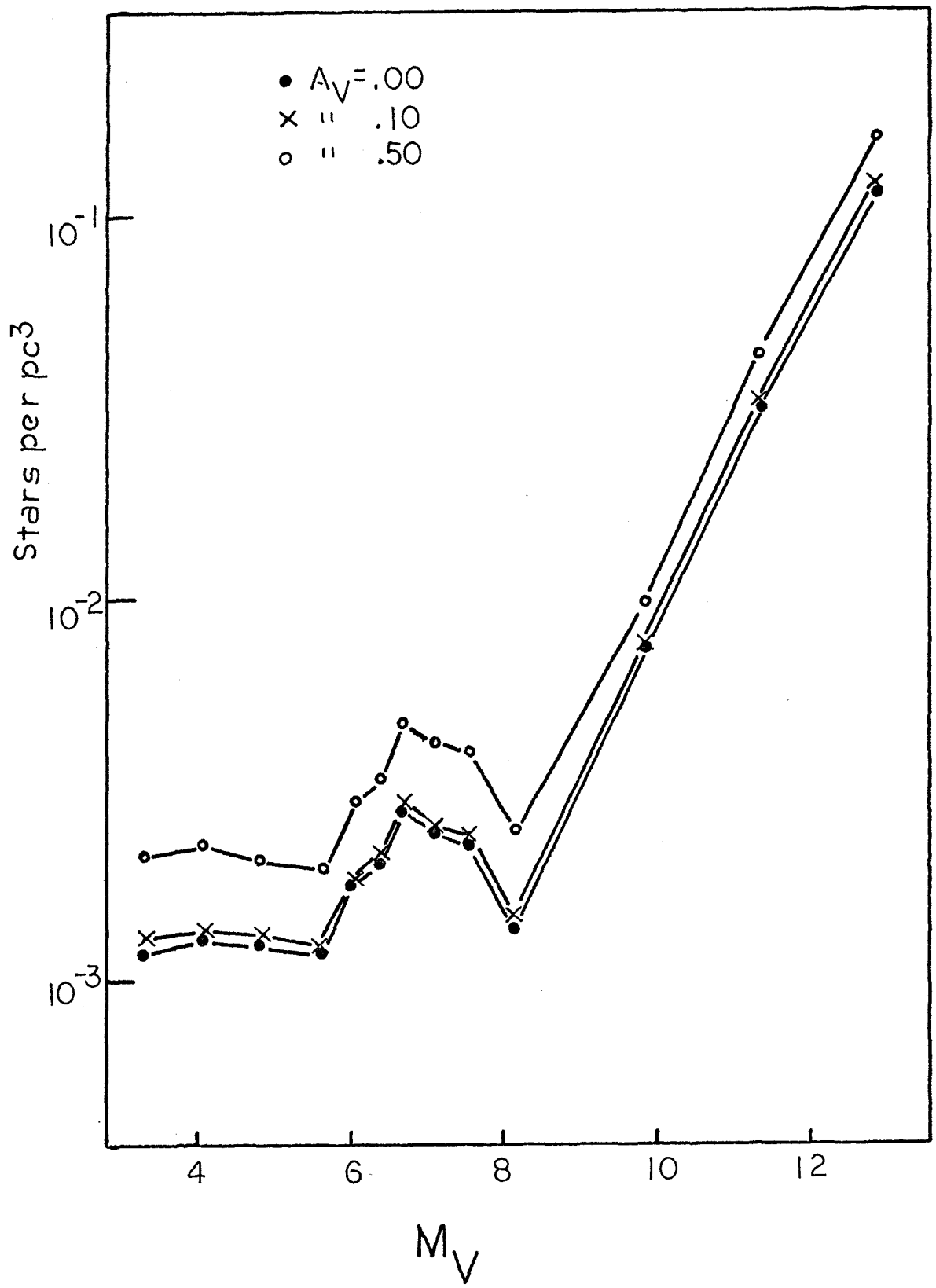
• A_V=.00
× " .10
○ " .50
10^{-1}
10^{-2}
10^{-3}
Stars per pc3
4
6
8
10
12
M_V

magnitudes. The difference between the luminosity functions for the .00 mag. and .10 mag. of absorption cases is negligible. The effect of the assumed absorption on the mass density of the stars (Table 20) just reflects the changes in the luminosity function.

Population II

In order to compare the derived upper limit of the local Population II density with the results of other authors, mass-luminosity ratios for M 3 and M 92 must be adopted. Oort and van Herk (1959) find values for M 3 which range from .19 to .62 in solar units, but suggest the most probable value is about .25 , indicating an upper limit to the local Population II density of 3×10^{-5} solar masses per pc^3 if model M 3, n=4, 1:2 is assumed (Table 12).

More up-to-date estimates of the mass-luminosity ratio can also be made. The integrated magnitudes determined by Kron and Mayall (1960) have been transformed to B magnitudes using the relations given in their paper. These values, combined with the distance moduli given by Sandage (1970), determine absolute integrated blue magnitudes of -7.9 and -7.6 for M 3 and M 92, respectively. Adopting Sandage's distance modulus, the mass determined by Schwarzschild and Bernstein (1955) for M 92 becomes 1.15×10^5 solar masses. The mass of M 3 has

been taken as 1.4×10^5 suns, following Sandage (1954). This value does not disagree with the results of Oort and van Herk, who find the best model for M 3 to have a mass between 1.2×10^5 and 1.9×10^5 solar masses. Using these masses and absolute magnitudes, $\mathcal{M}/L$ is $.7\,\mathcal{M}_\odot/L_\odot$ for both M 3 and M 92. Considering the uncertainty of the mass determinations, this agreement is probably coincidental. Mass-luminosity ratios of $.7\,\mathcal{M}_\odot/L_\odot$ predict an upper limit of $7\text{-}8 \times 10^{-5}$ solar masses per pc^3 for the density of Population II stars in the neighborhood of the sun.

Eggen (1968a) finds three suspected halo population members within 8 pc of the sun. Because his investigation was principally limited to stars with visual magnitude brighter than 10, the survey for stars as faint as the suspected Population II members (M_V = 10.9 , 13.2) is complete to only 6.6 pc and 2.6 pc , respectively. (Eggen's data for these stars are given in Table 21.) The third suspected halo population member has been eliminated, as it is part of a much more restricted sample of stars with apparent magnitudes fainter than 10. Eggen observed 90% of the stars in a survey 60% complete over the northern half of the sky (Vyssotsky and Mateer, 1952). The density derived from the two suspected Population II members being considered must therefore be multiplied by 4, yielding a

Table 21

Eggen's Data for Suspected Halo Members

Eggen No.	Name	M_V	$\mu_\alpha \cos\delta$	μ_δ	RV km sec^{-1}	U km sec^{-1}	V km sec^{-1}	W km sec^{-1}	π_{tr}	Wt
73	HD 33793	10.9	6".564	-5".722	+244	-22	-289	-50	".251	18
349	V/799	13.2	-".689	10".256	-107	+138	+6	+18	".545	92

local Population II density of about 9×10^{-3} solar masses per pc^3. It must be emphasized that this result is determined principally by star No. 349. If that star is not a subdwarf, the local density, as derived from No. 73, is 1.1×10^{-3} solar masses per pc^3. Oort (1965), applying similar arguments to the material presented by Joy (1947), finds a local Population II density of 4×10^{-4} solar masses per pc^3. Both these results are substantially larger than the local density derived here, and differ greatly from each other. The statistics used to obtain the densities are very poor; the Oort result consisting of data for four stars, and that from Eggen, two. Also, Eggen is careful to note that his stars are only suspected of halo membership. Another cause of the discrepancy between the results cited and those derived may lie in the different methods used to arrive at the local Population II mass density. The results from Oort and Eggen's data are based on very nearby stars, while the density derived here is determined from the number of stars far from the plane, and the assumed density distribution perpendicular to the plane. If the Population II density gradient were actually steeper than we have assumed, the true local Population II density would be higher than the value calculated.

Bond (1970) has found that for stars with

Henry Draper types F5 - G5 the relative number of extremely metal-deficient stars ([Fe/H] < - 1.20) in the neighborhood of the sun is roughly one in a thousand. If this percentage is valid for metal-poor stars of all spectral types, and the luminosity function and mass-luminosity relation for Population II are assumed similar to those for the disk population, then, from the values for the disk star density determined below, the local mass density for Population II stars is approximately 1.5×10^{-4} solar masses per pc^3. Considering the uncertainties in both analyses, the agreement with the density derived in the present study is excellent.

The effect of the uncertainty in the globular cluster mass - luminosity ratio on the Population II density derived should be emphasized. Values ranging from .25 to .7 in solar units have been considered. If future determinations should increase the larger value significantly, the difference between the local Population II density derived by Oort, and the density computed in this analysis could be greatly reduced.

In addition, the question of whether the globular cluster mass-luminosity ratios are representative of field Population II should be considered. The calculations of Oort and van Herk indicate that the number of faint stars in M 3 is depressed relative to the van Rhijn luminosity function, possibly due to evaporation of such stars from

the cluster. If this is actually the case, the field Population II might well be expected to have a higher mass-luminosity ratio than is found for the clusters. The applicability of this argument to the above result for M 3 is uncertain, since Sandage, using his counts for M 3 extrapolated with a van Rhijn luminosity function, and Oort and van Herk, assuming fewer faint stars than the van Rhijn luminosity function indicates, calculate approximately the same mass (an indication of the uncertainties involved). The local Population II density determined from M 92 would, however, be influenced by the absence of subdwarfs in the cluster, as the mass determination used here is based on dynamical arguments.

Composite Disk Density Distributions

Figure 19 compares the disk density distribution derived from stars with $M_V = 3\text{-}9$ for model M 92, n=4, 1:2, Case I with Oort's curve (1960) for K giants and Fenkart's curve (1967) for stars with $M_G = 3\text{-}8$. The dashed line indicates the extrapolation adopted due to the uncertainty in $D(z)$ for small z , as described in Chapter III. Fenkart's curve is slightly high, probably due to the normalization at 250 pc from the galactic plane. If Fenkart's result is forced to coincide with Oort's at 250 pc , the agreement with Oort is excellent to $z = 1000$ pc. Beyond 1000 pc, Fenkart's curve falls off faster

Figure 19

Comparison of density distributions derived for disk stars. The kind of stars used to determine each curve is indicated after the author's name. (Dashed line indicates extrapolated portion of curve.)

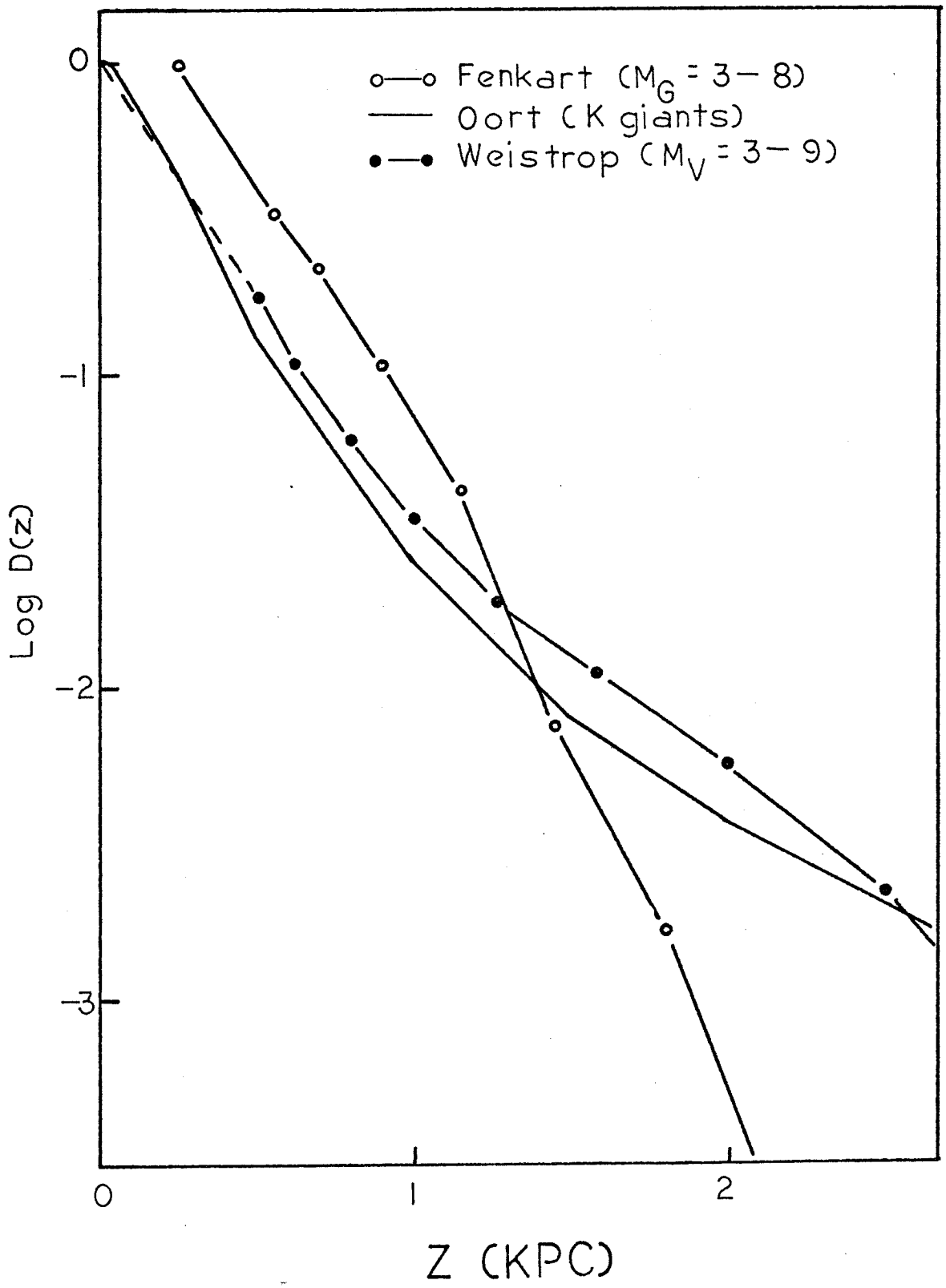
Fenkart (M_G = 3 – 8)
Oort (K giants)
Weistrop (M_V = 3 – 9)
Log D(z)
0
-1
-2
-3
0
1
2
Z (KPC)

than either Oort's or the result found here. The derived curve is consistent with the renormalized Fenkart curve to 1 kpc , and with Oort to 2 kpc . Considering the uncertainties in the data beyond 2 kpc , the agreement with Oort at those distances is not unsatisfactory.

The discrepancy between the Fenkart curve and the one derived here arises in the different methods used to assign stars to either Population II or the disk. Fenkart makes use of the location of the stars in the two color diagram to separate halo and disk populations. Such a procedure is dangerous, considering the errors in the colors are of a size comparable with the ultraviolet excesses (see Chapter III). Using the ultraviolet excess as a population discriminant, Fenkart has assigned a larger fraction of the faint stars to the halo population than has been done here, producing the observed difference in the disk density curves.

The Case II curve for M 92, n=4, 1:2 is compared with the density distribution of the gas (Schmidt, 1957) in Figure 20. The agreement is good to 200 pc , beyond which point the star density remains higher than that of the gas. The divergence occurs at the distance at which the density distribution of the brighter stars is used to extrapolate the curve derived from the faint stars. Figure 20 suggests the possibility that the intrinsically

Figure 20

Comparison of relative density distributions for intrinsically faint stars and gas.

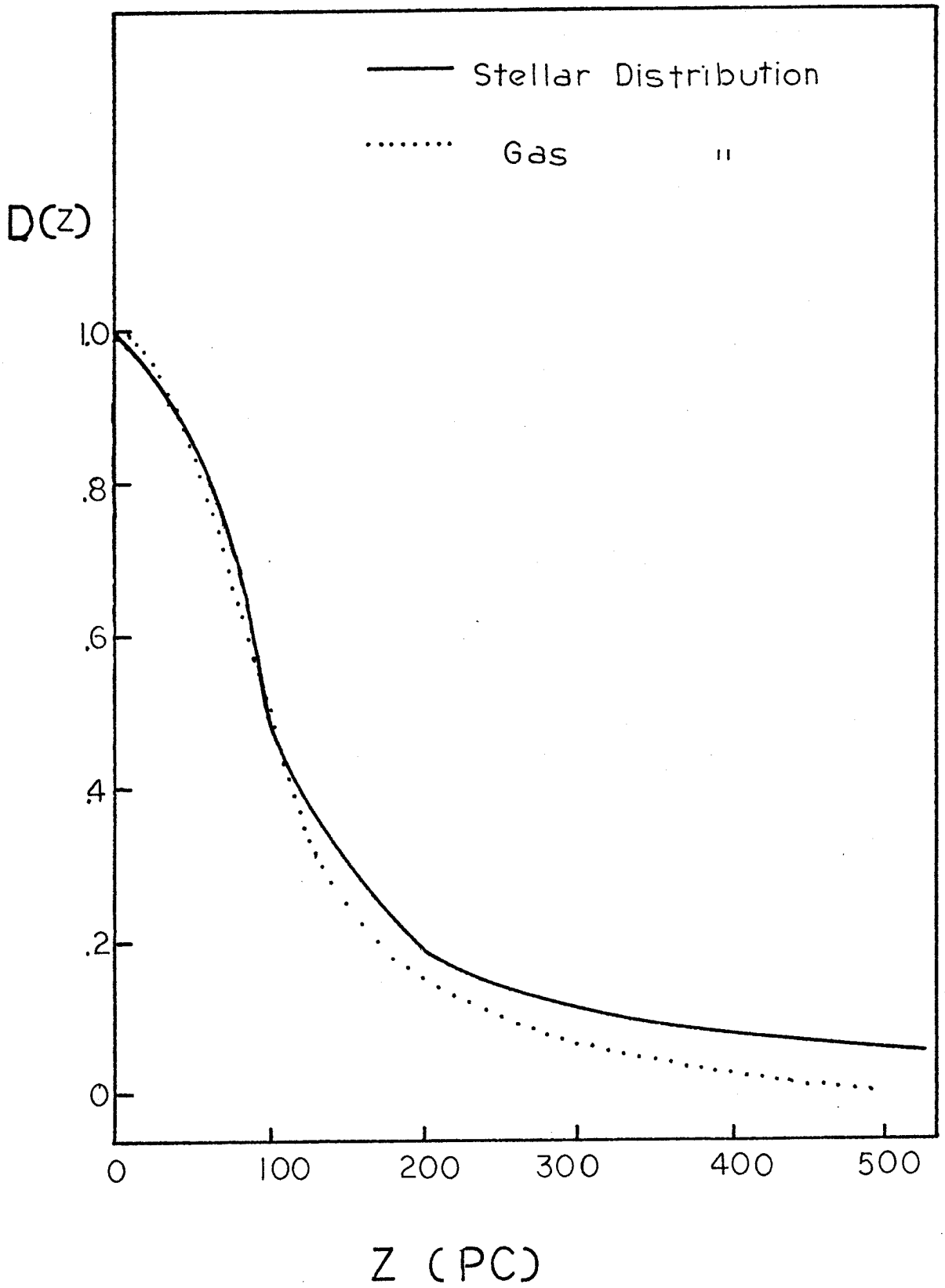
Stellar Distribution
Gas "
D(Z)
1.0
.8
.6
.4
.2
0
0
100
200
300
400
500
Z (PC)

faint stars may in fact be very young stars, recently formed from the gas. However, it should be noted that the dispersion of the velocities perpendicular to the plane for red dwarfs does not indicate such a narrow layer. Using Eggen's data (1968a) for stars selected without reference to velocity criteria, the velocity dispersion as a function of color was calculated (Table 22). As can be seen from the result, no narrowing of the layer occurs for stars bluer than $B-V = 1.60$. The number of redder stars is insufficient to determine the velocity dispersion with any accuracy. It should also be noted that while a smooth, monotonically decreasing curve has been fitted to the Case II density distributions, as can be seen from Figure 12, the individual points are not inconsistent with a peak in the density distribution at $z = 50$ pc , as suggested by Elvius (1965).

Luminosity Functions and Mass Density

The increased luminosity function for intrinsically faint stars is probably the most striking result of this study. Before discussing its consequences, it is necessary to investigate whether these stars could in fact be attributed to some other source. Four possibilities will be considered, that the stars are Population II giants, Population II dwarfs, disk giants, or disk dwarfs. In order to account for the number of stars observed as

Table 22

Velocity Dispersion as a Function of Color

B-V	Disp_Z km sec^{-1}	No.Stars
1.05	21	58
1.15	20	62
1.25	23	65
1.35	33	73
1.45	19	68
1.55	22	32
1.65	5	6
1.75	8	2

Population II giants, it is necessary to increase the number of giants at 100 kpc by a factor of one hundred to one thousand. Such an increase may be accomplished by increasing the number of giants relative to dwarfs in the luminosity function or assuming the density distribution falls off more slowly than is the case for the models we have used. Neither of these possibilities seems likely. If the relative number of giants in the luminosity function is increased by the required factor, the number of Population II stars predicted for magnitudes V = 12-14 is at least a factor of five more than the total number of stars observed. Figure 21 shows the steepest and flattest of the density distributions assumed for Population II. The increase required to account for the observations is indicated by the circled points, the circled cross representing the increases for distribution n=4, 1:2 , and that for n=3 , 1:1 represented by the circled dot. As the figure shows, the change in the n=4, 1:2 model is such that it would become flatter than the n=3, 1:1 case. Even that would not satisfy the observations, however, since the new curve would essentially present the same situation as the n=3, 1:1 model, but that model cannot account for the observations in question, either. From the observed star counts at V = 12-14 , the maximum increase possible for the relative luminosity function of the

Figure 21

Steepest and flattest of the Population II density distributions assumed. See text for explanation of circled points.

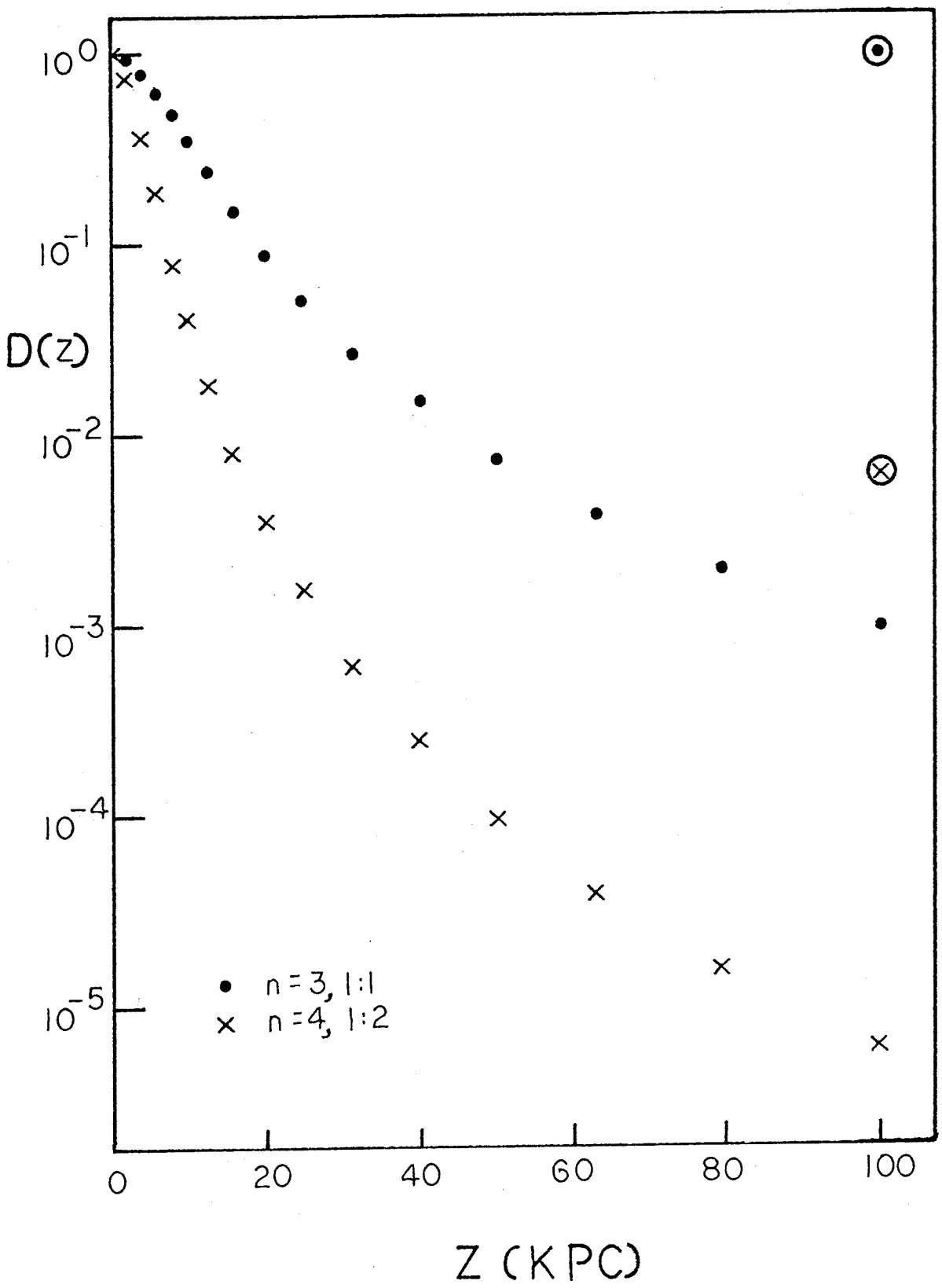
10^0
10^{-1}
10^{-2}
10^{-3}
10^{-4}
10^{-5}
D(Z)
n = 3, 1:1
n = 4, 1:2
0
20
40
60
80
100
Z (KPC)

giants is a factor ten. It also seems possible to increase the density distribution a factor ten at $z = 100$ kpc without disturbing the curve for z less than 30 kpc. If these factors worked together, the observed star counts could be explained for $(B-V)_o = 1.40$ to 1.60, but an increase of an additional factor of ten would still be required to explain the counts at $(B-V)_o = 1.60\text{-}1.70$. The observed star counts probably cannot be attributed to Population II dwarfs, either, as it is extremely unlikely that such stars would be distributed in a very narrow layer, as is indicated for the stars in question.

The argument against the observations being due to disk giants is similar to that for the Population II giants. Since we have tied the luminosity function of the giants to observations for $V = 11\text{-}12$ (see Chapter III), only a change in the density distribution can be used to fit the estimated number of disk giants to the observed number of red stars at faint magnitudes. The increase in density required to make that fit is indicated in Figure 22. The crosses represent the Oort giant density distribution, extrapolated as indicated by the solid line. The circle at 30 kpc represents the density needed to represent the observations. The data currently available do not seem to warrant a density distribution of the required shape. Thus, there seems no alternative to the assignment

Figure 22

Extrapolated Oort K giant density distribution. Points taken from Oort's curve are indicated by (x). See text for explanation of (o).

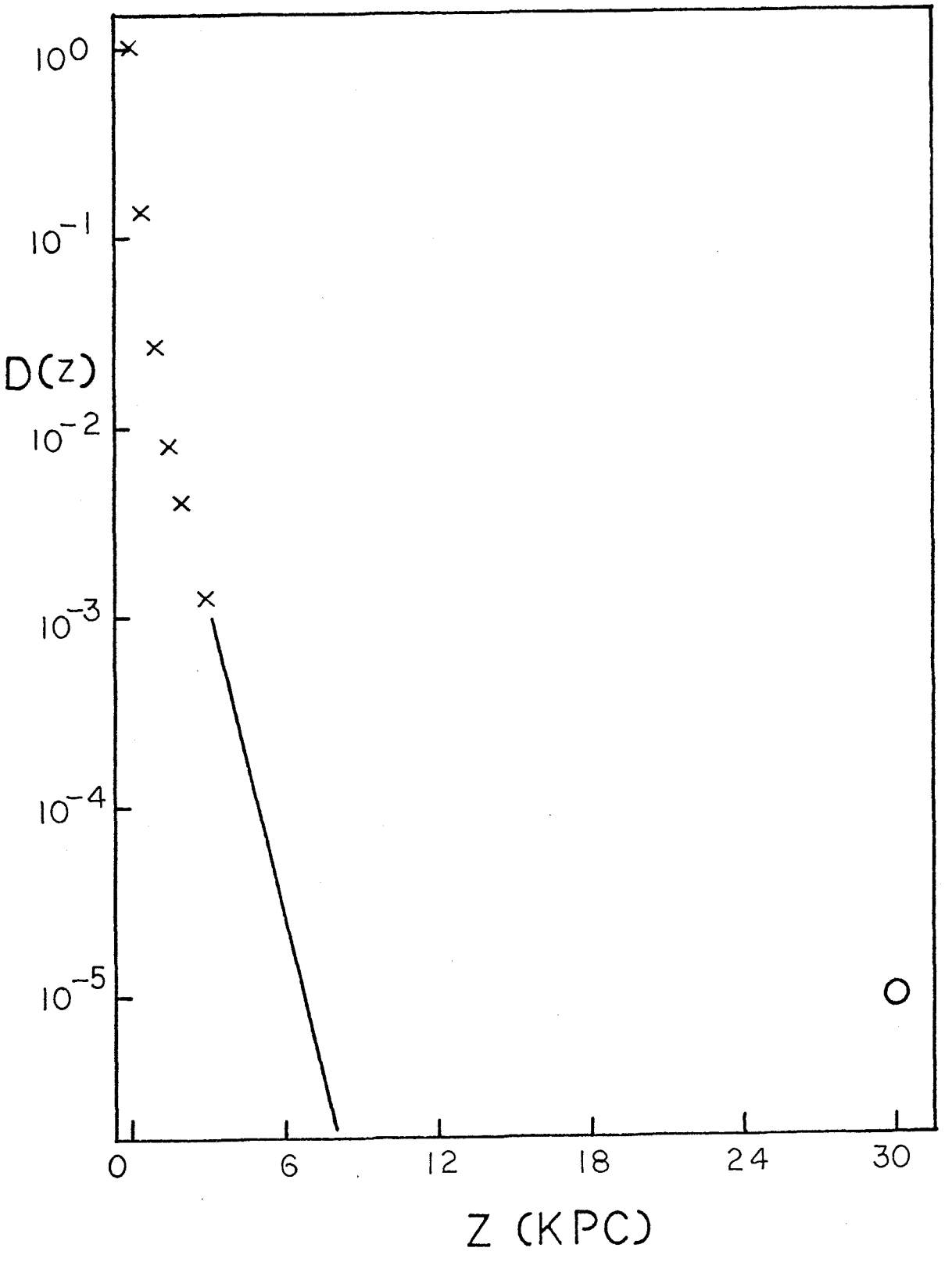
10^0
10^{-1}
D(z)
10^{-2}
10^{-3}
10^{-4}
10^{-5}
0
6
12
18
24
30
Z (KPC)

of the observed stars to the disk dwarf population.

The local mass density calculated for disk stars is greater than that previously determined, as can be seen from Table 18. The difference in the total masses computed is due to the increased number of intrinsically faint stars, except in Case II, where there is also an increased contribution from brighter stars, due to the assumed shape of the density distribution near the plane. To estimate the total mass near the sun due to disk stars, the combined van Rhijn - Case III and van Rhijn - Case I luminosity functions will be considered. The red end of the van Rhijn - Case I function is shown in Figure 23a, along with two extensions. The dashed curve represents the arbitrary assumption that the luminosity function is flat for stars fainter than $M_V = 14$. The dotted curve has been constructed so that the mass contribution from the stars is sufficient to supply all the missing mass in the solar neighborhood, some of which has already been accounted for by the increased luminosity function for faint stars reported here. Table 23a shows the total mass in the solar neighborhood contributed by stars, as calculated for each of the extensions under consideration. To this must be added .006-.010 solar masses per pc^3 for the white dwarfs (Gliese, 1956) and .010-.025 solar masses per pc^3 for the interstellar matter (Oort, 1958; and Westerhout,

Figure 23

Extrapolations of the combined luminosity functions, (a) van Rhijn - Case I, and (b) van Rhijn - Case III. The dashed curves are arbitrary horizontal extensions of the functions. The dotted curves represent the luminosity functions required to supply the missing mass in the solar neighborhood.

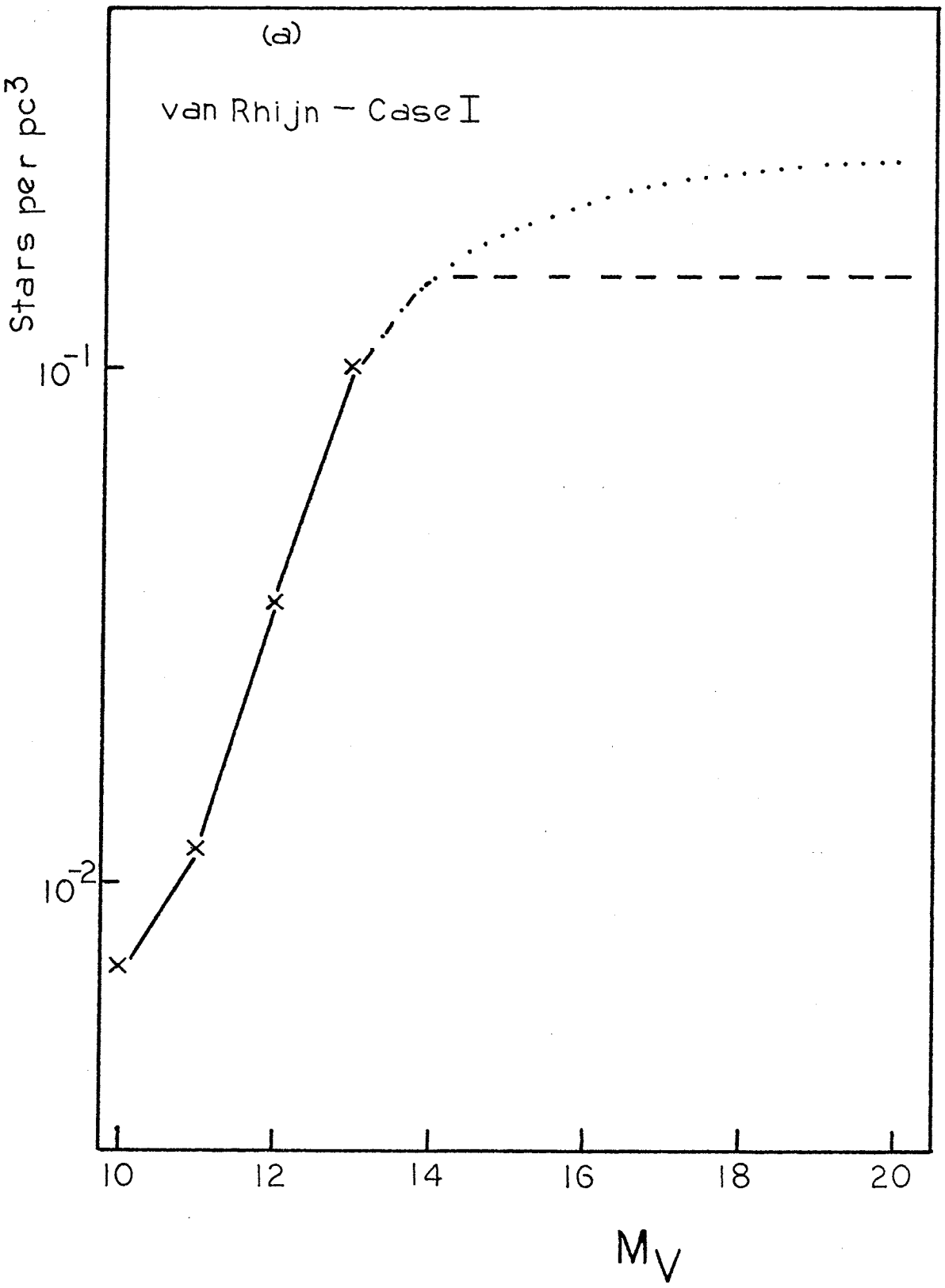
(a)
van Rhijn – Case I
Stars per pc3
10-1
10-2
10
12
14
16
18
20
MV

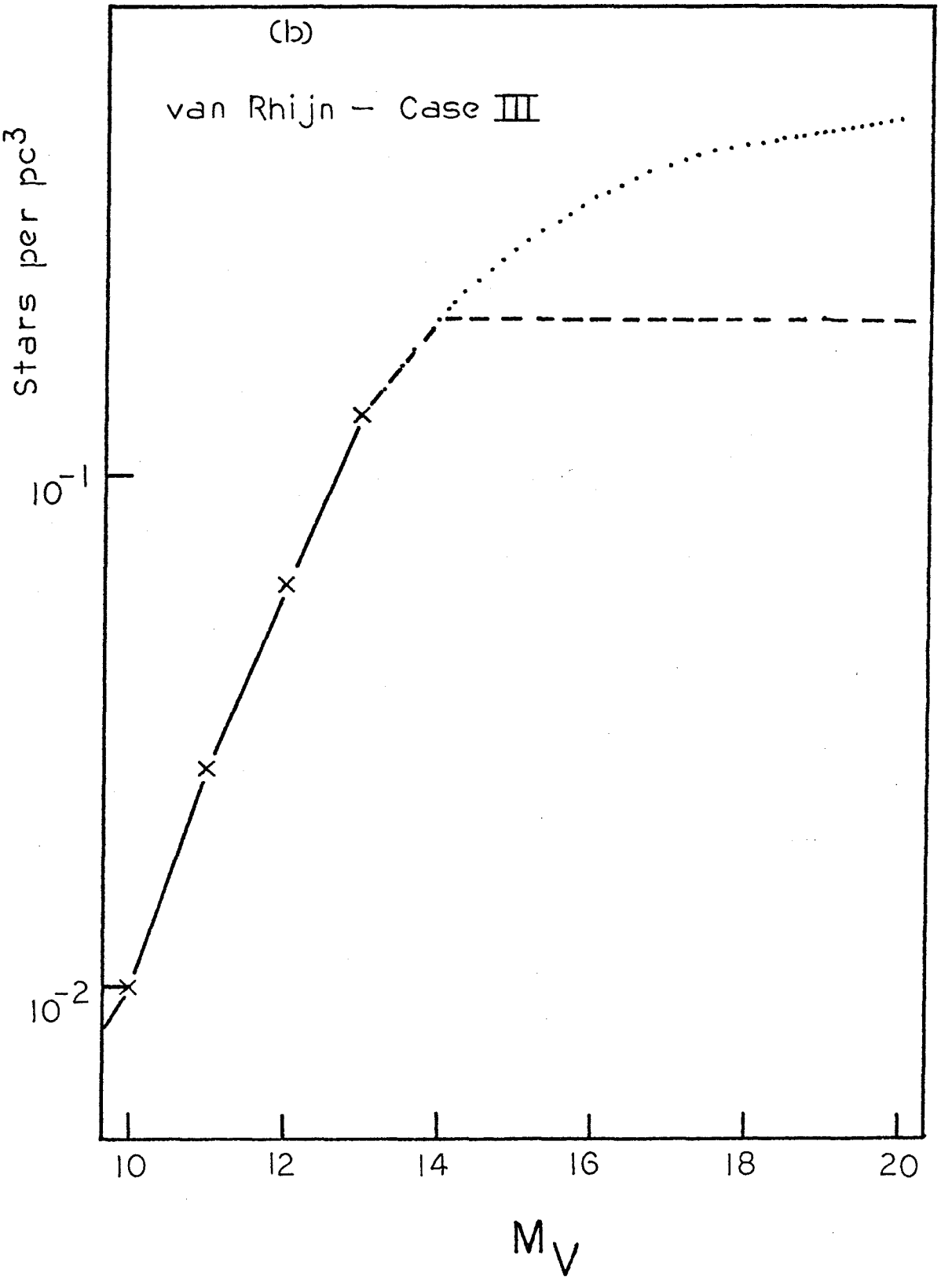
(b)
van Rhijn – Case III
Stars per pc3
10-1
10-2
10
12
14
16
18
20
MV

Table 23a

Luminosity Functions and Mass Densities

(solar masses per pc^3)

for Faint Stars, van Rhijn-Case I

	Horizontal Lum. Fcn.		Maximum Lum. Fcn.	
M_V	Lum.Fcn.	Mass Den.	Lum.Fcn.	Mass Den.
≤ 13		.050		.050
14	.15	.018	.15	.018
15	.15	.012	.18	.014
16	.15	.009	.21	.013
17	.15	.006	.23	.009
18	.15	.004	.24	.007
19	.15	.003	.25	.005
20	.15	.002	.25	.004
		.104		.120
Other Sources		.03	Other Sources	.03
Total		.13	Total	.15

Table 23b

Luminosity Functions and Mass Densities

(solar masses per pc^3)

for Faint Stars, van Rhijn–CaseIII

	Horizontal Lum. Fcn.		Maximum Lum. Fcn.	
M_V	Lum.Fcn.	Mass Den.	Lum.Fcn.	Mass Den.
≤13		.067		.067
14	.20	.024	.20	.024
15	.20	.016	.28	.022
16	.20	.012	.35	.021
17	.20	.008	.40	.016
18	.20	.006	.44	.013
19	.20	.004	.47	.009
20	.20	.003	.50	.007
		.140		.179
Other Sources		.03	Other Sources	.03
Total		.17	Total	.21

1957), for an addition of about .03 solar masses per pc^3. Thus, if the horizontally extended luminosity function represents the real stellar distribution, the total mass accounted for is .13 solar masses per pc^3. To account for the .15 solar masses per pc^3 thought to be in the solar neighborhood from dynamical arguments (Oort, 1960), a luminosity function like the one represented by the dotted line in Figure 23a is required.

When considering the van Rhijn - Case III luminosity function, we must also take into account Oort's calculation (1965) that the amount of unknown mass in the plane is increased 40% , to .21 solar masses per pc^3 , if it is distributed in a narrow layer. Figure 23b shows the van Rhijn - Case III luminosity function with an arbitrarily chosen horizontal extension (dashed line) and an extension (dotted line) which can account for all the mass required under the assumption of a narrow layer for the faint stars. The extended luminosity functions and their mass contributions are tabulated in Table 23b. For the horizontal extension, the total mass in the solar neighborhood is .17 solar masses per pc^3 , while, using the other luminosity function, all the required mass, .21 solar masses per pc^3 is accounted for. Thus, without making extremely unreasonable extrapolations of the luminosity function, it is possible to account for all the mass in

the solar neighborhood, for either of the density distributions close to the plane that have been considered.

Conclusions

The local density for Population II is still very uncertain. Unfortunately a lengthy program of photoelectric observations of ultraviolet excesses seems necessary to accurately determine both the density distribution and local density of members of the halo population.

For the disk population, a reasonably reliable density distribution to distances of $z = 2500$ pc has been derived. The steep density distribution indicated by the intrinsically faint stars needs further investigation, perhaps by extending the study to still fainter stars, or determining velocities perpendicular to the plane for the stars in question. At least part of the missing mass in the solar neighborhood has been found in the increased number of faint stars. By extending the observed luminosity functions in a fairly reasonable way, it is possible to account for all the missing mass, whether distributed in a narrow layer or as the brighter disk stars.

Appendix

Total Star Counts

Though the major part of the analysis has dealt with stars separated into intervals of color as well as magnitude, it is of some interest to consider star counts as a function of apparent magnitude only, as will be done in this section. First, a change in the reduction procedure to improve the calibration for the faintest stars will be discussed. The corrections to the star counts necessary to account for errors in the magnitudes will also be considered. The counts for various sections of the plate will be used to discuss the possibility of variable absorption over the area investigated. Finally, the adopted relation between star counts and apparent magnitude is presented and compared with previous work.

Because the photoelectric sequence derived in the study does not extend beyond apparent visual magnitude 18 , it was necessary to strengthen the calibration for the faintest stars from external sources. Photographic plates in B and V taken with the 200-inch telescope and a faint photoelectric sequence, all for SA 57 , were supplied for this purpose by Dr. Sandage. For 83 of the stars in the investigation, B and V magnitudes were determined from measurements of the 200-inch plates. The measuring and reduction procedures were the same as

those described for the 48-inch plate material. Calibration curves for the 48-inch plates, determined from these magnitudes and all photoelectrically determined magnitudes, are shown in Figures Ala-b for B and V . The dots indicate magnitudes determined from the 200-inch plates; the crosses represent magnitudes of the photoelectric sequence observed in this study. As can be seen from the graphs, the curves are quite steep and the scatter large at faint magnitudes, making it difficult to accurately define the calibration relations.

Because iris measurements of these secondary, photographically determined standards, were not made for every measuring session, the calibration of iris readings for faint stars was accomplished in two steps. All stars were reduced using the calibration relation derived from the photoelectric standards measured daily, extrapolated where necessary. Then magnitudes fainter than $V = 18.1$ or $B = 19.7$ were corrected for the difference between the extrapolated curve and the curve defined by the secondary standards, using the relations in Figures A2a-b. None of the results discussed in Chapters I - IV were influenced by this procedure, as only stars brighter than $V = 18.0$ and $B = 19.7$ were considered in that analysis.

The observed counts should be corrected for errors in the magnitudes. The effect of errors on the observations may be described by equation (A1), where

Figure A1

Calibration curves for (a) faint V, and (b) faint B magnitudes. Photoelectric standards are represented by (x). Magnitudes of stars measured on 200-inch plates are indicated by (•).

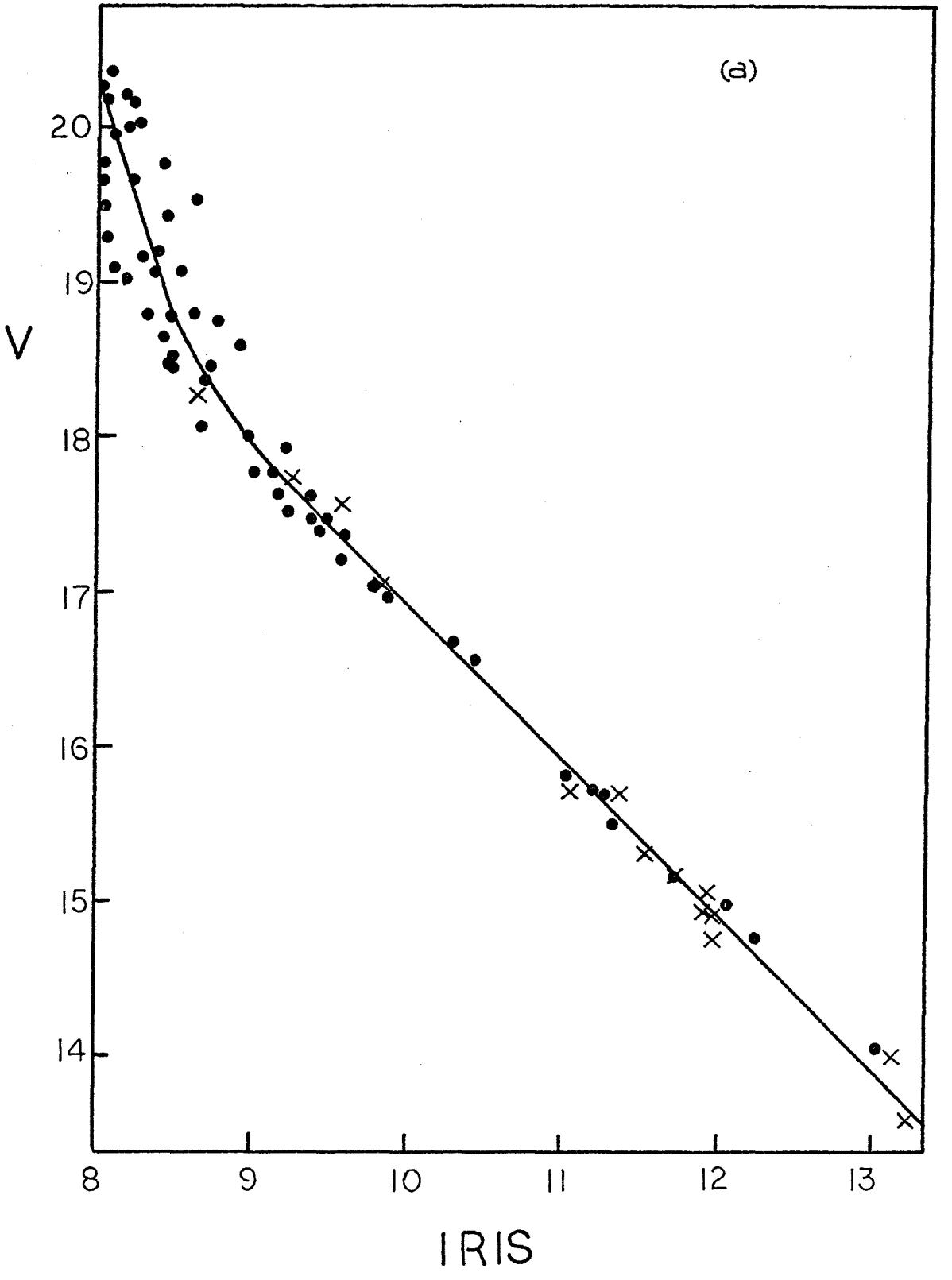
(a)
20
19
18
17
16
15
14
V
8
9
10
11
12
13
IRIS

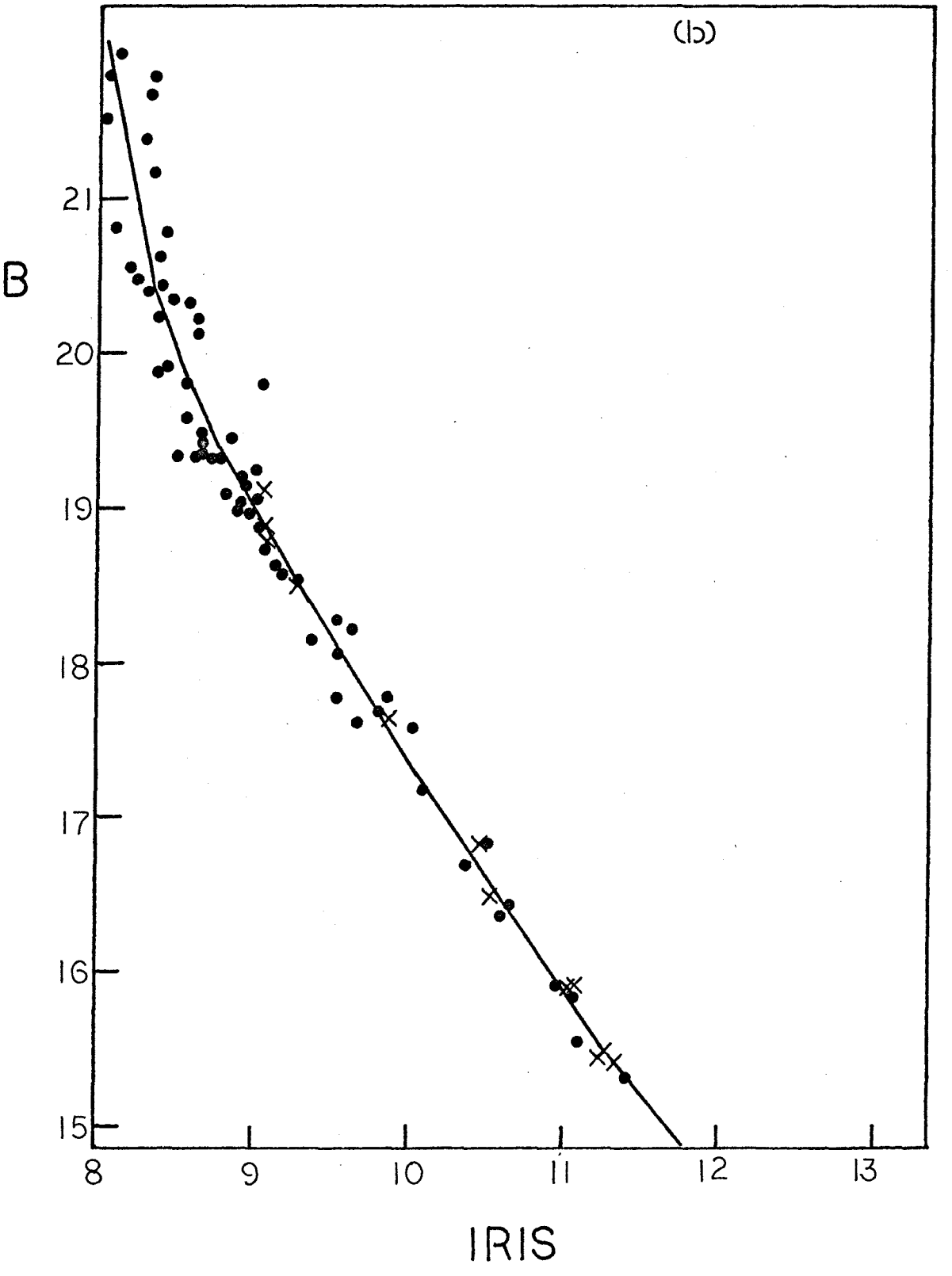
(b)
B
21
20
19
18
17
16
15
8
9
10
11
12
13
IRIS

Figure A2

Corrections for (a) faint V , and (b) faint B magnitudes as a function of magnitude determined from daily measuring sessions. (The latter are indicated by subscript "d".)

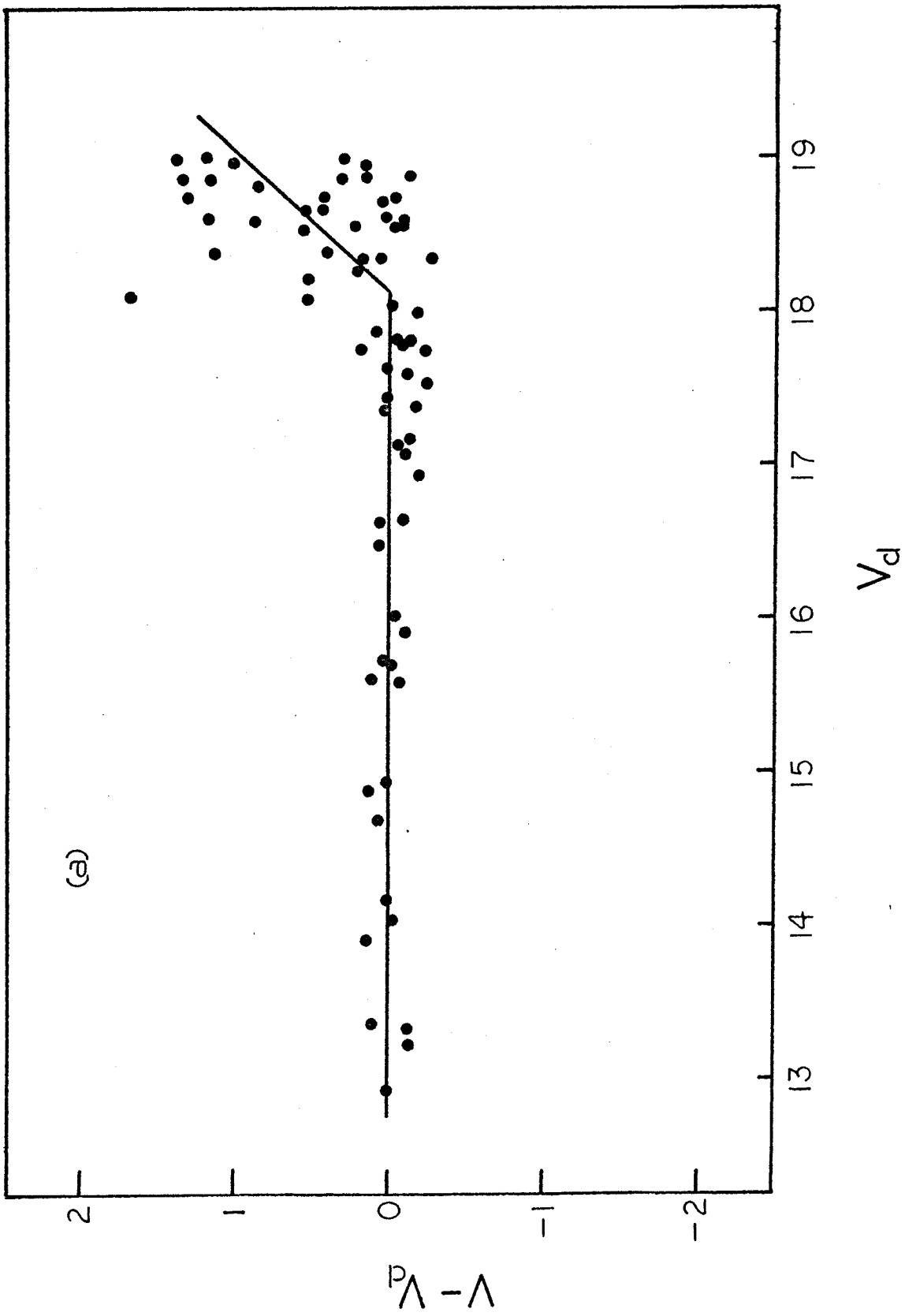
(a)
2
1
0
-1
-2
V - Vd
13
14
15
16
17
18
19
Vd

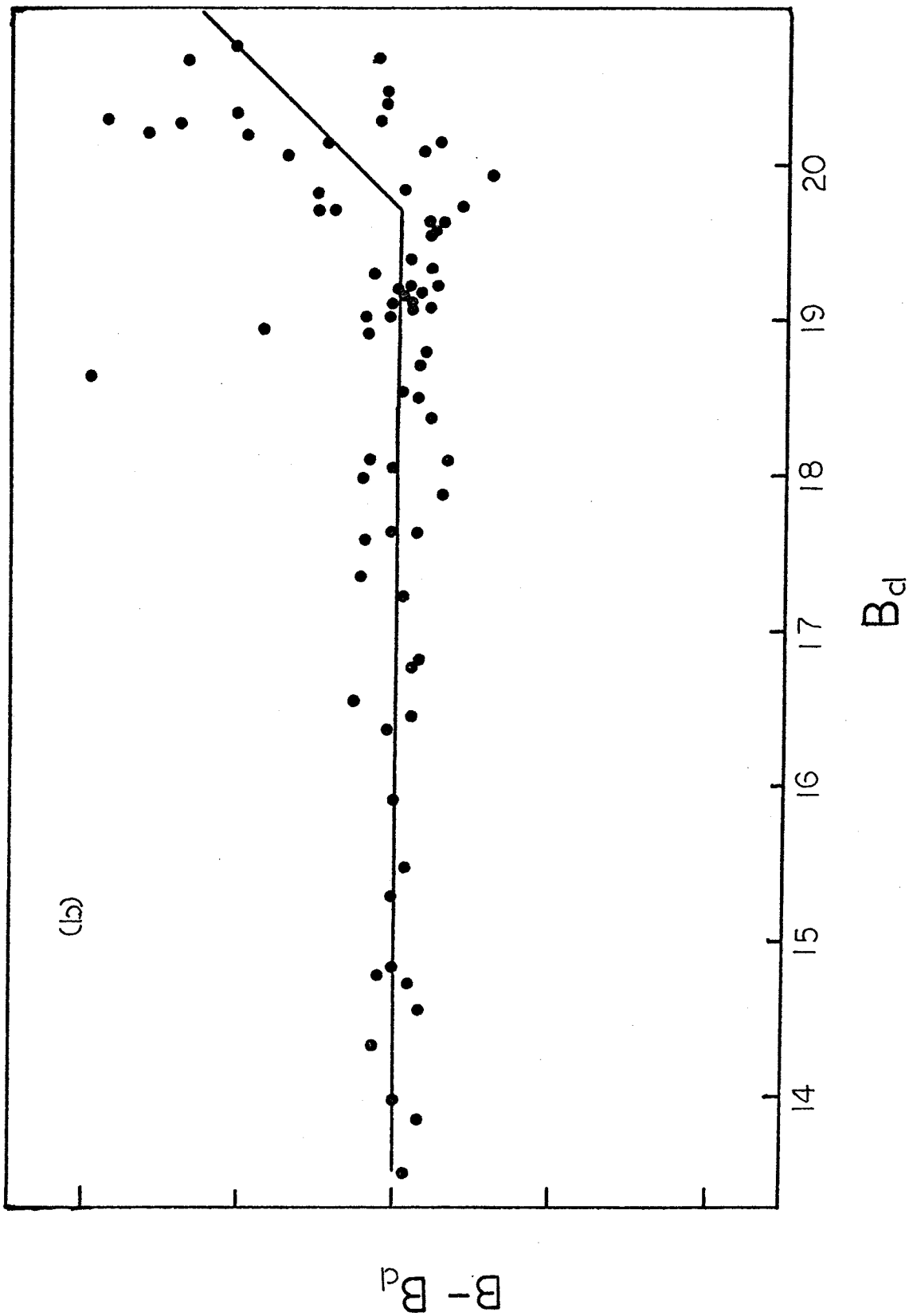
(b)
14
15
16
17
18
19
20
B_d
$B - B_d$

$F_t(x)$ is the true function, $K(y-x)$

$$F_o(y) = \int_{-\infty}^{\infty} F_t(x)\ K(y-x)\ dx \qquad (A1)$$

is the error distribution, and $F_o(y)$ is the observed function. If the error distribution can be represented by a Gaussian, the solution to equation (A1) may be given in series form (A2), using a method described by Eddington (Trumpler and Weaver, 1962). Substituting

$$F_t(y) = F_o(y) - \frac{\sigma^2}{2} F_o''(y) + \frac{\sigma^4}{8} F_o^{iv}(y) - \ldots \qquad (A2)$$

the star counts, $A(m)$, for the general function $F(y)$ in (A2) and assuming the mean error, σ, is relatively small, the series may be truncated after the second term, producing equation (A3), where A_t

$$A_t(m) = A_o(m) \left[1 - \frac{\sigma^2}{2} \left(\frac{b^2}{\log^2 e} \right) \right] \qquad (A3)$$

is the true number of stars per apparent magnitude, A_o is the observed number, and b is the slope of the curve defined by $\log A_o(m)$ plotted against m, which may be approximated by a straight line over a large range in magnitude. Assuming σ = .15 mag. and b = .25, the steepest slope for the data, the correction is 0.4% ;

that is, the observed counts are too large by 0.4% . The corrected values for the counts lie within the symbols representing the observed counts in Figures A3 and A4.

To determine whether any variable absorption exists within the area of the sky investigated, the field was divided into nine equal parts. For each region, the total number of stars in intervals of one magnitude was counted for V between magnitude 12 and 18 . The average number of stars per region was computed for each magnitude interval. Comparison of the root mean square deviation of the number of stars per region with the square root of the averaged counts shows little difference, (Table A1), indicating the absence of non-statistical variations across the plate. Similar results were found for star counts as a function of U and B magnitudes, supporting the conclusion that no variable absorption is present over the area of the sky investigated. The final star counts were determined by combining data from the entire plate.

Figure A3 shows the adopted value of log A(V) as a function of V , normalized to counts per square degree. The dip beyond V = 18 and the rise beyond V = 19 are probably due to the difficulty in defining the calibration relation for faint stars. The solid line has been extended to indicate what is thought to be the

Table A1

V	$\bar{A}$, Ave. No. Stars per Region	$\sqrt{\bar{A}}$	RMS Dev. of Stars per Region from $\bar{A}$
12.5	28	5.3	6.2
13.5	52	7.2	7.7
14.5	91	9.5	9.6
15.5	126	11.2	10.7
16.5	169	13.0	17.2
17.5	265	16.3	20.2

Figure A3

Logarithm of the number of stars per square degree as a function of V. The solid line indicates what is thought to be the true relation. The constant density case is represented by the dashed line.

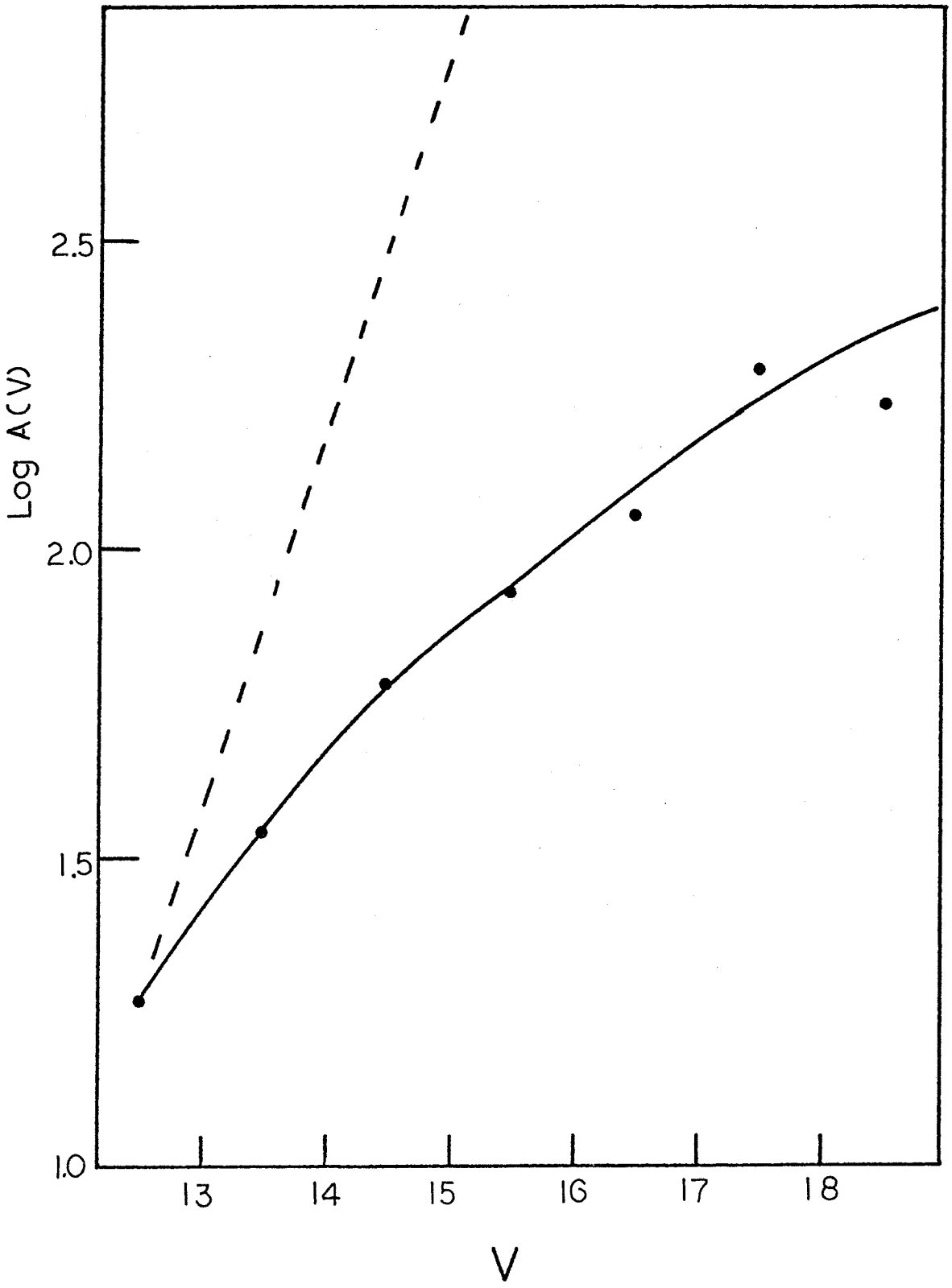
2.5
2.0
1.5
1.0
Log A(V)
13
14
15
16
17
18
V

correct relation. The leveling off of the curve at faint magnitudes, due to the decreasing star density far from the plane, is apparent. The dashed line in Figure A3 indicates the log A(V) - V relation expected if the density remains constant with increasing z, normalized to the observed counts at V = 12.5. Log A(B) for the data normalized to one square degree is represented by the dots in Figure A4. The crosses indicate van Rhijn's star counts (1929) for Selected Area 57, corrected for the error in the m_{pg} magnitude scale and the difference between B and m_{pg} (Arp, 1965). The comparison is not unsatisfactory.

Figure A4

Comparison of log A(B) with van Rhijn's star counts.

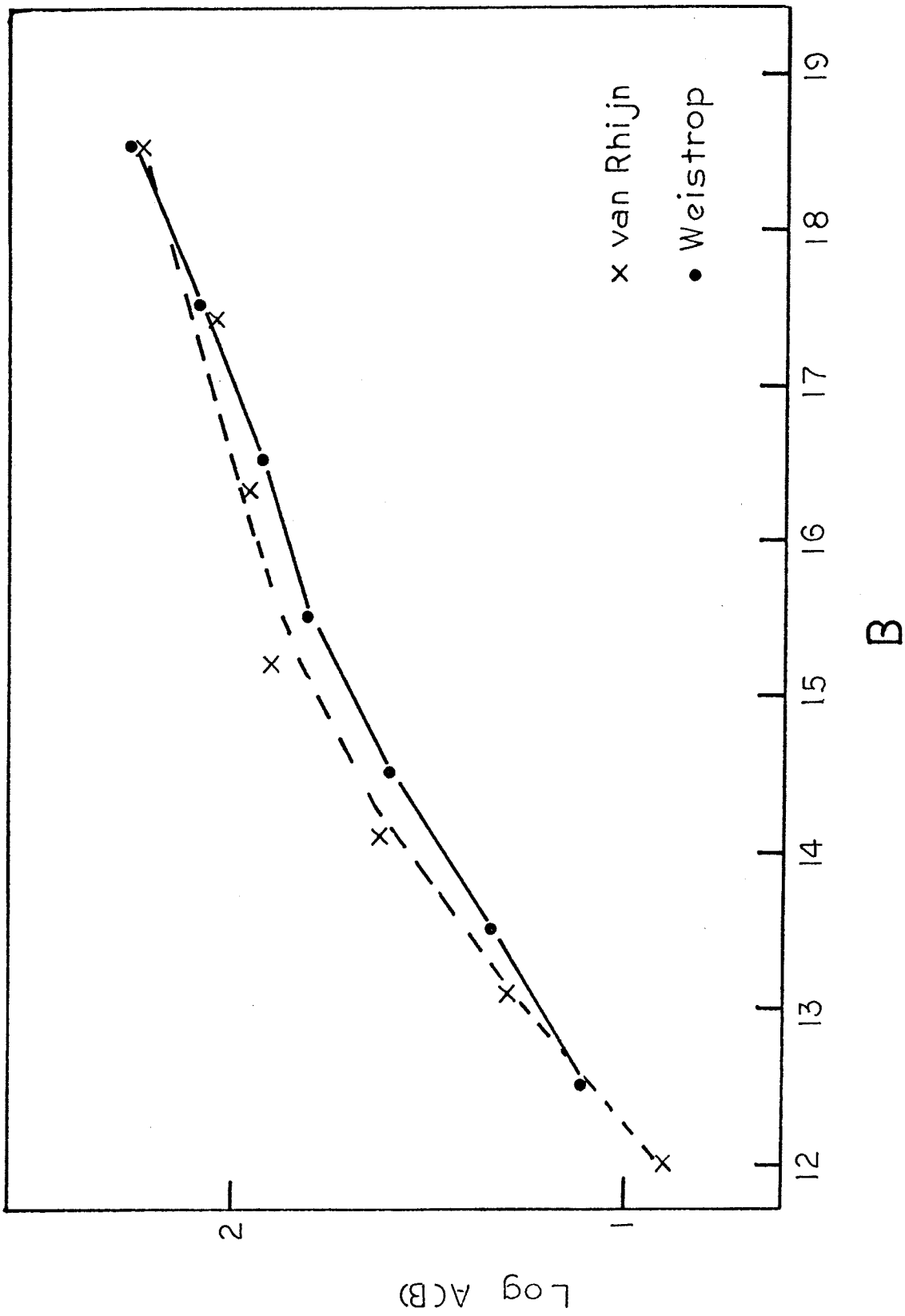
x van Rhijn
• Weistrop
Log A(B)
2
1
12
13
14
15
16
17
18
19
B

References

Allen,C.W. 1963,Astrophysical Quantities (2nd ed.; London:The Athlone Press), p.104.

Arp,H.C. 1965, Galactic Structure, ed. A.Blaauw and M.Schmidt (Chicago: U. of Chicago Press), p.409.

Becker,F. 1940, Zs.f.Ap.,19,50.

Blaauw,A. 1963, Basic Astronomical Data, ed. K.Aa.Strand (Chicago: U. of Chicago Press), p.383.

Bok,B.J.,and MacRae,D.A. 1941, Ann.N.Y. Acad. Sci.,42,Art.2,219.

Bond,H.E. 1970, Ap.J.Supp.,22,117.

Crawford,D.L., and Barnes,J.V. 1969, A.J.,74,1008.

Eggen,O.J. 1965, First Conference on Faint Blue Stars, ed. W.J.Luyten (Minneapolis:U. of Minnesota Observatory),p.37.

_____. 1967, Ann. Rev. Astr. and Ap.,5,105.

_____. 1968a, Ap.J.Supp.,16,49.

_____. 1968b, ibid., p.97.

Eggen,O.J., Lynden-Bell,D., and Sandage,A.R. 1962, Ap.J.,136,748.

Eggen,O.J., and Sandage,A.R. 1964, Ap.J.,140,130.

_____. 1969, Ap.J.,158,669.

Elvius,T. 1965, Galactic Structure, ed.A.Blaauw and M.Schmidt (Chicago: U. of Chicago Press), p.41.

Fenkart,R.P. 1967, Zs.f.Ap.,66,390.

Gliese,W. 1956, Zs.f.Ap.,39,1.

Greenstein,J.L. 1966, Ap.J.,144,496.

Greenstein,J.L., and Eggen,O.J. 1965, Ap.J.,141,83.

Halliday,I. 1955, Ap.J.,122,222.

Harris,D.L.,III,Strand,K.Aa., and Worley,C.E. 1963, Basic Astronomical Data, ed.K.Aa.Strand (Chicago: U. of Chicago Press),p.273.

Hartwick,F.D.A. 1970, Ap.J.,161,845.

Hill,E.R. 1960, B.A.N.,15,1.

Hoffleit,D. 1964, Catalogue of Bright Stars (3rd ed.;New Haven: Yale University Press).

Humason,M.L., and Zwicky,F. 1947, Ap.J.,105,85.

Jenaer Glaswerk Schott & Gen. 1962, Color Filter Glass (Mainz: Jenaer Glaswerk Schott & Gen.).

Johnson,H.L. 1954, Ap.J.,119,181.

_____. 1955, Ann.d'ap.,18,292.

Johnson,H.L., and Morgan,W.W. 1953, Ap.J.,117,313.

Johnson,H.L., and Sandage,A.R. 1955, Ap.J.,121,616.

Joy,A.H. 1947, Ap.J.,105,96.

Kinman,T.D. 1965, Ap.J.,142,655.

Kodak Co. 1948, Photographic Plates for Scientific and Technical Use (6th ed.; Rochester: Eastman Kodak Co.).

_____. 1968, Kodak Wratten Filters (22nd ed.;Rochester: Eastman Kodak Co.).

Kron,G.E., and Mayall,N.U. 1960, A.J.,65,581.

Malmquist,K.G. 1936, Stockholms Obs. Medd.,No. 26.

McClure,R.D., and Crawford,D.L. 1971, A.J.,76,31.

McCuskey,S.W. 1956, Ap.J.,123,458.

Minkowski,R.L., and Abell,G.O. 1963, Basic Astronomical Data, ed. K.Aa.Strand (Chicago: U. of Chicago Press),p.481.

Morgan,W.W. 1959, A.J.,64,432.

Oort,J.H. 1932, B.A.N.,6,249.

_____. 1958, Stellar Populations,ed. D.J.K. O'Connell (Vatican City: Vatican Obs.),p.415.

_____. 1960, B.A.N.,15,45.

_____. 1965, Galactic Structure, ed. A.Blaauw and M.Schmidt (Chicago: U. of Chicago Press), p.455.

Oort, J.H., and Herk, G. van 1959, B.A.N., 14, 299.

Peterson, B.A. 1970, A.J., 75, 695.

Philip, A.G.D. 1968, A.J., 73, 1000.

Plaut, L., and Soudan, A. 1963, B.A.N., 17, 70.

Rhijn, P.J. van 1929, Pub. Kapteyn Astr. Lab. Groningen, No.43.

_____. 1936, ibid., No. 47.

Rhijn, P.J.van, and Schwassmann, A. 1935, Zs.f.Ap., 10, 161.

Sandage, A.R. 1954, A.J., 59, 162.

_____. 1957a, Ap.J., 125, 422.

_____. 1957b, ibid., p.435.

_____. 1962, Ap.J., 135, 333.

_____. 1968 (private communication).

_____. 1969a, Ap.J., 157, 515.

_____. 1969b, ibid., 158, 1115.

_____. 1970, ibid., 162, 841.

Sandage, A.R., and Luyten, W.J. 1967, Ap.J., 148, 767.

_____. 1969, ibid., 155, 913.

Sandage, A.R., and Smith, L.L. 1963, Ap.J., 137, 1057.

Schmidt, M. 1957, B.A.N., 13, 247.

_____. 1959, Ap.J., 129, 243.

Schwarzschild, M., and Bernstein, S. 1955, Ap.J., 122, 200.

Seares, F.H., Kapteyn, J.C., and Rhijn, P.J.van 1930, Mount Wilson Catalogue of Photographic Magnitudes in Selected Areas 1-139 (Washington: Carnegie Institution of Washington).

Shane, C.D., and Wirtanen, C.A. 1967, Pub. Lick Obs., 22, 1.

Slettebak,A.,Wright,R.R., and Graham,J.A. 1968, A.J.,73,152.

Stebbins,J.,Whitford,A.E., and Johnson,H.L. 1950, Ap.J.,112,469.

Sturch,C. 1966, Ap.J.,143,774.

Trumpler,R.J., and Weaver,H.F. 1962, Statistical Astronomy (New York: Dover Publications,Inc.),p.123.

Upgren,A.R. 1962, A.J.,67,37.

_____. 1963, A.J.,68,194.

Vyssotsky,A.N., and Mateer,B.A. 1952, Ap.J.,116,117.

Westerhout,G. 1957, B.A.N.,13,201.

Wildey,R.L.,Burbidge,E.M.,Sandage,A.R., and Burbidge,G.R. 1962,Ap.J., 135,94.